Title

Mechanisms of Neuroprotection and Remyelination in Demyelinating Disease Models of Multiple Sclerosis: A Lesson From Estrogen Receptor Specific Ligands

Author

Kim, Youn-Jung Roy

Publication Date

2018

Peer reviewed|Thesis/dissertation

UNIVERSITY OF CALIFORNIA

Los Angeles

Mechanisms of Neuroprotection and Remyelination in Demyelinating Disease Models of Multiple Sclerosis: A Lesson From Estrogen Receptor Specific Ligands

A dissertation submitted in partial satisfaction of the requirements

for the degree Doctor of Philosophy

in Molecular Cellular and Integrative Physiology

by

Youn-Jung Roy Kim

2018

ABSTRACT OF THE DISSERTATION

Mechanisms of Neuroprotection and Remyelination in Demyelinating Disease Models of Multiple Sclerosis: A Lesson From Estrogen Receptor Specific Ligands

by

Youn-Jung Roy Kim

Doctor of Philosophy in Molecular Cellular and Integrative Physiology

University of California, Los Angeles, 2018

Professor Rhonda Renee Voskuhl, Chair

Currently, available drugs for multiple sclerosis (MS) are predominantly immune-modulatory. They are effective in reducing relapses, but not in slowing down or stopping progressive disease course. Therefore, there is a need to develop treatment strategies that will provide neuroprotection and halt disability progression. Pregnancy is neuroprotective in patients with MS. A pregnancy hormone and a moderate estrogen receptor beta (ERβ)-ligand, estriol, has been reported to have beneficial effects on reducing relapses and improving cognition when treated in MS patients. Although, the mechanisms of ERβ-ligand mediated treatment effects on neuroprotection remains poorly understood. Here I hypothesized that ERβ signaling on $CD11c^+$ immune cells and $Olig1^+$ oligodendrocytes plays an essential role in providing neuroprotection and enhancing remyelination. To test the hypothesis, I created conditional knockout mice (CKO) with ERβ deleted from each cell type using the Cre-LoxP recombinase system and investigated

neuroprotective effects of ERβ-ligand treatment in experimental autoimmune encephalomyelitis (EAE) and cuprizone diet-induced demyelinating disease models. Also, I used RiboTag mice to determine oligodendrocyte specific gene expression to understand the molecular mechanisms of remyelination. Subsequently, I studied the mechanisms of ERβ-ligand treatment effects in oligodendrocytes during remyelination.

The results revealed that ERβ-ligand treatment reduced pro-inflammatory responses through ERβ on $CD11c^+$ myeloid DC/MΦ and increased oligodendrocyte maturation through ERβ on $Olig1^+$ oligodendrocytes during EAE. The use of CKO mice proved that both were necessary as one without the other was not sufficient. Mechanistic insights on remyelination using the RiboTag mice revealed that oligodendrocytes upregulate *de novo* cholesterol biosynthesis during remyelination after chronic demyelination. Furthermore, when compared to vehicle treated naturally remyelinating mice, ERβ-ligand treated mice showed enhanced remyelination by increasing oligodendrocyte maturation, increasing cholesterol synthesis pathway genes, increasing oligodendrocyte progenitor cells (OPCs), and increasing Sox2 expression in OPCs during remyelination. I extended our investigation of ERβ-ligand treatment in the cuprizone model to the EAE model, to discover that ERβ-ligand treated mice showed neuroprotection by increasing oligodendrocyte maturation, and increasing cholesterol synthesis pathway genes, but not by increasing OPC Sox2 expression. This comprehensive approach using two different demyelinating disease models of MS and two transgenic mouse models provided critical insights regarding treatment effects of ERβ-ligand on neuroprotection and remyelination *in vivo*.

The dissertation of Youn-Jung Roy Kim is approved

Arthur P. Arnold

Stephanie Correa Van Veen

Andrea L. Hevener

Rhonda Renee Voskuhl, Committee Chair

University of California, Los Angeles

2018

TABLE OF CONTENTS

Abstract	ii
Table of content	v
List of Tables	ix
List of Figures	x
Acknowledgment	xiii
Biographical Sketch	xv
CHAPTER 1. General Introduction	1
1.1 Multiple Sclerosis (MS)	1
1.2 Experimental autoimmune encephalomyelitis (EAE)	2
1.3 Cuprizone diet-induced demyelination model	3
1.4 Estrogen receptor alpha (ERα) ligand treatment effects in EAE	3
1.5 Estrogen receptor beta (ERβ) ligands treatment effects in EAE	4
1.6 Objectives	6
1.7 Bibliography	7
CHAPTER 2 Astrocytes CCL2 sustains inflammation in chronic EAE: a lesson from ERα-ligand treatment effects on astrocytes.	12
2.1 Introduction	12
2.2 Results	14
2.2.1 Verification of the GFAP-cre line	14
2.2.2 Validation of CCL2 deletion in astrocytes	15

2.2.3 CCL2 deletion from astrocytes provides clinical disease protection late during EAE	17
2.2.4 CCL2 deletion from astrocytes reduces macrophage and T cell infiltration during EAE	19
2.2.5 CCL2 deletion from astrocytes reduces activation of astrocytes and microglial during EAE	20
2.2.6 CCL2 deletion from astrocytes preserves myelin and protects against axonal loss during EAE	22
2.2.7 CCL2 deletion from astrocytes did not affect early EAE	24
2.3 Discussion	26
2.4 Methods and materials	29
2.5 Bibliography	31
CHAPTER 3 Neuroprotection requires modulation of inflammation and remyelination during EAE: a lesson from estrogen receptor beta ligand	39
3.1 Introduction	39
3.2 Results	41
3.2.1 Specification of $CD11c^+$ cells in the CNS during EAE	41
3.2.2 Validation of ERβ specific deletion in $CD11c^+$ cells	42
3.2.3 ERβ activation on $CD11c^+$ cells is important for neuroprotection during EAE	44
3.2.4 ERβ on $CD11c^+$ cells is necessary for ERβ-ligand mediated myelin preservation and remyelination during EAE	48

3.2.5 ERβ activation on CD11c$^+$ cells had no quantitative effects on immune cells during EAE	50
3.2.6 ERβ activation on CD11c$^+$ cells has qualitative effects on CNS myeloid cells during EAE	51
3.2.7 ERβ signaling reduces pro-inflammatory phenotypes of CD11c$^+$ myeloid DC/MΦ during EAE	53
3.2.8 ERβ activation on CD11c$^+$ microglia is not important for neuroprotection during EAE	54
3.2.9 ERβ activation on CD11c$^+$ myeloid DC/MΦ is important for neuroprotection during EAE	58
3.2.10 ERβ activation on CD11c$^+$ cells is important for permitting oligodendrocyte maturation	61
3.2.11 ERβ on Olig1$^+$ oligodendrocytes is necessary for ERβ-ligand mediated neuroprotection	63
3.3 Discussion	65
3.4 Methods and materials	69
3.5 Bibilography	78
CHAPTER 4 Estrogen acts on oligodendrocytes to upregulate cholesterol synthesis genes during remyelination in the cuprizone and EAE models	86
4.1 Introduction	86
4.2 Results	88
4.2.1 Oligodendrocyte specific RNA isolation from Olig1-RiboTag mice	88

4.2.2 Remyelination after chronic demyelination in the cuprizone diet-induced model	90
4.2.3 Dominance of enrichment of cholesterol synthesis pathways during remyelination after chronic demyelination	92
4.2.4 ERβ-ligand treatment enhances remyelination and increases oligodendrocytes during remyelination in the cuprizone diet-induced model	96
4.2.5 No effects of ERβ-ligand treatment on microglia and reactive astrocytes during remyelination	101
4.2.6 ERβ-ligand treatment upregulates cholesterol synthesis pathway genes in oligodendrocytes	103
4.2.7 ERβ-ligand treatment increases cholesterol synthesis pathway gene expression in oligodendrocytes during remyelination in EAE	105
4.3 Discussion	109
4.4 Methods and materials	112
4.5 Bibliography	121
CHAPTER 5 General Conclusion, Limitations and Future Directions	128

LIST OF TABLES

Table		Page
3.1	Statistics of clinical EAE severity scores shown in Figures.	47
4.1	Mean MBP intensity, Mean difference, standard errors and significance levels for each comparison in all experiments.	101

LIST OF FIGURES

Figures		Page
2.1	Verification of extent and selectivity of Cre targeting to astrocytes.	15
2.2	Validation of CCL2 deletion specificity in $GFAP^+$ astrocytes during EAE.	16
2.3	Astrocyte CCL2-CKO, as compared to CCL2-WT, has less severe EAE late in the disease.	18
2.4	Astrocyte CCL2-CKO mice with EAE have a reduction in macrophage and T cell infiltrates during EAE.	20
2.5	Selective deletion of CCL2 from astrocytes results in less activation of astrocytes diffusively in the spinal cords during EAE.	21
2.6	Selective deletion of CCL2 from astrocytes results in less microglial activation diffusively in the spinal cords during EAE.	22
2.7	Astrocyte CCL2-CKO, as compared to CCL2-WT littermates, has less demyelination and axonal loss during EAE.	23
2.8	No differences were found between CCL2-CKO mice as compared to CCL2-WT littermates during the early phase of EAE.	25
3.1	Specification of $CD11c^+$ cells in the CNS during EAE.	42
3.2	Validation of ERβ specific deletion in $CD11c^+$ cells via immunofluorescence and qPCR.	43
3.3	ERβ on $CD11c^+$ cells is necessary for ERβ-ligand mediated amelioration of clinical EAE and axonal protection during EAE.	45

3.4	ERβ on CD11c$^+$ cells is necessary for ERβ-ligand mediated myelin preservation and remyelination during EAE.	49
3.5	No quantitative effects on CNS resident and infiltrated immune cells.	50
3.6	Qualitative effects on inflammatory markers on CNS resident and infiltrated Iba1$^+$ myeloid cells.	52
3.7	ERβ-ligand treatment effects on CD11c$^+$ microglia and CD11c$^+$ myeloid DC/MΦ cells gene expression.	53
3.8	Reconstitution efficiency in BMC mice.	56
3.9	CD11c$^+$ microglial ERβ expression is not necessary for neuroprotection in EAE.	57
3.10	ERβ expression on CD11c$^+$ myeloid DC/MΦ is necessary for neuroprotection in EAE.	59
3.11	No quantitative effects on CNS resident and infiltrated immune cells in BMC EAE mice.	60
3.12	ERβ-ligand treatment acts on CD11c$^+$ cells to permit increases in mature oligodendrocytes during EAE.	62
3.13	ERβ expression on Olig1$^+$ cells is necessary for neuroprotection in EAE.	64
4.1	Isolation and validation of oligodendrocyte specific transcripts from Olig1-RiboTag mice.	89
4.2	Time course of remyelination after chronic demyelination in the cuprizone model.	91
4.3	Oligodendrocyte specific transcriptome changes during remyelination	94

	after chronic demyelination.	
4.4	Validation of upregulated cholesterol synthesis genes in oligodendrocytes during remyelination.	95
4.5	ERβ-ligand treatment during the remyelination phase of the cuprizone model further enhances remyelination and increases mature oligodendrocytes and OPCs.	99
4.6	ERβ-ligand treatment has no effect on microglia and reactive astrocytes during remyelination.	102
4.7	ERβ-ligand treatment during the remyelination phase of the cuprizone model further increases cholesterol synthesis gene expression in oligodendrocytes.	104
4.8	ERβ-ligand treatment induces remyelination during EAE.	106
4.9	ERβ-ligand treatment during EAE.	108
5.1	Mechanisms of ERβ-ligand treatment effects during EAE.	130
5.2	Mechanisms of ERβ-ligand treatment effects during EAE with insights from an investigation in the cuprizone model	133
5.3	ERβ-ligand treatment increases Sox2 expression in OPCs in the cuprizone model, but not in the EAE model.	138

ACKNOWLEDGMENT

First, I would like to thank my supervisor Dr. Rhonda R. Voskuhl, for her guidance and mentorship. Also, for giving me this great opportunity to be a part of her journey to study sex differences in multiple sclerosis (MS) and to develop treatments for MS using sex hormones. The past 6 years, through her kindness I was able to participate in making critical decisions and write grants for my research projects. I want to thank her for allowing me the freedom to make my own mistakes and pursue my passion for research. It has been a great experience.

I want to thank my committee members Dr. Arthur P. Arnold, Dr. Stephanie Correa, and Dr. Andrea Hevener for their guidance on how to strengthen my experimental designs, wisdoms on interpretation of my data, and giving me constructive feedback. Without Dr. Voskuhl and committee members, I would not have been able to prepare myself to become an independent research scientist.

I'm grateful to have such wonderful lab members, Noriko Itoh, Yuichiro Itoh, Alessia Tassoni, and Lisa Golden, and past members, Laura Kammel, Sienmi Du and Rory Spence. Without them, I doubt that I would have survived the past 6 years of my graduate years. Over the years I have created a special bond of friendship with them, and I feel fortunate to have such fun and supportive lab members. I'm also thankful to have such great undergraduate students that worked with me throughout the years, Alexandria Hoffman, Rojan Kavosh, Eunice Jung, Darian Mangu, Raul Alejandro-Rodrigez and Kevin Herrera. All of them were such hard working and dedicated students and have contributed greatly to all my projects. I want to also thank Dr. Allan Mackenzie-Graham and his lab members, Cassandra Meyers and Stefano Lepore, for being such a supportive group.

I also gratefully acknowledge sources of financial support for my work. I want to thank the Laboratory of Neuroendocrinology training grant (T32-HD07228) for accepting me as a trainee for two years and Ruth L. Kirschstein National Research Service Award from National Institute of Neurological Disorders and Stroke (F31-NS096906) for supporting me for two years.

Finally, I would like to thank my family for their excellent support and cheering me on throughout the years. Especially, my wife Michelle Yu who endured through the toughest times in her life taking care of our newborn Nicolas Kim alone at crucial times. You are the strongest person I have ever encountered in my life. Thank you for all that you have done.

BIOGRAPHICAL SKETCH

Education

Chungnam National University, Daejeon, Korea

B.S. in Microbiology 2007

Research Experience

Dr. Robert Raffai's Laboratory, Department of Surgery UCSF, San Francisco, CA

Position: Research Associate September 2008 – July 2012

Dr. Rhonda Voskuhl's Laboratory, Department of Neurology UCLA, Los Angeles, CA

Position: Graduate Student Researcher September 2012 – Present

Teaching Experience

UCLA Teaching Assistant - Life Science 2, Spring 2014

UCLA Teaching Assistant - Life Science 2, Spring 2013

Awards and Grants

NRSA Individual Predoctoral Fellowship (F31-NS096906) April 2016 – March 2018

Superior Poster Presentation, UCLA MCIP Program Retreat Febuary 2014

UCLA LNE Training grant (T32-HD07228) August 2013 – July 2015

Presentations

Oral presentations

ERβ-ligand acts on $CD11c^{+}$ cells to mediate neuroprotection in EAE. Laboratory of Neuroendocrinology (LNE) Seminar Brain Research Institute (BRI), UCLA. March 2018.

Mechanisms of estrogen mediated neuroprotection in EAE. MCIP Ph.D. Program Student seminar, UCLA. September 2017

Neuroprotective effects of estrogens in EAE; mechanisms of ERβ mediated treatment effects. Neural Repair Seminar BRI, UCLA. May 2017.

Understanding the mechanisms of ERβ mediated neuroprotective effects in EAE. LNE Seminar BRI, UCLA. March 2015

Mechanism of estrogen receptor alpha (ERα) mediated neuroprotection in EAE. LNE Seminar BRI, UCLA. May 2014

Poster presentations

ERβ-ligand acts on peripheral myeloid cells to mediate protection in EAE. MCIP Ph.D. program retreat, UCLA. February 2018.

Regulation of myeloid immune cells and remyelination are both necessary for neuroprotection in autoimmune encephalomyelitis. 15th Annual CNSR Symposium, UCLA. February 2017.

ERβ is required on $CD11c^+$ for ERβ-ligand mediated neuroprotection during EAE. Society for Neuroscience San Diego, CA. November 2016

ERβ is required on CD11c expressing cells for ERβ-ligand mediated neuroprotection during EAE. OSSD Meeting Stanford, CA. May 2015

ERβ is required on CD11c expressing cells for ERβ-ligand mediated neuroprotection during EAE. 7th Annual Neurology Science Day, UCLA. Mar 2015

ERβ on $CD11c^+$ microglia/dendritic cell is required for ERβ-ligand mediated neuroprotection during EAE. MCIP Ph.D. Program Retreat, UCLA. Feb 2015

The role of chemokine (C-C motif) ligand 2 (CCL2) in astrocytes EAE. MCIP Ph.D. Program Retreat, UCLA. Feb 2014

Publications

Kim RY, Tassoni A, Itoh Y, Itoh N, Mangu D, Jung E, Alejandro-Ramirez R, Herrera K, Hoffman A, Kovash R, Peng M, Farkhondeh V, Voskuhl R. Oligodendrocyte upregulate *de novo* cholesterol biosynthesis during remyelination and estrogen receptor beta activation enhances this process. *Manuscript in preparation*

Kim RY, Mangu D, Hoffman AS, Kovash R, Jung E, Itoh N, Voskuhl R. ERβ ligand acts on $CD11c^+$ cells to mediate protection in EAE. Brain. 2018 Jan 1;141(1):132-147.

Itoh N, **Kim RY**, Peng M, DiFilippo E, Johnsonbaugh H, MacKenzie-Graham A, Voskuhl RR. Bedside to bench to bedside research: ERβ-ligand as a candidate neuroprotective treatment for multiple sclerosis. J Neuroimmunol. 2017 Mar 15; 304:63-71.

Kim RY, Hoffman AS, Itoh N, Ao Y, Spence R, Sofroniew MV, Voskuhl RR., Astrocyte CCL2 sustains immune cell infiltration in chronic EAE. J Neuroimmunol. Sep 2014; 274(1-2):53-61

Chapter 1

General Introduction

1.1 Multiple Sclerosis (MS)

MS is a chronic autoimmune disease of the central nervous system. The autoimmunity against myelin and myelin producing oligodendrocytes causes axonal damage and neurodegeneration leading to neurological disability (Steinman, 1996). The etiology is unknown but genetic, and epidemiology studies suggest that heritable factors such as major histocompatibility complex (MHC) and non-heritable factors such as geographical location both play a role (Compston and Coles, 2008; Mechelli et al., 2010). This devastating neurological disease occurs in young adults with a higher susceptibility in women compared to men (~3:1). Although, men show an earlier progressive disease course compared to women, demonstrating an apparent sexual dimorphism (Voskuhl, 2016).

There are mainly three types of disease courses in MS. Relapse-remitting MS (RRMS) is the most common where nearly 85% of patients develop. RRMS is characterized by inflammatory attacks followed by partial or complete recovery. Patients experiencing RRMS disease course often eventually develop into chronic secondary progressive (SPMS). SPMS is characterized by worsening of disease symptoms and permanent deficits in neurological functions. Patients with worse disease symptoms without early relapses or remissions are considered to have developed primary progressive MS (PPMS).

Current treatments available for MS patients are drugs that target peripheral immune responses and are effective in reducing relapse rates, but not in slowing down disability progression. Therefore, to halt disease progression and improve disability, there is a need to

develop treatment strategies targeting oligodendrocytes that will protect them against inflammation and promote remyelination (Plemel et al., 2017).

1.2 Experimental Autoimmune Encephalomyelitis (EAE)

EAE is an animal model for MS. In EAE, mice are subjected to immunization with myelin protein emulsified in Complete Freund's Adjuvant to initiate the autoimmune response. The primed T cells, namely Th1 and Th17, followed by macrophages, infiltrate into the CNS and attack myelin proteins initiating the EAE disease course. After the initial attack by infiltrated T cells and macrophages, more immune cells are recruited, further damaging the CNS (Wujek et al., 2002). After induction of EAE, mice display clinical MS symptoms such as walking disability, vision impairment, and cognitive decline. Due to these similarities with MS, EAE has been the most widely used model for developing therapeutics (Constantinescu et al., 2011).

EAE disease course varies between mouse strains. C57BL/6 EAE model has a chronic progressive disease course. All investigations conducted in this dissertation used the C57BL/6 strain for EAE, as we are interested in developing treatment strategies for neuroprotection during the chronic progressive disease course. Despite the benefits of EAE on understanding the pathophysiology of MS, there are some limitations. EAE has strong immune-mediated responses leading to demyelination and neurodegeneration, which limits studying molecular and cellular mechanisms of remyelination in oligodendrocytes. Therefore, other non-invasive demyelinating disease models such as cuprizone diet-induced models or lysolecithin can be used concomitantly.

1.3 Cuprizone diet-induced demyelination model

The cuprizone diet-induced demyelination model has been extensively used to study the pathophysiological mechanisms of demyelination and remyelination (Matsushima and Morell, 2001; Skripuletz et al., 2011). Cuprizone (bis-cyclohexanone oxaldihydrazone) is a copper-chelating agent targeting mature oligodendrocytes in the CNS (Suzuki and Kikkawa, 1969). When animals are fed with cuprizone containing diet, it causes oligodendrocyte death resulting in demyelination over time. After the death of oligodendrocytes occurs, newly produced OPCs and oligodendrocytes start a spontaneous remyelination process (Blakemore, 1972; Matsushima and Morell, 2001). Also, removing cuprizone in the diet induces remyelination (Morell et al., 1998). When cuprizone diet is used chronically (9 to 12 weeks) the newly generated oligodendrocytes undergo apoptosis, leading to a reduction in the OPC pool and remyelination capacity (Mason et al., 2004). Chronic treatment with cuprizone can also lead to severe axonal damage, slowing down the remyelination process. Unlike EAE, the cuprizone model does not have a robust immune response from the periphery and inflammation is mainly entails glial activation within the CNS (Matsushima and Morell, 2001; Gudi et al., 2014).

1.4 Estrogen receptor alpha (ERα) ligands treatment effects in EAE

Estrogens and specific ligands of estrogen receptors (ER) are known to be neuroprotective in murine models of neurodegenerative diseases such as Alzheimer disease, Parkinson disease, ischemic stroke, spinal cord injury and EAE (Samantaray et al., 2010; Spence and Voskuhl, 2012). Estrogens signal through binding to estrogen receptors (ER), alpha (ERα) and/or beta (ERβ), as well as the G-protein coupled estrogen receptor (GPER, previously termed GPR30).

ERα-ligand treatment provides disease protection during EAE. Treatment effects include reduced production of pro-inflammatory cytokines such as TNFα and IFNγ and increased anti-inflammatory cytokines such as IL-10 and IL-5 by peripheral immune cells. Also, decrease in infiltration of macrophages and T cells in the CNS, and protection against axonal loss and demyelination (Morales et al., 2006; Tiwari-Woodruff et al., 2007; Spence et al., 2011; Spence et al., 2013). Investigating the importance of ERα expression on peripheral immune cells led to findings that CD4 T cells, but not B cells, macrophages, or dendritic cells, are essential in mediating ERα-ligand treatment effects during EAE (Morales et al., 2006; Zhu et al., 2010; Lelu et al., 2011). Also, investigations on CNS cell types showed that astrocytes, but not neurons, mediate ERα-ligand treatment effects during EAE (Spence et al., 2011). Unfortunately, treatments using estradiol or ERα-ligands for years in humans might cause adverse effects on the breast and uterus, so targeted strategies are needed to achieve neuroprotection while minimizing off-target toxicity. One approach is to use drugs designed to act in a tissue-specific manner in the CNS, but not in the periphery (Prokai et al., 2015). Another is to develop estrogen compounds or selective estrogen receptor modifiers (SERMs) that are neuroprotective through ERβ activation with minimal ERα activation (Nilsson et al., 2011; Paterni et al., 2014). Alternatively, by targeting downstream effects of ERα-ligand mediated neuroprotection during EAE, such as reduction of CCL2 or NFκB from astrocytes could be another approach to develop treatment strategies for MS (Kim et al., 2014; Giraud et al., 2010; Brambilla et al., 2009).

1.5 Estrogen receptor beta (ERβ) ligands treatment effects in EAE

ERβ-ligands were initially shown to be neuroprotective during EAE without decreasing levels of immune cell infiltration in the CNS or modulating peripheral immune responses (Tiwari-

Woodruff et al., 2007). This study also describes that ER-ligands have differential effects on disease protection, where ERα-ligands are anti-inflammatory and neuroprotective, whereas ERβ-ligands are neuroprotective. Investigating the importance of ERβ expression on CNS cell types showed that oligodendrocytes, but not astrocytes or neurons, are important in mediating disease protection during EAE (Khalaj et al., 2013; Spence et al., 2013), perhaps through enhancing remyelination (Kumar et al., 2013; Crawford et al., 2010). However, the mechanisms regarding its beneficial effects on remyelination in oligodendrocytes remain poorly understood.

More recently, studies reported moderate effects of ERβ-ligands on modulating CNS resident and peripheral immune cells. Treatment with LY3201 ameliorated clinical EAE in SJL/J mice by reducing iNOS and NFkB expression on $Iba1^+$ microglia and T cells in the spinal cord (Wu et al., 2013). Indazoles and 5-androstene-3β,17β-diol (ADIOL) reduced pro-inflammatory iNOS, IL-1β, IL-6 and IL-23 expression in cultured glial cells, and provided EAE protection in an ERβ dependent manner (Saijo et al., 2011). In a subsequent study, indazole-Cl suppressed the peripheral immune system and prevented immune cell infiltration into the CNS during EAE (Moore et al., 2014). AC-186, an ERβ-ligand with a selectivity of approximately 830:1 over ERα (McFarland et al., 2013), prevented CNS infiltration of $CD45^+$ cells, specifically, $Iba1^+$ globoid macrophages (Itoh et al., 2017). Lastly, diarylpropionitrile (DPN), the most commonly used ERβ-ligand, reduced the ability of $CD11c^+CD11b^+$ DC in the CNS to produce TNFα and MHCII during EAE (Du et al., 2011). Together these studies showed that ERβ-ligand treatment modulates immune cells during EAE, but whether the treatment effects were mediated directly through ERβ on immune cells remained unknown.

1.6 Objectives

This dissertation examines the mechanisms of neuroprotection provided directly and indirectly through estrogen receptor specific ligands in two different demyelinating disease models for MS, EAE model and cuprizone model. I first investigated the indirect effects of ERα-ligand on neuroprotection aimed for alternative treatment strategies, as a chronic treatment of estradiol or ERα-ligands in humans may cause adverse effects. Previous studies have shown that ERα signaling on astrocytes reduced expression of chemokines CCL2. Interestingly, deletion of ERα selectively from astrocytes reversed ERα-ligand mediated reduction of astrocyte CCL2 expression, and subsequently, neuroprotection during EAE. These results suggested that targeting astrocyte's ability to downregulate CCL2 could be a promising approach for neuroprotective therapies. However, whether CCL2 expression on astrocytes has a significant role in EAE pathogenesis was unknown. To investigate this, I generated mice with CCL2 deleted specifically in astrocytes. (CHAPTER 2)

Next, I aimed to investigate the mechanisms ERβ-ligands on neuroprotection and remyelination, as they are proven to be safe in humans and have the potential to be developed as treatments for MS. However, the mechanisms underlying its effects on neuroprotection and remyelination remains poorly understood. Here I investigated the direct effects of ERβ-ligand treatment on $CD11c^+$ immune cells (myeloid dendritic cells and macrophages, DC/MΦ) and $Olig1^+$ oligodendrocytes in EAE, using mice with specific deletion of ERβ from each cell type (CHAPTER 3).

In the EAE model, studying neuroprotection and remyelination in oligodendrocytes is limited, as remyelination rarely occurs. Therefore, I used the cuprizone model for investigating molecular mechanisms of remyelination in oligodendrocytes. I first investigated transcriptional

changes in oligodendrocytes during remyelination to understand the natural process of remyelination in oligodendrocytes. Until now, the limitation to perform this type of investigation *in vivo* was obtaining oligodendrocyte specific transcripts without *ex vivo* manipulations and artifacts. The use of RiboTag technology allowed isolation of oligodendrocyte specific ribosome associated transcripts from whole tissue samples *in vivo*. Using the RiboTag mouse model and mice with specific deletion of ERβ on $Olig1^{+}$ oligodendrocytes, I investigated the treatment effects of ERβ-ligand on oligodendrocytes during remyelination after chronic demyelination (CHAPTER 4).

1.7 Bibliography

Blakemore WF. Observations on oligodendrocyte degeneration, the resolution of status spongiosus and remyelination in cuprizone intoxication in mice. J Neurocytol 1972; 1(4): 413-26.

Brambilla R, Persaud T, Hu X, Karmally S, Shestopalov VI, Dvoriantchikova G, et al. Transgenic inhibition of astroglial NF-kappa B improves functional outcome in experimental autoimmune encephalomyelitis by suppressing chronic central nervous system inflammation. J Immunol 2009; 182(5): 2628-40.

Compston A, Coles A. Multiple sclerosis. Lancet 2008; 372(9648): 1502-17.

Constantinescu CS, Farooqi N, O'Brien K, Gran B. Experimental autoimmune encephalomyelitis (EAE) as a model for multiple sclerosis (MS). Br J Pharmacol 2011; 164(4): 1079-106.

Crawford DK, Mangiardi M, Song B, Patel R, Du S, Sofroniew MV, et al. Oestrogen receptor beta ligand: a novel treatment to enhance endogenous functional remyelination. Brain 2010; 133(10): 2999-3016.

Du S, Sandoval F, Trinh P, Umeda E, Voskuhl R. Estrogen receptor-beta ligand treatment modulates dendritic cells in the target organ during autoimmune demyelinating disease. Eur J Immunol 2011; 41(1): 140-50.

Giraud SN, Caron CM, Pham-Dinh D, Kitabgi P, Nicot AB. Estradiol inhibits ongoing autoimmune neuroinflammation and NFkappaB-dependent CCL2 expression in reactive astrocytes. Proc Natl Acad Sci U S A 2010; 107(18): 8416-21.

Gudi V, Gingele S, Skripuletz T, Stangel M. Glial response during cuprizone-induced de- and remyelination in the CNS: lessons learned. Front Cell Neurosci 2014; 8: 73.

Itoh N, Kim R, Peng M, DiFilippo E, Johnsonbaugh H, MacKenzie-Graham A, et al. Bedside to bench to bedside research: Estrogen receptor beta ligand as a candidate neuroprotective treatment for multiple sclerosis. J Neuroimmunol 2017; 304: 63-71.

Khalaj AJ, Yoon J, Nakai J, Winchester Z, Moore SM, Yoo T, et al. Estrogen receptor (ER) beta expression in oligodendrocytes is required for attenuation of clinical disease by an ERbeta ligand. Proc Natl Acad Sci U S A 2013; 110(47): 19125-30.

Kim RY, Hoffman AS, Itoh N, Ao Y, Spence R, Sofroniew MV, et al. Astrocyte CCL2 sustains immune cell infiltration in chronic experimental autoimmune encephalomyelitis. J Neuroimmunol 2014; 274(1-2): 53-61.

Kumar S, Patel R, Moore S, Crawford DK, Suwanna N, Mangiardi M, et al. Estrogen receptor beta ligand therapy activates PI3K/Akt/mTOR signaling in oligodendrocytes and promotes remyelination in a mouse model of multiple sclerosis. Neurobiol Dis 2013; 56: 131-44.

Lelu K, Laffont S, Delpy L, Paulet PE, Perinat T, Tschanz SA, et al. Estrogen receptor alpha signaling in T lymphocytes is required for estradiol-mediated inhibition of Th1 and Th17

cell differentiation and protection against experimental autoimmune encephalomyelitis. J Immunol 2011; 187(5): 2386-93.

Mason JL, Toews A, Hostettler JD, Morell P, Suzuki K, Goldman JE, et al. Oligodendrocytes and progenitors become progressively depleted within chronically demyelinated lesions. Am J Pathol 2004; 164(5): 1673-82.

Matsushima GK, Morell P. The neurotoxicant, cuprizone, as a model to study demyelination and remyelination in the central nervous system. Brain Pathol 2001; 11(1): 107-16.

McFarland K, Price DL, Davis CN, Ma JN, Bonhaus DW, Burstein ES, et al. AC-186, a selective nonsteroidal estrogen receptor beta agonist, shows gender specific neuroprotection in a Parkinson's disease rat model. ACS Chem Neurosci 2013; 4(9): 1249-55.

Mechelli R, Annibali V, Ristori G, Vittori D, Coarelli G, Salvetti M. Multiple sclerosis etiology: beyond genes and environment. Expert Rev Clin Immunol 2010; 6(3): 481-90.

Moore SM, Khalaj AJ, Kumar S, Winchester Z, Yoon J, Yoo T, et al. Multiple functional therapeutic effects of the estrogen receptor beta agonist indazole-Cl in a mouse model of multiple sclerosis. Proc Natl Acad Sci U S A 2014; 111(50): 18061-6.

Morales LB, Loo KK, Liu HB, Peterson C, Tiwari-Woodruff S, Voskuhl RR. Treatment with an estrogen receptor alpha ligand is neuroprotective in experimental autoimmune encephalomyelitis. J Neurosci 2006; 26(25): 6823-33.

Morell P, Barrett CV, Mason JL, Toews AD, Hostettler JD, Knapp GW, et al. Gene expression in brain during cuprizone-induced demyelination and remyelination. Mol Cell Neurosci 1998; 12(4-5): 220-7.

Nilsson S, Koehler KF, Gustafsson JA. Development of subtype-selective oestrogen receptor-based therapeutics. Nat Rev Drug Discov 2011; 10(10): 778-92.

Paterni I, Granchi C, Katzenellenbogen JA, Minutolo F. Estrogen receptors alpha (ERalpha) and beta (ERbeta): subtype-selective ligands and clinical potential. Steroids 2014; 90: 13-29.

Plemel JR, Liu WQ, Yong VW. Remyelination therapies: a new direction and challenge in multiple sclerosis. Nat Rev Drug Discov 2017; 16(9): 617-34.

Prokai L, Nguyen V, Szarka S, Garg P, Sabnis G, Bimonte-Nelson HA, et al. The prodrug DHED selectively delivers 17beta-estradiol to the brain for treating estrogen-responsive disorders. Sci Transl Med 2015; 7(297): 297ra113.

Saijo K, Collier JG, Li AC, Katzenellenbogen JA, Glass CK. An ADIOL-ERbeta-CtBP transrepression pathway negatively regulates microglia-mediated inflammation. Cell 2011; 145(4): 584-95.

Samantaray S, Sribnick EA, Das A, Thakore NP, Matzelle D, Yu SP, et al. Neuroprotective efficacy of estrogen in experimental spinal cord injury in rats. Ann N Y Acad Sci 2010; 1199: 90-4.

Skripuletz T, Gudi V, Hackstette D, Stangel M. De- and remyelination in the CNS white and grey matter induced by cuprizone: the old, the new, and the unexpected. Histol Histopathol 2011; 26(12): 1585-97.

Spence RD, Hamby ME, Umeda E, Itoh N, Du S, Wisdom AJ, et al. Neuroprotection mediated through estrogen receptor-alpha in astrocytes. Proc Natl Acad Sci U S A 2011; 108(21): 8867-72.

Spence RD, Voskuhl RR. Neuroprotective effects of estrogens and androgens in CNS inflammation and neurodegeneration. Front Neuroendocrinol 2012; 33(1): 105-15.

Spence RD, Wisdom AJ, Cao Y, Hill HM, Mongerson CR, Stapornkul B, et al. Estrogen mediates neuroprotection and anti-inflammatory effects during EAE through ERalpha

signaling on astrocytes but not through ERbeta signaling on astrocytes or neurons. J Neurosci 2013; 33(26): 10924-33.

Steinman L. Multiple sclerosis: a coordinated immunological attack against myelin in the central nervous system. Cell 1996; 85(3): 299-302.

Suzuki K, Kikkawa Y. Status spongiosus of CNS and hepatic changes induced by cuprizone (biscyclohexanone oxalyldihydrazone). Am J Pathol 1969; 54(2): 307-25.

Tiwari-Woodruff S, Morales LB, Lee R, Voskuhl RR. Differential neuroprotective and antiinflammatory effects of estrogen receptor (ER)alpha and ERbeta ligand treatment. Proc Natl Acad Sci U S A 2007; 104(37): 14813-8.

Voskuhl R. Preclinical studies of sex differences: a clinical perspective. Biol Sex Differ 2016; 7: 7.

Wu WF, Tan XJ, Dai YB, Krishnan V, Warner M, Gustafsson JA. Targeting estrogen receptor beta in microglia and T cells to treat experimental autoimmune encephalomyelitis. Proc Natl Acad Sci U S A 2013; 110(9): 3543-8.

Wujek JR, Bjartmar C, Richer E, Ransohoff RM, Yu M, Tuohy VK, et al. Axon loss in the spinal cord determines permanent neurological disability in an animal model of multiple sclerosis. J Neuropathol Exp Neurol 2002; 61(1): 23-32.

CHAPTER 2

Astrocytes CCL2 sustains inflammation in chronic EAE

: a lesson from ERα-ligand treatment effects on astrocytes.

2.1 Introduction

Inflammation characterizes many disorders of the central nervous system (CNS), including neurodegenerative, traumatic and autoimmune disorders. In neurodegenerative and traumatic disorders, CNS inflammation is locally restricted and tends to resolve over time (Bush et al., 1999; Schnell et al., 1999; Donnelly and Popovich, 2008). In contrast, in autoimmune disorders, CNS inflammation is widespread and continuous or recurring (Raine et al., 1980; Lucchinetti et al., 2000; McFarland and Martin, 2007). Understanding which molecule on which cell regulates the continuous influx of inflammatory cells into the CNS during autoimmune disease is central to the developing treatment strategies aiming for neuroprotection.

Astrocytes are intimately associated with and signal to blood vessels (Iadecola and Nedergaard, 2007) and are recognized as playing essential roles in regulating leukocyte trafficking and inflammation in the CNS. They produce a wide variety of pro-inflammatory chemokines and cytokines, as well as reactive oxygen species (ROS) *in vitro*, consistent with a pro-inflammatory role (Dong and Benveniste, 2001; Chen and Swanson, 2003; Farina et al., 2007; Nair et al., 2008). Conversely, astrocytes also produce anti-inflammatory cytokines and ROS scavengers, thereby suggesting a role in mitigating inflammation (Aloisi et al., 1997; Dong and Benveniste, 2001; Dringen and Hirrlinger, 2003; Nair et al., 2008). Astrocytes have been implicated *in vivo* in locally triggering innate pro-inflammatory responses after CNS trauma and stroke (Farina et al., 2007). On the other hand, scar-forming reactive astrocytes form essential

barriers that restricted leukocyte migration from areas of damaged tissue into neighboring healthy tissue (Bush et al., 1999; Faulkner et al., 2004; Myer et al., 2006; Okada et al., 2006; Herrmann et al., 2008; Li et al., 2008). Thus, astrocytes are thought to play complex roles in regulating leukocyte trafficking in the CNS (John et al., 2005). Reactive astrocytosis is a prominent feature of chronic inflammation of the CNS during EAE and MS (Eng et al., 1970; Liedtke et al., 1998; Eng et al., 2000). Transgenically targeted ablation of proliferating, scar-forming reactive astrocytes during EAE revealed loss of astrocyte barrier function resulting in widespread inflammation and worsening of EAE outcomes (Voskuhl et al., 2009).

Chemokine (C-C motif) ligand 2 (CCL2) is a chemokine initially identified as monocyte chemoattractant protein-1 (MCP-1). Upon tissue specific expression of CCL2, it can attract macrophages, T cells, dendritic cells, mast cells and basophils to tissue sites (Rollins et al., 1991, 1997). CCL2 expression in the CNS occurs during chronic relapsing EAE, with higher CCL2 expression correlating with relapses, and antibody mediated blocking decreasing disease severity and reducing macrophage infiltration (Kennedy et al., 1998). Global knockouts of CCL2 (Huang et al., 2001) and its receptor CCR2 (Fife et al., 2000) were resistant to EAE induction. Adoptive transfer of encephalitogenic cells that were devoid of CCL2 induced EAE in wild type recipients showing that CCL2 expression in the peripheral immune induction phase was not required. However, EAE was suppressed when recipients of adoptively transferred wild type encephalitogenic cells were devoid of CCL2, thereby showing that CCL2 expression in the recipient was required for disease. CCL2 expression in the recipient could be required either in the recipient's CNS or peripheral immune cells recruited during disease (Fife et al., 2000). Bone marrow chimeras using global CCL2 gene deletion separated out effects of CCL2 in the immune system versus the CNS. Specifically, CCL2 expression in the reconstituted immune system was

not necessary for active EAE induction in chimeras, while CCL2 expression in the engrafted recipient was required (Dogan et al., 2008). Together these reports showed that CCL2 expression in a CNS cell is central to chronic EAE pathogenesis, which remains unknown.

In this study, we have ascertained whether CCL2 expression in astrocytes may be critical to EAE pathogenesis. We have created a conditional knock out of CCL2 in astrocytes and asked whether this affects the clinical course, focal macrophage and T cell infiltration, diffuse activation of astrocytes and microglial cells, as well as axonal and myelin loss during EAE.

2.2 Results

2.2.1 Verification of the GFAP-cre line

To target the deletion of CCL2 in astrocytes, we used a well characterized mGFAP-Cre line previously shown to target Cre activity selectively in astrocytes in the CNS (Herrmann et al., 2008; Spence et al., 2011, 2013). This mGFAP-Cre line targets 98% of all astrocytes in the spinal cord, the tissue evaluated in this study, with no targeting of other cells, such as oligodendrocytes, microglia, and neurons (Herrmann et al., 2008). We confirmed the specific targeting of Cre activity to essentially all astrocytes and only to astrocytes in the spinal cord of healthy, untreated young adult mice of this transgenic line by showing complete overlap in the expression of GFAP with the highly sensitive reporter protein tdTomato whose expression requires Cre expression activity (Figure 2.1).

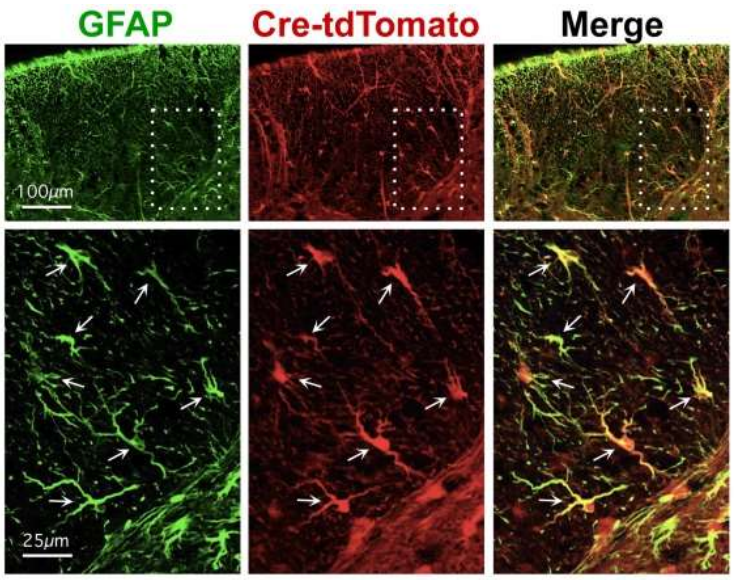

Figure 2.1 Verification of extent and selectivity of Cre targeting to astrocytes. Immunofluorescence shows complete GFAP (green) with tdTomato reporter protein (red) in healthy, untreated young adult mice mGFAP-Cre-tdTomato reporter mice. Merged images ($GFAP^+$ tdTomato) show co-localization in yellow. Survey images (top row) show dorsal column white matter. Scale bar, 100 μm. Boxed areas indicate areas shown in detail below. Scale bar, 25 μm. Arrows indicate double-labeled astrocytes. All detectable astrocytes express both GFAP and tdTomato.

2.2.2 Validation of CCL2 deletion in astrocytes

We then crossed mGFAP-Cre mice with $CCL2^{floxed/floxed}$ mice ($CCL2^{fl/fl}$ mice) to generate mice with astrocyte specific conditional knockout of CCL2 (CCL2-CKO) and wildtype littermate controls (CCL2-WT) (Shi et al., 2011). To confirm the selectivity of CCL2 deletion in astrocytes during EAE, we assessed CCL2 expression by immunohistochemistry using double staining for CCL2 (green) and GFAP (red). Genetically unmanipulated C57BL/6 control mice with EAE exhibited readily detectable immunoreactive CCL2, with some colocalization of CCL2 with

GFAP and some CCL2 not colocalizing with GFAP (Figure 2.2A, top row), thereby demonstrating CCL2 expression both in astrocytes as well as in other cells during EAE. In contrast, CCL2-CKO mice with EAE no longer showed co-localization of CCL2 with GFAP, as CCL2 staining limited to non-GFAP staining cells (Figure 2.2A, middle row). CCL2-CKO littermate CCL2-WT mice with EAE (Figure 2.2A, bottom row) were the same as C57BL/6 mice with EAE (Figure 2.2A, top row). CCL2 staining in dorsal column of thoracic spinal cord confirmed that deletion of CCL2 from astrocytes in our CCL2-CKO mice resulted in the overall partial deletion of CCL2 in cord during EAE (Figure 2.2B,C). Specifically, CCL2-CKO mice had removal of CCL2 from astrocytes, but not other cells, during EAE.

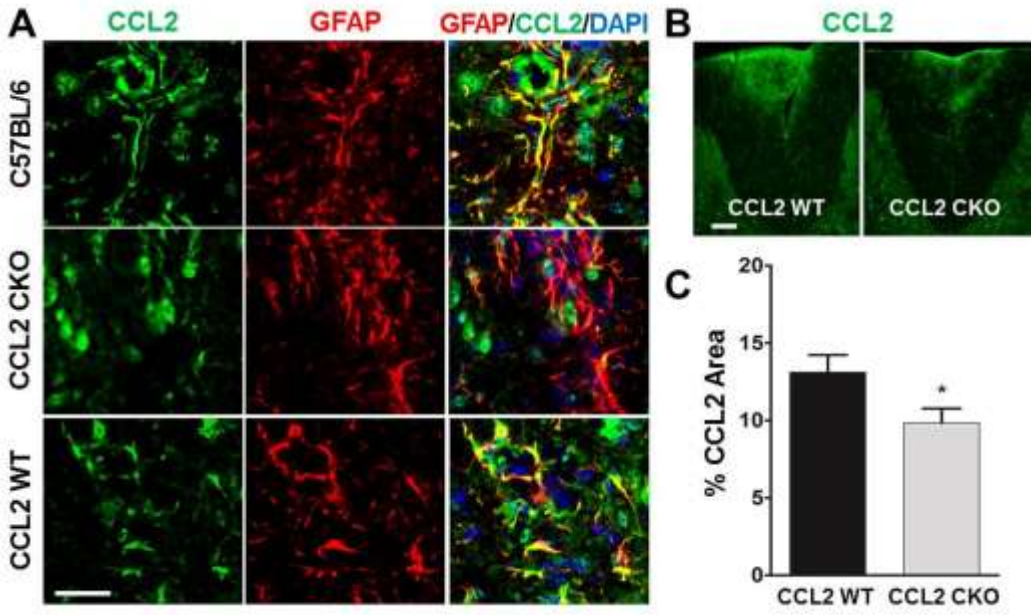

Figure 2.2 Validation of CCL2 deletion specificity in GFAP$^+$ astrocytes during EAE. (A) Immunofluorescence shows co-localization of CCL2 (green) with GFAP (red) in C57BL/6 wildtype (top row) and CCL2 wildtype littermate controls (CCL2-WT bottom row), but not in mice with astrocyte CCL2 conditional gene deletion (CCL2-CKO middle row) during EAE.

Merged images ($GFAP^+CCL2^+$) show co-localization in yellow. Scale bar, 20 μm. **(B)** Immunofluorescence shows significantly reduced CCL2 expression in the spinal cord dorsal column of CCL2-CKO mice compared to CCL2-WT mice during EAE. Scale bar, 100 μm. **(C)** Quantification shows reduced % CCL2 expression area in the spinal cord dorsal column of CCL2-CKO mice. *$p < 0.05$ versus CCL2-WT (mean ± SEM).

2.2.3 CCL2 deletion from astrocytes provides clinical disease protection late during EAE

To determine whether CCL2 from astrocytes play a role in EAE, we compared standard EAE clinical scores in CCL2-CKO versus CCL2-WT littermates. CCL2-CKO mice had significantly less severe EAE late in the disease while having a similar incidence and severity of disease at onset (Figure 2.3). This result showed a role for CCL2 from astrocytes in mechanisms related to disease progression, but not in acute disease onset.

A

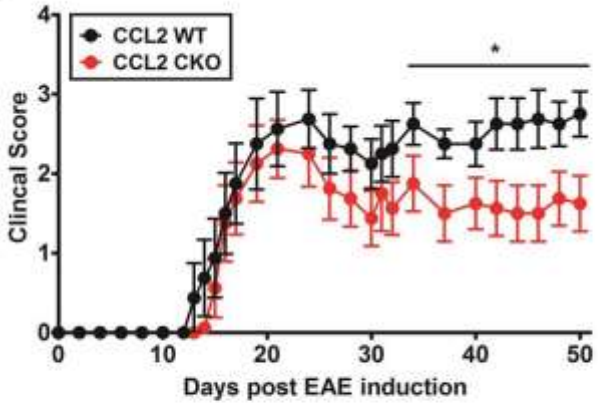

B *Summary of EAE experiments*

	Group	Incidence[a]	Mean Day of Onset[b]	Mean Peak Clinical Score[c]	Cumulative Disease Index (All days)[d]	Cumulative Disease Index (After Day 30)[d]
1	WT	4/5	13.0 ± 0.8	3.4 ± 0.5	55.2 ± 34.0	21.1 ± 13.7
	CKO	7/7	15.6 ± 1.0 *	2.2 ± 0.9 *	24.5 ± 20.0	5.9 ± 6.6 *
2	WT	8/8	16.0 ± 3.3	3.4 ± 0.7	88.4 ± 31.8	51.1 ± 14.1
	CKO	8/8	16.3 ± 2.1	2.4 ± 0.8 *	62.8 ± 35.0	33.4 ± 18.4 *
3	WT	5/5	16.6 ± 2.1	2.7 ± 0.3	76.1 ± 12.7	46.3 ± 5.4
	CKO	8/8	16.0 ± 2.4	2.3 ± 1.0	56.1 ± 38.8	30.1 ± 18.6 †

Figure 2.3 Astrocyte CCL2-CKO, as compared to CCL2-WT, has less severe EAE late in the disease. (A) CCL2-CKO mice had significantly better clinical EAE scores late (after EAE day 30) compared with CCL2-WT mice. *$p < 0.05$ (repeated-measures ANOVA with post hoc Bonferroni analysis). **(B)** The table is showing clinical assessments in three separate experiments. [a]Incidence is the number of mice that developed EAE signs from the total number of mice in each group. [b]Mean day of onset (±SEM) was assessed when mice showed first clinical disease signs (score of >1) after EAE induction. [c]Mean peak clinical score (±SEM) was assessed when each mouse reached its maximum clinical score. [d]Cumulative disease index (±SEM) was calculated by summing the daily clinical scores of each mouse and averaging them within each

group. “All days” signifies all the days of EAE, while “After Day 30” is from day 30 of EAE until end of the experiment. *$p < 0.05$, †$p < 0.08$ versus CCL2-WT (mean ± SEM).

2.2.4 CCL2 deletion from astrocytes reduces macrophage and T cell infiltration during EAE

To understand how CCL2 in astrocytes may affect the progression of EAE, we sacrificed mice during late disease and assessed immune cell infiltrates by immunofluorescence using a T lymphocyte marker (anti-CD3) and macrophage marker (anti-Iba1). To identify macrophages, distinct from microglia, we used immunohistochemistry for Iba1 and counted cells with a globoid shape, as previously described (Voskuhl et al., 2009). We found that CCL2-CKO mice, compared to CCL2-WT littermate controls, had a significant reduction in both macrophage and T cell infiltrates in both the dorsal and ventrolateral white matter of spinal cords (Figure 2.4). Representative images of CCL2-CKO and CCL2-WT EAE mice showed the differences in infiltrates with anti-Iba-1 (arrowhead) and anti-CD3 (arrow) staining (Figure 2.4A,B), while quantitative analysis confirmed the significant reduction of macrophages (Figure 2.4C) and T cells (Figure 2.4D) in CCL2-CKO mice. These results showed a role for CCL2 in astrocytes in recruiting macrophages and T cells to the CNS during progressive EAE.

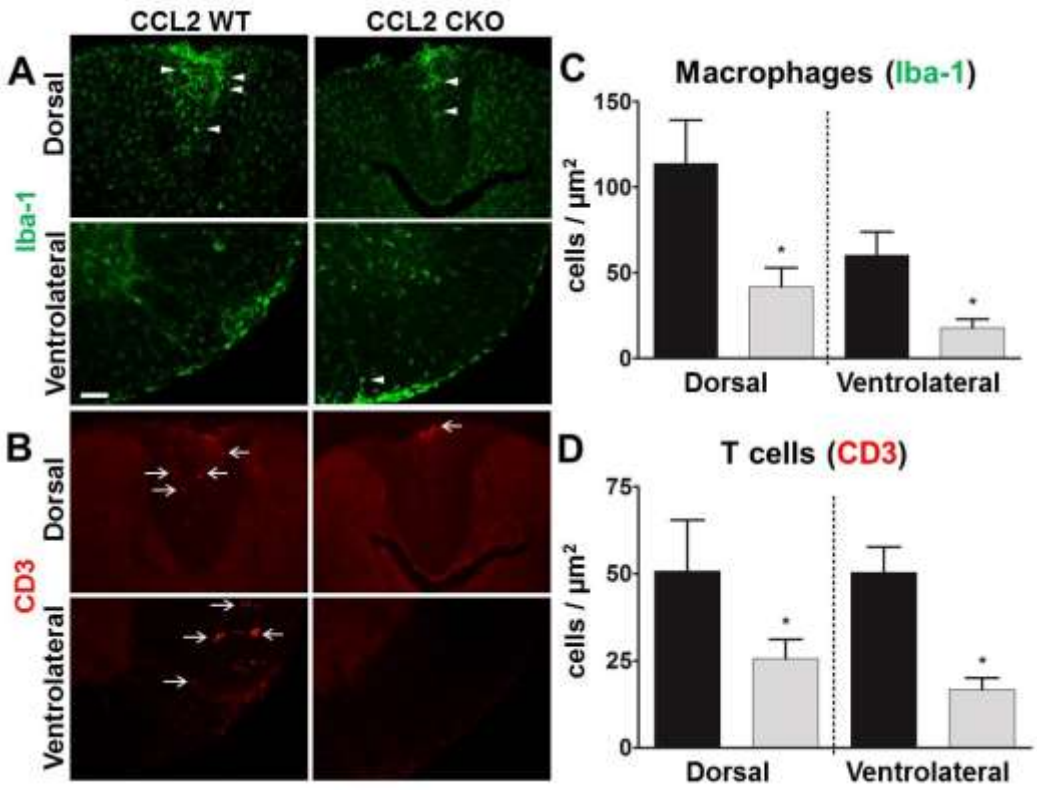

Figure 2.4 Astrocyte CCL2-CKO mice with EAE have a reduction in macrophage and T cell infiltrates during EAE. Representative immunofluorescence images of **(A)** Iba-1 (green) globoid macrophage (arrowhead) and **(B)** CD3 (red) T cell (arrow) infiltrates, each reduced in the dorsal (top rows) and ventrolateral (bottom rows) white matter of spinal cords during EAE. Scale bar, 100 µm. Quantitative analysis shows that CCL2-CKO mice have a significant reduction in **(C)** Iba-1 globoid macrophages and **(D)** CD3 T cells in the dorsal and ventrolateral white matter of the spinal cord during EAE. *$p < 0.05$ versus CCL2-WT (mean ± SEM).

2.2.5 CCL2 deletion from astrocytes reduces activation of astrocytes and microglial during EAE

Astrocytes are known to become reactive and increase in number, not only in focal lesions but also diffusively in both white and gray matter throughout the CNS during EAE (Liedtke et al.,

1998; Voskuhl et al., 2009). Also, microglial cells are known to change their morphology to a more ramified state and increase in number diffusely during EAE (Rasmussen et al., 2007). Thus, we next went beyond classic focal white matter lesions containing macrophage and T cell infiltrates to assess a role for CCL2 in astrocytes on diffuse glial activation in both white and gray matter of spinal cords during progressive EAE. CCL2-CKO mice showed a significant reduction in reactive astrocytes as compared to CCL2-WT littermates in white matter and gray matter (Figure 2.5). Also, less ramified/activated microglia was observed when comparing CCL2-CKO versus CCL2-WT littermates with EAE, and quantitative analysis showed fewer microglia in both white and gray matter of the spinal cords of CCL2-CKO EAE mice compared to CCL2-WT mice (Figure 2.6). Together these results demonstrated a role of CCL2 in astrocytes on diffuse glial activation in the CNS during progressive EAE.

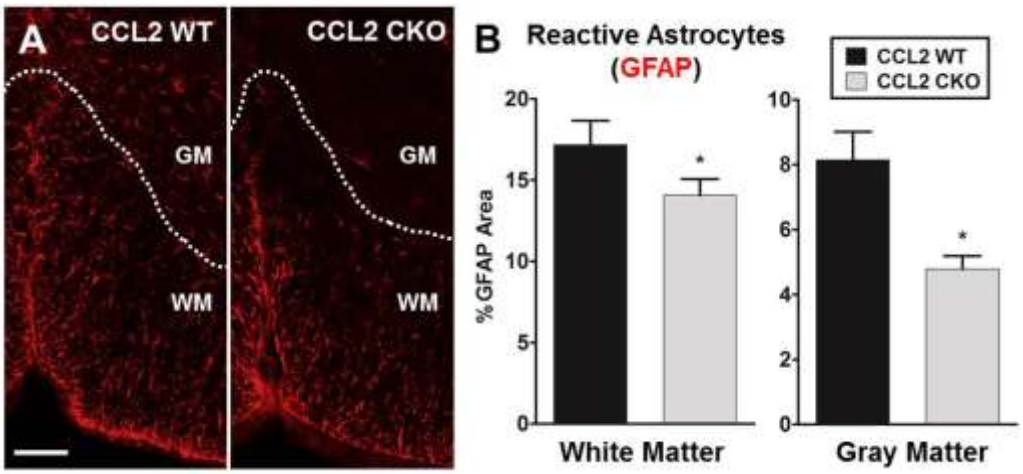

Figure 2.5 Selective deletion of CCL2 from astrocytes results in less activation of astrocytes diffusively in the spinal cords during EAE. (A) Representative immunofluorescence images show that CCL2-CKO mice have less reactive $GFAP^+$ astrocytes (red) in the gray matter (GM) and white matter (WM) of the spinal cord compared to CCL2-WT mice during EAE. Scale bar,

100 μm. **(B)** Quantitative analysis shows that CCL2-CKO mice have a significant reduction of GFAP expression in both white and gray matter of the spinal cord compared to CCL2-WT. *p < 0.05 versus CCL2-WT (mean ± SEM).

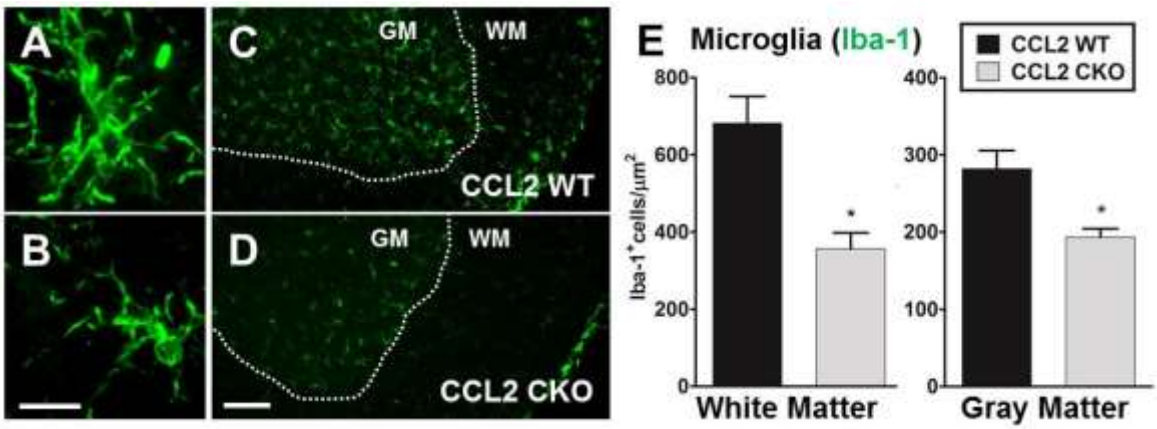

Figure 2.6 Selective deletion of CCL2 from astrocytes results in less microglial activation diffusively in the spinal cords during EAE. Representative immunofluorescence image of **(A)** activated and **(B)** resting microglial cells using Iba1 staining (green). Scale bar, 10 μm. **(C and D)** CCL2-CKO mice show a reduced number of ramified/activated microglial cells in white matter (WM) and gray matter (GM) of the spinal cord compared to CCL2-WT mice during EAE. Scale bar, 100 μm. **(E)** Quantitative analysis confirms that CCL2-CKO mice have reduced activated microglial cells in the white and gray matter of the spinal cord during EAE. *p < 0.05 versus CCL2-WT (mean ± SEM).

2.2.6 CCL2 deletion from astrocytes preserves myelin and protects against axonal loss during EAE

We evaluated EAE neuropathology, namely demyelination and axonal loss in spinal cord white matter, using immunofluorescence staining with anti-myelin basic protein (MBP) and anti-

neurofilament (NF200) antibody staining, respectively. CCL2-CKO mice with EAE had more myelin (green) and more axonal (red) staining as compared to CCL2-WT littermates with EAE (Figure 2.7A,B). Quantitative analysis of myelin (Figure 2.7C) and axons (Figure 2.7D) confirmed the significant preservation myelin and axons in CCL2-CKO spinal cords as compared to CCL2-WT. These results are consistent with differences in EAE clinical scores of CCL2-CKO mice versus WT (Figure 2.3) since axonal loss has been shown to correlate with clinical disease severity (Wujek et al., 2002). Together, these results confirm the functional significance of CCL2 in astrocytes during the later progressive phase of EAE.

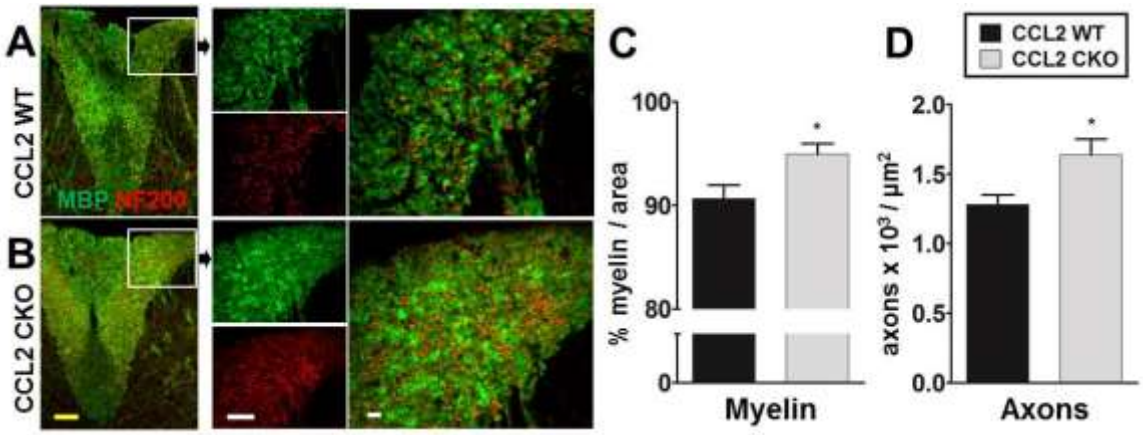

Figure 2.7 Astrocyte CCL2-CKO, as compared to CCL2-WT littermates, has less demyelination and axonal loss during EAE. (A and B) Immunofluorescence images of MBP^+ myelin (green) and $NF200^+$ axon (red) in the spinal cord dorsal column of CCL2-CKO and CCL2-WT mice induced with EAE. Left images show the entire dorsal column of the spinal cord, with images in boxes shown in higher magnification. CCL2-CKO, compared to CCL2-WT, has more myelin and axons in the dorsal column shown in individual (left) and merged (right) images. Scale bars; yellow, 100 µm: white, 20 µm. Quantitative analysis shows that CCL2-CKO

mice have more **(C)** myelin and **(D)** axons in the dorsal column of the spinal cord compared to CCL2-WT mice during EAE. *$p < 0.05$ versus CCL2-WT (mean ± SEM).

2.2.7 CCL2 deletion from astrocytes did not affect early EAE

Lastly, given our findings of effects of CCL2 on astrocytes during late EAE, we ascertained whether such effects might also be observed early during EAE. Thus, in additional experiments, mice were sacrificed early in EAE, before clinical disease scores began to differ between CCL2-CKO and CCL2-WT littermates, and assessed for potential differences in the immune cell (T cell and macrophage) infiltrates, diffuse glial (astrocytes and microglia), demyelination and axonal loss. In contrast to differences observed at late in EAE, such differences were not found early (Figure 2.8). This result revealed that effects of CCL2 in astrocytes that were observed late in EAE were not merely secondary to early differences, but rather were due to effects of CCL2 in astrocytes during late disease, which is consistent with our conclusion that CCL2 in astrocytes is essential for T cell and macrophage infiltration into the CNS during the late chronic phase of the disease.

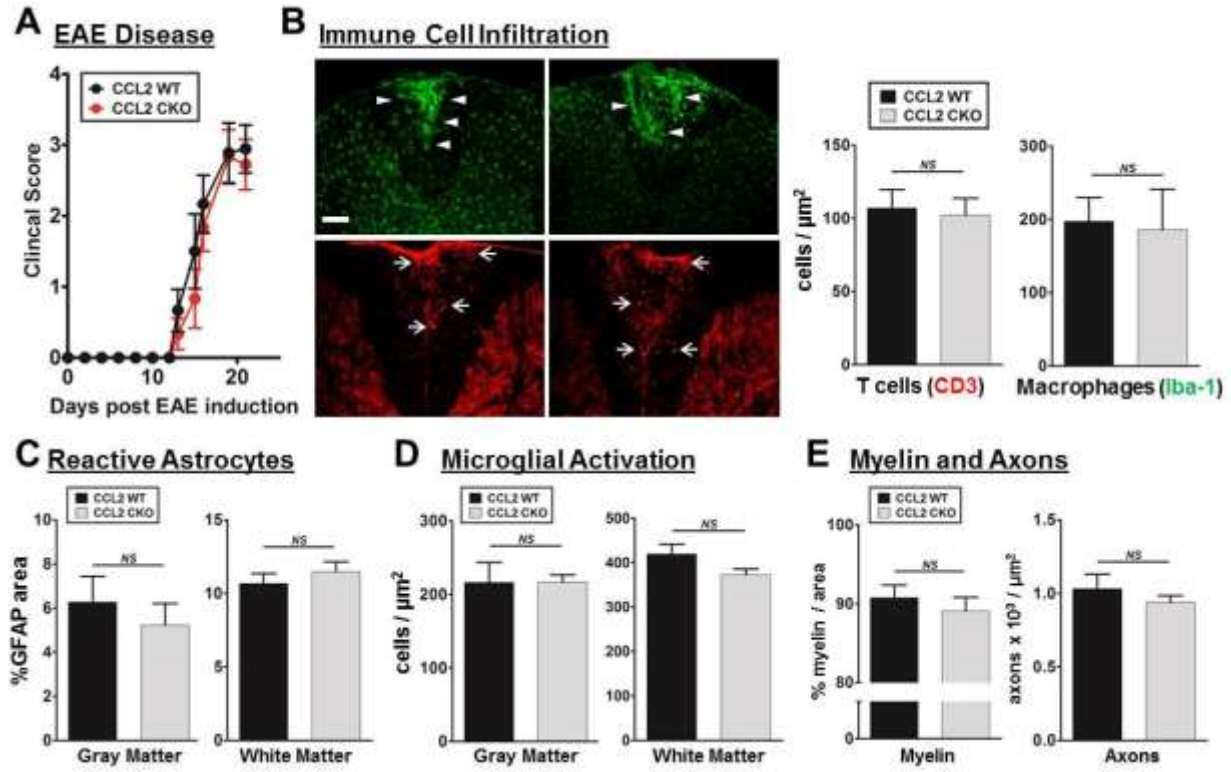

Figure 2.8 No differences were found between CCL2-CKO mice as compared to CCL2-WT littermates during the early phase of EAE. (A) CCL2-CKO mice have similar clinical disease scores as CCL2-WT mice early during EAE. **(B)** Representative immunofluorescence images and quantitative analysis show that CCL2-CKO and CCL2-WT have similar levels of Iba-1 (green) globoid macrophage (arrowhead) and CD3 (red) T cell (arrow) infiltrates in the spinal cord dorsal column. Scale bar, 100 µm. Quantitative analyses confirm that CCL2-CKO mice and CCL2-WT mice have similar levels of diffuse activation of **(C)** reactive astrocytes and **(D)** activated microglial cells in the white and gray matter of the spinal cord early during EAE. Quantitative analyses show that CCL2-CKO mice and CCL2-WT mice have similar levels of myelin and axons in the dorsal column of the spinal cord.

2.3 Discussion

By selectively removing CCL2 from astrocytes, we found that CCL2 expression in astrocytes is functionally significant during EAE. It plays a role in focal macrophage and T cell infiltration in spinal cord white matter as well as diffuse activation of astrocytes and microglia in both white and gray matter, consistent with the more severe EAE clinical scores, demyelination and axonal loss observed in wild type littermates compared to CCL2-CKOs.

Seminal work on the critical role of CCL2 in the pathogenesis of EAE was done by the Ransohoff group (Huang et al., 2001) and the Karpus group (Kennedy et al., 1998; Fife et al., 2000; Dogan et al., 2008). While originally, CCL2 was thought to be involved in the generation of encephalitogenic immune responses primarily, their elegant work involving knockouts during adoptive EAE, as well as induction of active EAE in bone marrow chimeras, together with revealed that CNS expression of CCL2 was critical in mediating macrophage and T cell infiltrates during EAE. Specifically, CCL2 production from resident CNS was thought to contribute to the recruitment of myeloid dendritic cells and macrophages expressing TNFα and iNOS during EAE (Dogan et al., 2008). Until now, the CNS resident cell with functionally significant CCL2 expression during EAE has remained unknown. Here, we created mice with a specific deletion of CCL2 in astrocytes and showed effects on the recruitment of macrophages and T cells to the CNS during EAE, thereby showing functional significance of CCL2 expression by astrocytes in mediating inflammation. This is consistent with previous reports showing a correlation between higher astrocyte CCL2 expression and worse disease severity in a variety of CNS injury models (Brambilla et al., 2005; Conductier et al., 2010; Carrillo-de Sauvage et al., 2012; Hamby et al., 2012), and that CCL2 is expressed in astrocytes surrounding lesions in MS patients (McManus et al., 1998; Simpson et al., 1998). That said, our finding of a role for

CCL2 in astrocytes is not mutually exclusive of an additional role for CCL2 in other CNS resident cells. Indeed, we found that CCL2-CKO mice had reduced EAE severity late in disease while having a similar incidence and severity of disease at onset as compared to wild type (CCL2-WT) control littermates. In this context it is important to note that our analysis of reporter gene expression demonstrates Cre-recombinase activity in essentially all spinal cord astrocytes in healthy, uninjured young adult mGFAP-Cre transgenic mice, indicating that CCL2 mediated deletion from astrocytes would have occurred before the onset of EAE. Given previous reports that global CCL2 knockouts were resistant to disease induction (Fife et al., 2000), together this may suggest that CCL2 on astrocytes is critical to ongoing, continuing inflammation late in chronic EAE, while CCL2 expression on other CNS resident cells, such as endothelial cells (Berman et al., 1996; dos Santos et al., 2005; Ge et al., 2009), may be needed in initial early inflammatory processes at disease onset. Distinguishing between earlier versus later inflammatory mechanisms may be essential in developing the most appropriate treatment strategies for various phases of MS.

Reactive astrocytosis producing NFkappaB (NFκB)-dependent pro-inflammatory molecules including CCL2 are thought to play a role in continued inflammation and secondary injury processes not only in EAE and MS but also in other neurological disorders. This neuroinflammatory pathway may be therefore an important mechanism to target with candidate neuroprotective treatments. Indeed, the mechanism of estradiol as a neuroprotective treatment involves this neuroinflammatory pathway. Initially, estradiol treatment was shown to reduce EAE clinical disease severity and decrease CNS inflammation through its effects on peripheral immune responses, with global estrogen receptor (ER)α knockouts and selective ERα ligand treatments showing that this was mediated through ERα (Liu et al., 2003; Polanczyk et al., 2003;

Morales et al., 2006). Astrocytes were then shown to be a direct target of ERα ligand treatment using conditional deletion of ERα selectively removed from astrocytes. Mice with astro-ERα-CKO exhibited significantly reduced estrogen mediated clinical disease protection and less CNS anti-inflammatory effects (Spence et al., 2011) as well as complete loss of the estrogen mediated reduction in astrocyte CCL2 expression (Spence et al., 2013). Another complementary study showed that ERα ligand treatment ameliorated EAE and reduced astrocyte CCL2 production *in vivo* and inhibited TNFα induced CCL2 expression in vitro with direct suppression of NFκB recruitment to the CCL2 enhancer (Giraud et al., 2010). Finally, in both spinal cord injury and EAE, selective inactivation of NFκB in astrocytes lead to an improvement in clinical outcomes, with less white matter injury and reduced expression of pro-inflammatory chemokines and cytokines including CCL2 (Brambilla et al., 2005, 2009). Together these reports reinforce the conclusion that a promising approach for neuroprotective therapies would be to target the astrocyte's ability to upregulate CCL2 and other chemokines.

Designing neuroprotective treatments for neurological disorders is particularly challenging since many molecules, including chemokines, are expressed in the CNS, the immune system and other organ systems (Ransohoff, 2009). Thus, targeting specific molecules in the CNS can be confounded by off target binding with unexpected results. Targeting specific CNS cells is complicated by the various roles that a given cell may have during a disease process. Depending on the condition and the timing, astrocytes may have pro- or anti-inflammatory effects as well as neuroprotective effects mediated through glutamate uptake or neurotrophic factor production (Anderson et al., 2014; Sofroniew et al., 2014). In the MS model, EAE, CCL2 on astrocytes plays a role in attracting immune cell infiltrates to form CNS lesions, while the barrier function of scar forming astrocytes prevents focal inflammation from becoming

widespread (Voskuhl et al., 2009). Thus, the challenge of future neurotherapeutics will be to design both molecule specific and cell specific treatments to be delivered at the optimal phase of an evolving disease process.

2.4 Methods and materials

Animals CCL2 conditional gene deletion or knockouts (CKO) from astrocytes (CCL2-CKO) were generated by crossing transgenic mice that express Cre-recombinase under regulation of the mouse glial fibrillary acid protein (mGFAP) promoter, mGFAP-Cre line 73.12 (Herrmann et al., 2008), with mice carrying a *Ccl2* gene flanked by *loxP* sites ($CCL2^{fl/fl}$) (Shi et al., 2011). The $CCL2^{fl/fl}$ was a generous gift from Professor Eric G. Pamer (Sloan-Kettering Institute for Cancer Research). Reporter mice were generated by crossing mGFAP-Cre line 73.12 with transgenic mice harboring ROSA-tdTomato under the regulation of a *loxP*-flanked STOP cassette (JAX, Bar Harbor, ME). Animals were maintained under standard conditions in a 12 h dark/light cycle with access to food and water ad libitum. All procedures were done in accordance to the guidelines of the National Institutes of Health and the Chancellor's Animal Research Committee of the University of California, Los Angeles Office for the Protection of Research Subjects.

Active EAE induction and clinical scoring CCL2-CKO and littermate control (CCL2-WT) mice were immunized subcutaneously with myelin oligodendrocyte glycoprotein (MOG), amino acids 35–55 (200 μg/animal, American Peptides) emulsified in Complete Freund's Adjuvant, supplemented with Mycobacterium Tuberculosis H37Ra (400 μg/animal, Difco Laboratories), over two sites drained by left inguinal and auxiliary lymph nodes in a total volume of 0.1 ml/mouse. One week later, a booster immunization was delivered over contralateral lymph nodes.

The animals were daily monitored for EAE signs based on a standard EAE 0–5 scale scoring system: 0, healthy; 1, complete loss of tail tonicity; 2, loss of righting reflex; 3, partial paralysis; 4, complete paralysis of one or both hind limbs; and 5, moribund.

Histological preparation Mice were exposed to a lethal dose of isoflurane and perfused transcardially with ice-cold 1X PBS for 8–10 min, followed by 10% formalin for 8–10 min. Spinal cords were dissected and submerged in 10% formalin overnight at 4 ℃, followed by 30% sucrose for 24 hrs at 4 ℃. Spinal cords were embedded in optimal cutting temperature compound (Tissue Tek) and stored in −80 °C after flash frozen in an isopentane bath cooled with liquid nitrogen. Spinal cord cross-sections were obtained 40 μm thick with a microtome cryostat (model HM505E) at −20 °C. Tissues were collected serially and stored free floating in 1X PBS with 1% sodium azide in 4 ℃ for further analysis.

Immunofluorescence Before histological staining, 40-mm thick free-floating sections were thoroughly washed with 1X PBS to remove residual sodium azide. In the case of anti-MBP labeling, tissue sections were processed with an additional 2 h incubation with 5% glacial acetic acid in 100-proof ethanol at room temperature (RT). After washing tissue sections were permeabilized with 0.05% Tween20 and 2% normal goat serum in 1X PBS for 30 min at RT and blocked with 10% normal goat serum in 1X PBS for 1 hr. Without washing, tissues were then incubated with primary antibodies overnight in 4 ℃. The following primary antibodies were used: anti-CD3 at 1:2000 (BD Biosciences PharMingen), anti-Iba-1 at 1:10,000 (Wako Chemicals), anti-GFAP at 1:40,000 (Dako), anti-MCP-1 (CCL2) at 1:200 (Torrey Pines Biolabs), anti-NF200 at 1:750 dilutions (Sigma), and anti-MBP at 1:750 (Sigma). The next day tissues

were washed and incubated with secondary antibodies conjugated to Cy5 or Cy3 (Millipore) for 1 hr at RT. DAPI at 1:5000 (Molecular Probes) was used for nuclear stain. Sections were mounted on slides, allowed to semi-dry, and coverslipped in fluoromount G (Fisher Scientific) for confocal microscopy.

Microscopy and image processing Stained sections were examined and imaged using a confocal microscope (Leica TCS-SP) or a fluorescence microscope (BX51WI; Olympus) equipped with Plan Fluor objectives connected to a camera (DP70, Olympus). Images were processed using SlideBook™ 4.2 (Intelligent Imaging Innovations, Inc.) and assembled using Microsoft PowerPoint (Microsoft).

Statistical analysis Repeated measures one-way ANOVA determined differences in EAE clinical scores. One-way ANOVA determined statistical differences regarding the immunofluorescence data. For these analyses, one-way ANOVA and Bonferroni post hoc analysis was performed on F-stat values, and significance was determined at the 95% confidence interval (Prism).

2.5 Bibilography

Aloisi, F., Penna, G., Cerase, J., Menendez Iglesias, B., Adorini, L., 1997. IL-12 production by central nervous system microglia is inhibited by astrocytes. J. Immunol. 159, 1604–1612.

Anderson, M.A., Ao, Y., Sofroniew, M.V., 2014. Heterogeneity of reactive astrocytes. Neurosci. Lett. 565, 23–29.

Berman, J.W., Guida, M.P., Warren, J., Amat, J., Brosnan, C.F., 1996. Localization of monocyte chemoattractant peptide-1 expression in the central nervous system in experimental autoimmune encephalomyelitis and trauma in the rat. J. Immunol. 156, 3017–3023.

Brambilla, R., Bracchi-Ricard, V., Hu, W.H., Frydel, B., Bramwell, A., Karmally, S., et al., 2005. Inhibition of astroglial nuclear factor kappaB reduces inflammation and improves functional recovery after spinal cord injury. J. Exp. Med. 202, 145–156.

Brambilla, R., Persaud, T., Hu, X., Karmally, S., Shestopalov, V.I., Dvoriantchikova, G., et al., 2009. Transgenic inhibition of astroglial NF-kappa B improves functional outcome in experimental autoimmune encephalomyelitis by suppressing chronic central nervous system inflammation. J. Immunol. 182, 2628–2640.

Bush, T.G., Puvanachandra, N., Horner, C.H., Polito, A., Ostenfeld, T., Svendsen, C.N., et al., 1999. Leukocyte infiltration, neuronal degeneration and neurite outgrowth after ablation of scar-forming, reactive astrocytes in adult transgenic mice. Neuron 23, 297–308.

Carrillo-de Sauvage, M.A., Gomez, A., Ros, C.M., Ros-Bernal, F., Martin, E.D., Perez-Valles, A., et al., 2012. CCL2-expressing astrocytes mediate the extravasation of T lymphocytes in the brain. Evidence from patients with glioma and experimental models in vivo. PLoS One 7, e30762.

Chen, Y., Swanson, R.A., 2003. Astrocytes and brain injury. J. Cereb. Blood Flow Metab. 23, 137–149.

Conductier, G., Blondeau, N., Guyon, A., Nahon, J.L., Rovere, C., 2010. The role of monocyte chemoattractant protein MCP1/CCL2 in neuroinflammatory diseases. J. Neuroimmunol. 224, 93–100.

Dogan, R.N., Elhofy, A., Karpus, W.J., 2008. Production of CCL2 by central nervous system cells regulates development of murine experimental autoimmune encephalomyelitis through the recruitment of TNF- and iNOS-expressing macrophages and myeloid dendritic cells. J. Immunol. 180, 7376–7384.

Dong, Y., Benveniste, E.N., 2001. Immune function of astrocytes. Glia 36, 180–190.

Donnelly, D.J., Popovich, P.G., 2008. Inflammation and its role in neuroprotection, axonal regeneration and functional recovery after spinal cord injury. Exp. Neurol. 209, 378–388.

dos Santos, A.C., Barsante, M.M., Arantes, R.M., Bernard, C.C., Teixeira, M.M., Carvalho-Tavares, J., 2005. CCL2 and CCL5 mediate leukocyte adhesion in experimental autoimmune encephalomyelitis–an intravital microscopy study. J. Neuroimmunol. 162, 122–129.

Dringen, R., Hirrlinger, J., 2003. Glutathione pathways in the brain. Biol. Chem. 384, 505–516.

Eng, L.F., Gerstl, B., Vanderhaeghen, J.J., 1970. A study of proteins in old multiple sclerosis plaques. Trans. Am. Soc. Neurochem. 1, 42.

Eng, L.F., Ghirnikar, R.S., Lee, Y.L., 2000. Glial fibrillary acidic protein: GFAP-thirty-one years (1969-2000). Neurochem. Res. 25, 1439–1451.

Farina, C., Aloisi, F., Meinl, E., 2007. Astrocytes are active players in cerebral innate immunity. Trends Immunol. 28, 138–145.

Faulkner, J.R., Herrmann, J.E., Woo, M.J., Tansey, K.E., Doan, N.B., Sofroniew, M.V., 2004. Reactive astrocytes protect tissue and preserve function after spinal cord injury. J. Neurosci. 24, 2143–2155.

Fife, B.T., Huffnagle, G.B., Kuziel, W.A., Karpus, W.J., 2000. CC chemokine receptor 2 is critical for induction of experimental autoimmune encephalomyelitis. J. Exp. Med. 192, 899–905.

Ge, S., Murugesan, N., Pachter, J.S., 2009. Astrocyte- and endothelial-targeted CCL2 conditional knockout mice: critical tools for studying the pathogenesis of neuroinflammation. J. Mol. Neurosci. 39, 269–283.

Giraud, S.N., Caron, C.M., Pham-Dinh, D., Kitabgi, P., Nicot, A.B., 2010. Estradiol inhibits ongoing autoimmune neuroinflammation and NFkappaB-dependent CCL2 expression in reactive astrocytes. Proc. Natl. Acad. Sci. U. S. A. 107, 8416–8421.

Hamby, M.E., Coppola, G., Ao, Y., Geschwind, D.H., Khakh, B.S., Sofroniew, M.V., 2012. Inflammatory mediators alter the astrocyte transcriptome and calcium signaling elicited by multiple G-protein-coupled receptors. J. Neurosci. 32, 14489–14510.

Herrmann, J.E., Imura, T., Song, B., Qi, J., Ao, Y., Nguyen, T.K., et al., 2008. STAT3 is a critical regulator of astrogliosis and scar formation after spinal cord injury. J. Neurosci. 28, 7231–7243.

Huang, D.R., Wang, J., Kivisakk, P., Rollins, B.J., Ransohoff, R.M., 2001. Absence of monocyte chemoattractant protein 1 in mice leads to decreased local macrophage recruitment and antigen-specific T helper cell type 1 immune response in experimental autoimmune encephalomyelitis. J. Exp. Med. 193, 713–726.

Iadecola, C., Nedergaard, M., 2007. Glial regulation of the cerebral microvasculature. Nat. Neurosci. 10, 1369–1376.

John, G.R., Lee, S.C., Song, X., Rivieccio, M., Brosnan, C.F., 2005. IL-1-regulated responses in astrocytes: relevance to injury and recovery. Glia 49, 161–176.

Kennedy, K.J., Strieter, R.M., Kunkel, S.L., Lukacs, N.W., Karpus, W.J., 1998. Acute and relapsing experimental autoimmune encephalomyelitis are regulated by differential expression of the CC chemokines macrophage inflammatory protein-1alpha and monocyte chemotactic protein-1. J. Neuroimmunol. 92, 98–108.

Li, L., Lundkvist, A., Andersson, D., Wilhelmsson, U., Nagai, N., Pardo, A.C., et al., 2008. Protective role of reactive astrocytes in brain ischemia. J. Cereb. Blood Flow Metab. 28, 468–481.

Liedtke, W., Edelmann, W., Chiu, F.C., Kucherlapati, R., Raine, C.S., 1998. Experimental autoimmune encephalomyelitis in mice lacking glial fibrillary acidic protein is characterized by a more severe clinical course and an infiltrative central nervous system lesion. Am. J. Pathol. 152, 251–259.

Liu, H.B., Loo, K.K., Palaszynski, K., Ashouri, J., Lubahn, D.B., Voskuhl, R.R., 2003. Estrogen receptor alpha mediates estrogen's immune protection in autoimmune disease. J. Immunol. 171, 6936–6940.

Lucchinetti, C., Bruck, W., Parisi, J., Scheithauer, B., Rodriguez, M., Lassmann, H., 2000. Heterogeneity of multiple sclerosis lesions: implications for the pathogenesis of demyelination. Ann. Neurol. 47, 707–717.

McFarland, H.F., Martin, R., 2007. Multiple sclerosis: a complicated picture of autoimmunity. Nat. Immunol. 8, 913–919.

McManus, C., Berman, J.W., Brett, F.M., Staunton, H., Farrell, M., Brosnan, C.F., 1998. MCP-1, MCP-2 and MCP-3 expression in multiple sclerosis lesions: an immunohistochemical and in situ hybridization study. J. Neuroimmunol. 86, 20–29.

Morales, L.B., Loo, K.K., Liu, H.B., Peterson, C., Tiwari-Woodruff, S., Voskuhl, R.R., 2006. Treatment with an estrogen receptor alpha ligand is neuroprotective in experimental autoimmune encephalomyelitis. J. Neurosci. 26, 6823–6833.

Myer, D.J., Gurkoff, G.G., Lee, S.M., Hovda, D.A., Sofroniew, M.V., 2006. Essential protective roles of reactive astrocytes in traumatic brain injury. Brain 129, 2761–2772.

Nair, A., Frederick, T.J., Miller, S.D., 2008. Astrocytes in multiple sclerosis: a product of their environment. Cell. Mol. Life Sci. 65, 2702–2720.

Okada, S., Nakamura, M., Katoh, H., Miyao, T., Shimazaki, T., Ishii, K., et al., 2006. Conditional ablation of Stat3 or Socs3 discloses a dual role for reactive astrocytes after spinal cord injury. Nat. Med. 12, 829–834.

Polanczyk,M., Zamora, A., Subramanian, S., Matejuk, A., Hess, D.L., Blankenhorn, E.P., et al., 2003. The protective effect of 17beta-estradiol on experimental autoimmune encephalomyelitis is mediated through estrogen receptor-alpha. Am. J. Pathol. 163, 1599–1605.

Raine, C.S., Barnett, L.B., Brown, A., Behar, T., McFarlin, D.E., 1980. Neuropathology of experimental allergic encephalomyelitis in inbred strains of mice. Lab. Investig. 43, 150–157.

Ransohoff, R.M., 2009. Chemokines and chemokine receptors: standing at the crossroads of immunobiology and neurobiology. Immunity 31, 711–721.

Rasmussen, S., Wang, Y., Kivisakk, P., Bronson, R.T., Meyer, M., Imitola, J., et al., 2007. Persistent activation of microglia is associated with neuronal dysfunction of callosal projecting pathways and multiple sclerosis-like lesions in relapsing remitting experimental autoimmune encephalomyelitis. Brain 30, 2816–2829.

Rollins, B.J., 1991. JE/MCP-1: an early-response gene encodes a monocyte-specific cytokine. Cancer Cells 3, 517–524.

Rollins, B.J., 1997. Chemokines. Blood 90, 909–928.

Schnell, L., Fearn, S., Klassen, H., Schwab, M.E., Perry, V.H., 1999. Acute inflammatory responses to mechanical lesions in the CNS: differences between brain and spinal cord. Eur. J. Neurosci. 11, 3648–3658.

Shi, C., Jia, T., Mendez-Ferrer, S., Hohl, T.M., Serbina, N.V., Lipuma, L., et al., 2011. Bone marrow mesenchymal stem and progenitor cells induce monocyte emigration in response to circulating toll-like receptor ligands. Immunity 34, 590–601.

Simpson, J.E., Newcombe, J., Cuzner, M.L.,Woodroofe, M.N., 1998. Expression of monocyte chemoattractant protein-1 and other beta-chemokines by resident glia and inflammatory cells in multiple sclerosis lesions. J. Neuroimmunol. 84, 238–249.

Sofroniew, M.V., 2014. Multiple roles for astrocytes as effectors of cytokines and inflammatory mediators. Neuroscientist 20, 160–172.

Spence, R.D., Hamby, M.E., Umeda, E., Itoh, N., Du, S., Wisdom, A.J., et al., 2011. Neuroprotection mediated through estrogen receptor-{alpha} in astrocytes. Proc. Natl. Acad. Sci. U. S. A. 108, 8867–8872.

Spence, R.D., Wisdom, A.J., Cao, Y., Hill, H.M., Mongerson, C.R., Stapornkul, B., et al., 2013. Estrogen mediates neuroprotection and anti-inflammatory effects during EAE through ER alpha signaling on astrocytes but not through ER beta signaling on astrocytes or neurons. J. Neurosci. 33, 10924–10933.

Voskuhl, R.R., Peterson, R.S., Song, B., Ao, Y., Morales, L.B., Tiwari-Woodruff, S., et al., 2009. Reactive astrocytes form scar-like perivascular barriers to leukocytes during adaptive immune inflammation of the CNS. J. Neurosci. 29, 11511–11522.

Wujek, J.R., Bjartmar, C., Richer, E., Ransohoff, R.M., Yu, M., Tuohy, V.K., et al., 2002. Axon loss in the spinal cord determines permanent neurological disability in an animal model of multiple sclerosis. J. Neuropathol. Exp. Neurol. 61, 23–32.

CHAPTER 3

Neuroprotection requires modulation of inflammation and remyelination during EAE : a lesson from estrogen receptor beta ligand

3.1 Introduction

Estrogens are known to be neuroprotective in several models of neurodegenerative diseases including multiple sclerosis, Alzheimer's disease, Parkinson's disease, ischemic stroke and spinal cord injury (Suzuki et al., 2009; Samantaray et al., 2010; Spence and Voskuhl, 2012; McFarland et al., 2013; Uchoa et al., 2016). Estradiol signals through binding to estrogen receptors (ER), alpha (ERα) and/or beta (ERβ). ERα-ligand treatment mediates protection *in vivo* during EAE by acting on T lymphocytes (Morales et al., 2006; Lelu et al., 2011), and astrocytes (Spence et al., 2011), but not neurons (Spence et al., 2011). Unfortunately, treatments using estradiol or ERα ligands for years in humans may cause adverse effects on breast and uterus, so targeted strategies are needed to achieve neuroprotection while minimizing off-target toxicity. One approach is to use ERα ligands designed to act in a tissue-specific manner in the CNS, but not in the periphery (Prokai et al., 2015). Another is to use estrogen compounds or selective estrogen receptor modifiers (SERMs) that are neuroprotective through ERβ activation with minimum ERα activation.

Regarding a tailored estrogen receptor ligand approach, treatment with the classic ERβ-ligand diarylpropionitrile (DPN) is neuroprotective in the later phase of chronic EAE, sparing axons and myelin, while reducing grey matter atrophy by MRI (Tiwari-Woodruff et al., 2007; Mackenzie-Graham et al., 2012; Itoh et al., 2017). This occurs without decreasing peripheral

adaptive immune responses or reducing levels of white matter inflammation in the CNS (Tiwari-Woodruff et al., 2007), albeit with some qualitative effects on dendritic cells in the CNS (Du et al., 2011). Interestingly, two high-throughput in vitro screens to discover molecules to enhance maturation of oligodendrocytes and promote remyelination had identified SERMs (Mei et al., 2014; Lariosa-Willingham et al., 2016) as top candidates and suggested a role for ERβ specifically (Lariosa-Willingham et al., 2016). That said an effect on remyelination is not mutually exclusive of a direct effect of ERβ on the innate immune system during multiple sclerosis and other neurodegenerative diseases.

Here, we hypothesized that $CD11c^+$ immune cells could be a direct target of ERβ-ligand treatment. CD11c is a marker for dendritic cells in the peripheral immune system and is expressed in dendritic cells in perivascular areas in EAE (Bulloch et al., 2008; Prodinger et al., 2011). These cells release cytokines and chemokines to propagate an immunological cascade leading to demyelination and axonal degeneration (Karman et al., 2004; Greter et al., 2005). $CD11c^+$ resident microglia, as well as $CD11c^+$ peripheral myeloid dendritic cells and macrophages that have infiltrated into the CNS, are known to be critical in EAE pathogenesis (Bailey et al., 2007; King et al., 2009; Wlodarczyk et al., 2014; Clarkson et al., 2015). Involvement of $CD11c^+$ myeloid dendritic cells in the progression of later phases of EAE (Miller et al., 2007) was consistent with the timing of the ERβ-ligand treatment effect (Tiwari-Woodruff et al., 2007). That said, $CD11c^+$ resident microglia and $CD11c^+$ peripheral myeloid dendritic cells and macrophages have each demonstrated pro-inflammatory and anti-inflammatory properties (Wlodarczyk et al., 2015), and either could be a target of ERβ-ligand treatment. $CD11c^+$ cells express both ERα and ERβ during disease (Paharkova-Vatchkova et al., 2004), but effects of ERβ signaling on these cells *in vivo* during neurodegenerative diseases has remained

unknown. Finally, cells of this lineage have been implicated in human diseases, namely multiple sclerosis (Mishra and Yong, 2016) and Alzheimer's disease (Srinivasan et al., 2016), and cell-type specific similarities in gene expression changes have been observed across these distinct diseases (Itoh and Voskuhl, 2017). Here we determine the functional significance of ERβ in $CD11c^+$ cells *in vivo* during EAE using cell-specific conditional knockouts (CKO) of ERβ in $CD11c^+$ cells, and then use bone marrow chimeras to discern whether ERβ-ligand treatment effects are directly mediated through ERβ in $CD11c^+$ myeloid dendritic cells and macrophages versus $CD11c^+$ resident microglia.

3.2 Results

3.2.1 Specification of $CD11c^+$ cells in the CNS during EAE

To determine whether ERβ drives ERβ-ligand treatment effects *in vivo* during EAE in CNS resident microglia and peripherally derived myeloid dendritic cells and macrophages, we focused on $CD11c^+$ cells. Since CD11c expression is low in the healthy CNS, we first verified which population of cells express CD11c in the CNS during disease using flow cytometry of CNS mononuclear immune cells isolated from brains and spinal cords of EAE mice. CNS $CD45^+$ cells were divided into two distinct populations; $CD45^{int}$ CNS resident microglia and $CD45^{hi}$ peripherally derived immune cells. The populations were then further divided into: $CD45^{int}CD11c^+CD11b^+$ or $CD45^{int}CD11c^-CD11b^+$ microglia, $CD45^{hi}CD11c^+CD11b^+$ myeloid dendritic cells and macrophages, $CD45^{hi}CD11c^-CD11b^+$ macrophages and $CD45^{hi}CD11c^-CD11b^-$ lymphocytes (Figure 3.1). These data demonstrate CD11c expression in microglia and myeloid dendritic cells and macrophages in the CNS during EAE.

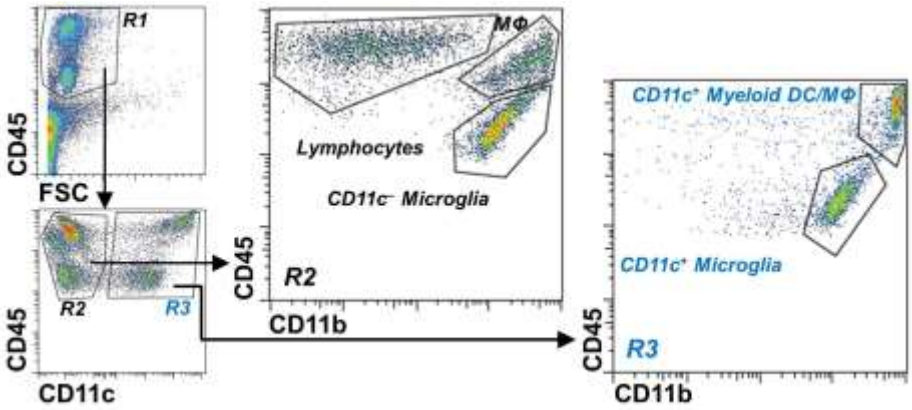

Figure 3.1 Specification of CD11c$^+$ cells in the CNS during EAE. Flow cytometry dot plots of CNS mononuclear immune cells isolated from brains and spinal cords of EAE mice. CNS mononuclear immune cells were gated based on FSC and CD45 expression. CNS CD45$^+$ gated cells included two separate populations, CD45^{hi} and CD45^{int}, within the R1 gate. CD45$^+$ cells were further gated based on CD11c expression into R2: CD45$^+$CD11c$^-$ and R3: CD45$^+$CD11c$^+$. CD11b staining revealed that R2 included CD45^{hi}CD11c$^-$CD11b$^-$ lymphocytes, CD45^{hi}CD11c$^-$CD11b$^+$ macrophages, and CD45^{int}CD11c$^-$CD11b$^+$ resident microglia, and R3 included CD45^{hi}CD11c$^+$CD11b$^+$ peripherally derived myeloid dendritic cells and macrophages (DC/MΦ) and CD45^{int}CD11c$^+$CD11b$^+$ resident microglia. FSC = forward scatter.

3.2.2 Validation of ERβ specific deletion in CD11c$^+$ cells

To investigate whether neuroprotective effects of ERβ-ligand treatment are mediated through CD11c$^+$ cells *in vivo* during EAE, we created mice with specific deletion of ERβ in CD11c$^+$ cells using the Cre-loxP system, by crossing CD11c-cre-GFP$^+$ mice with ERβ$^{floxed/floxed}$ (ERβ$^{fl/fl}$) mice to obtain CD11c-cre-GFP$^+$;ERβ$^{fl/fl}$ mice (CD11c ERβ CKO). We then confirmed the specific deletion of ERβ in CD11c$^+$ cells in the CNS in CKO mice by inducing EAE and collecting spinal

cord tissues for immunofluorescence. ERβ expression in CD11c$^+$ cells was shown by co-localization (merge) of ERβ (red) and CD11c-EGFP (green) in control EAE spinal cord tissues, while CKO EAE spinal cords did not show co-localization (Figure 3.2A). Quantification of co-localization confirmed the efficiency of ERβ deletion in CD11c$^+$ cells (Figure 3.2B). FACS sorted mononuclear immune cells from the CNS of EAE mice with analysis of ERβ (*Esr2*) mRNA expression by quantitative PCR showed deletion of ERβ from CD11c$^+$ microglia and CD11c$^+$ myeloid dendritic cells and macrophages, but not from CD11c$^-$ cells (Figure 3.2C,D). Together, these data validated the deletion of ERβ from CD11c$^+$ microglia and CD11c$^+$ myeloid dendritic cells and macrophages in the CNS of mice with EAE.

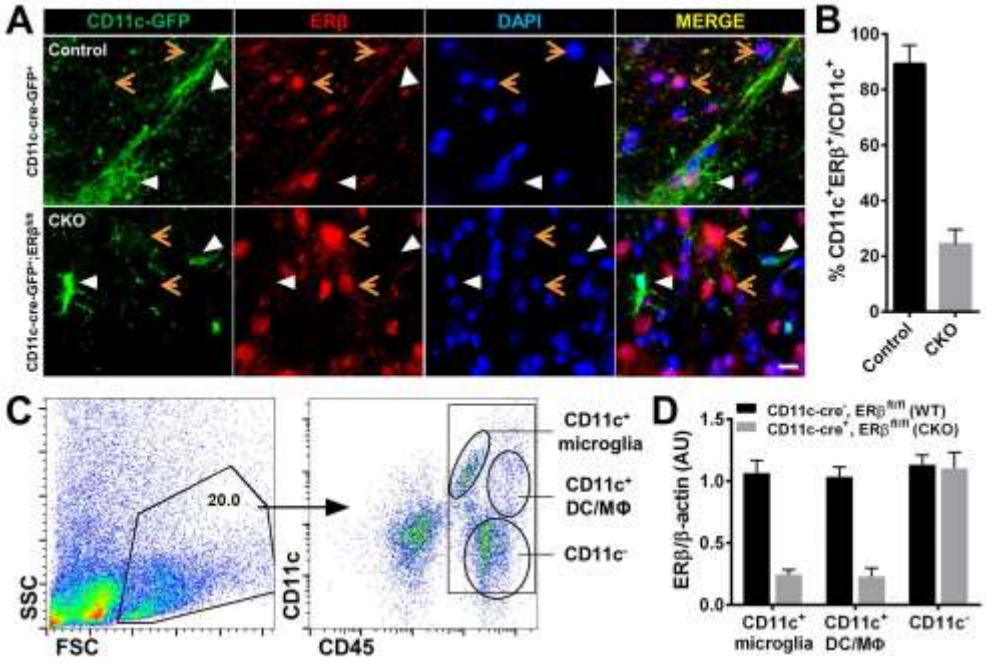

Figure 3.2 Validation of ERβ specific deletion in CD11c$^+$ cells via immunofluorescence and qPCR (A) Immunofluorescence images of spinal cord tissues stained with CD11c-GFP (green), ERβ (red) and nuclear stain DAPI (blue) with merged images for colocalization (yellow) on the right. Top row: CD11c-cre-GFP$^+$ control mice showed colocalization (white arrows) of CD11c-

GFP and ERβ. Bottom row: CD11c-cre-GFP^{+};ERβ$^{fl/fl}$ (CD11c ERβ CKO, CKO) mice did not show co-localization (white arrows). Orange arrows represent other cells in the CNS expressing ERβ. Scale bar, 20 μm. **(B)** Quantitative analysis of CD11c-GFP and ERβ co-localization in immunofluorescence images of CD11c-cre-GFP^{+} (Control) and CKO mice with EAE. **(C)** Representative flow cytometry plots of isolated CNS mononuclear immune cells from a pool of three individual mice. CNS mononuclear immune cells were gated based on SSC and FSC (left), and subpopulations were identified using CD11c and CD45 staining (right). Cell populations labeled as CD11c^{+} microglia, CD11c^{+} myeloid DC/MΦ, and CD11c^{-} cells were FACS sorted for mRNA isolation and quantitative PCR analysis. **(D)** Quantitative analysis of ERβ (*Esr2*) mRNA expression in sorted CNS CD11c^{+} microglia, CD11c^{+} myeloid DC/MΦ, and CD11c^{-} cells from CKO and littermate control CD11c-cre-GFP^{-}; ERβ$^{fl/fl}$ (CD11c ERβ WT, WT) mice, each with EAE.

3.2.3 ERβ activation on CD11c^{+} cells is important for neuroprotection during EAE

To determine the functional significance of ERβ expression in CD11c^{+} cells, we assessed effects of ERβ-ligand treatment during EAE in CKO and CD11c-cre-GFP^{-}; ERβ$^{fl/fl}$ (wild-type, WT) littermates (Figure 3.3A). For ERβ-ligand treatment we used DPN. Vehicle treated wild-type EAE mice exhibited the typical EAE disease course in C57BL/6J mice, whereas ERβ-ligand treated WT EAE mice showed amelioration of EAE during the chronic phase, consistent with previous reports (Tiwari-Woodruff et al., 2007; Spence et al., 2013). In contrast, ERβ-ligand treated CKO EAE mice did not exhibit clinical disease protection, with EAE scores identical to those in vehicle treated CKO EAE mice (Figure 3.3A, Table 1). Next, we performed neuropathological studies on the CKO and WT EAE mice.

Healthy axons were evaluated by counting the number of phosphorylated neurofilament 200 (NF200) positive intact axons, and injured axons by the number of non-phosphorylated NF200 (SMI32) and beta amyloid precursor protein (βAPP)-positive axons in spinal cord white matter. We observed a reduction of $NF200^+$ healthy axons and an increase in $SMI32^+$ and βAPP^+ injured axons in vehicle treated wild-type EAE mice compared to healthy controls. Axons were protected in ERβ-ligand treated wild-type EAE mice as shown by an increase in $NF200^+$ axons and a decrease in $SMI32^+$ and βAPP^+ axons. In contrast, ERβ-ligand treatment of CKO EAE mice failed to protect axons during EAE (Figure 3.3B).

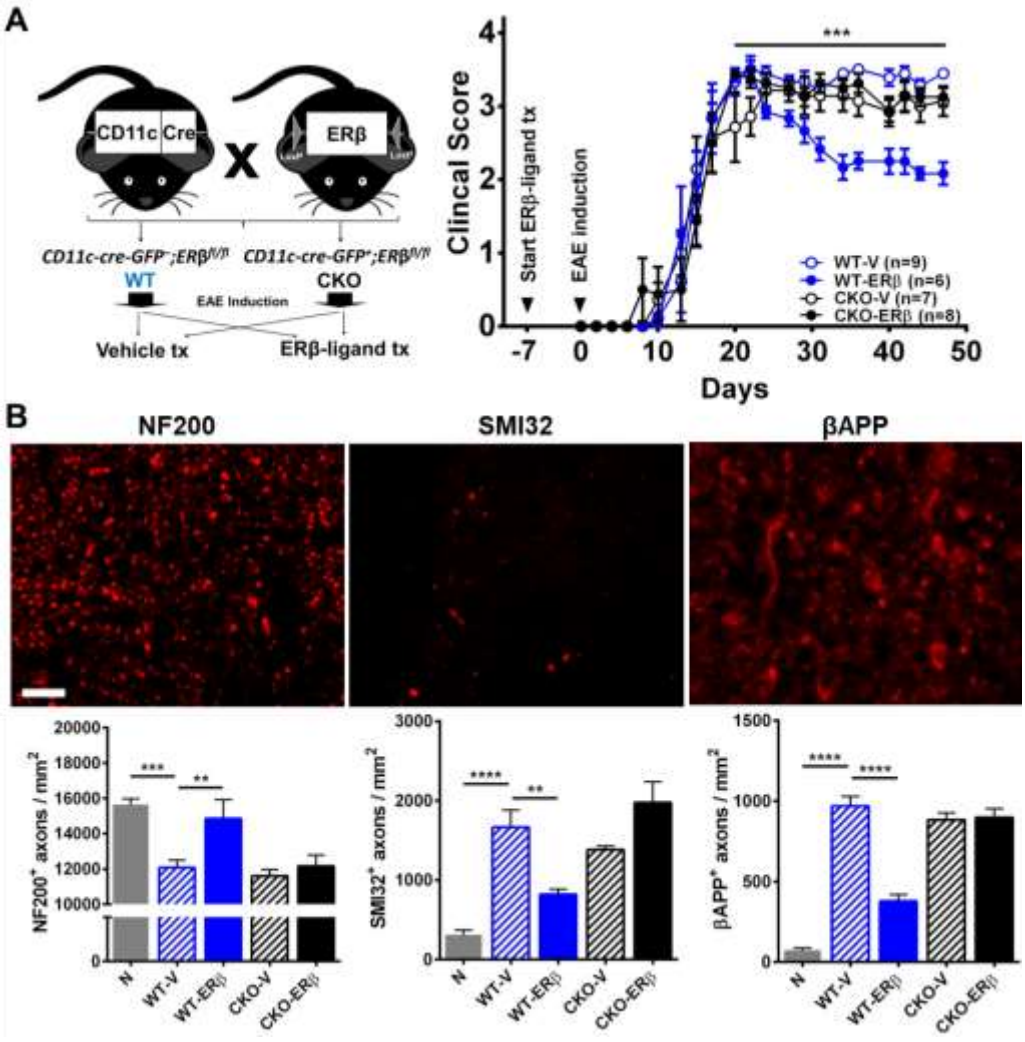

Figure 3.3 ERβ on CD11c$^+$ cells is necessary for ERβ-ligand mediated amelioration of clinical EAE and axonal protection during EAE. (A) Breeding scheme for creating WT and CKO mice of ERβ in CD11c$^+$ cells and experimental paradigm to investigate direct effects of ERβ-ligand treatment in EAE. ERβ-ligand treated WT EAE mice (WT-ERβ, blue solid) had significantly better clinical scores compared to vehicle treated WT EAE mice (WT-V, blue clear). In contrast, ERβ-ligand mediated protection did not occur in ERβ-ligand treated CKO EAE mice (CKO-ERβ, black solid) when compared to vehicle treated CKO EAE mice (CKO-V, black clear). Detailed EAE statistics are in Table 1. **(B)** Representative images and quantitative analyses of NF200$^+$, SMI32$^+$, and βAPP$^+$ axons in dorsal white matter of the spinal cord. Images were taken at 40× magnification. Scale bar, 20 μm. *$P < 0.05$; **$P < 0.01$; ***$P < 0.001$; ****$P < 0.0001$. Data are representative of three repeated experiments.

			P value	Degrees of freedom
Fig2.	Multiple comparison			
	WT-V vs WT-ERβ	***	0.0002	t(26)=4.975
	CKO-V vs CKO-ERβ	ns	> 0.9999	t(26)=1.053
	WT-V vs CKO-V	ns	0.2573	t(26)=2.129
	WT-V vs CKO-ERβ	ns	> 0.9999	t(26)=1.086
	WT-ERβ vs CKO-V	ns	0.0592	t(26)=2.784
	WT-ERβ vs CKO-ERβ	**	0.0039	t(26)=3.878
Fig5.	Multiple comparison			
	Olig1-WT-V vs Olig1-WT-ERβ	**	0.0095	t(17)=3.751
	Olig1-CKO-V vs Olig1-CKO-ERβ	ns	> 0.9999	t(17)=0.9283
	Olig1-WT-V vs Olig1-CKO-V	ns	> 0.9999	t(17)=0.01304
	Olig1-WT-V vs Olig1-CKO-ERβ	ns	> 0.9999	t(17)=1.004
	Olig1-WT-ERβ vs Olig1-CKO-V	*	0.0231	t(17)=3.343
	Olig1-WT-ERβ vs Olig1-CKO-ERβ	ns	0.208	t(17)=2.296
Fig6.	Multiple comparison			
	WT→WT-V vs WT→WT-ERβ	*	0.0188	t(25)=3.269
	WT→CKO-V vs WT→CKO-ERβ	**	0.0077	t(25)=3.629
	WT→WT-V vs WT→CKO-V	ns	> 0.9999	t(25)=0.06194
	WT→WT-V vs WT→CKO-ERβ	**	0.0067	t(25)=3.684
	WT→WT-ERβ vs WT→CKO-V	*	0.0214	t(25)=3.217
	WT→WT-ERβ vs WT→CKO-ERβ	ns	> 0.9999	t(25)=0.1953
Fig7.	Multiple comparison			
	WT→WT-V vs WT→WT-ERβ	***	0.0005	t(20)=4.932
	CKO→WT-V vs CKO→WT-ERβ	ns	> 0.9999	t(20)=1.169
	WT→WT-V vs CKO→WT-V	ns	> 0.9999	t(20)=0.4652
	WT→WT-V vs CKO→WT-ERβ	ns	0.7717	t(20)=1.585
	WT→WT-ERβ vs CKO→WT-V	**	0.0015	t(20)=4.435
	WT→WT-ERβ vs CKO→WT-ERβ	ns	0.0866	t(20)=2.679

Table 3.1 Statistics of clinical EAE severity scores shown in Figures. Repeated measures two-way ANOVA, with Bonferroni's multiple comparisons test. Shading highlights ERβ ligand (ERβ) versus vehicle control (V) treatment in WT, as well as ERβ ligand (ERβ) versus Vehicle control (V) treatment in the conditional knock out (CKO).

3.2.4 ERβ on CD11c$^+$ cells is necessary for ERβ-ligand mediated myelin preservation and remyelination during EAE.

Myelin pathology was evaluated by measuring the intensity of MBP and 2,3-cyclic-nucleotide 3-phosphodiesterase (CNPase). We observed a reduction of myelin intensity in vehicle treated WT EAE mice compared to healthy controls. Myelin was protected in ERβ-ligand treated WT EAE mice, but not in ERβ-ligand treated CKO EAE mice (Figure 3.4A). Lastly, ultrastructural analysis of myelination using electron microscopy showed that vehicle treated WT EAE mice had an increased g-ratio [axon diameter / (axon + outer myelin diameter)] compared to healthy controls. ERβ-ligand treatment in WT EAE mice decreased the g-ratio compared to vehicle treated, consistent with increased myelin staining by immunofluorescence during ERβ-ligand treatment. In contrast, ERβ-ligand treated CKO EAE mice did not show this protective effect on myelin (Figure 3.4B). Together, these results show that ERβ expression in CD11c$^+$ cells is necessary for ERβ-ligand treatment to provide neuroprotection during EAE.

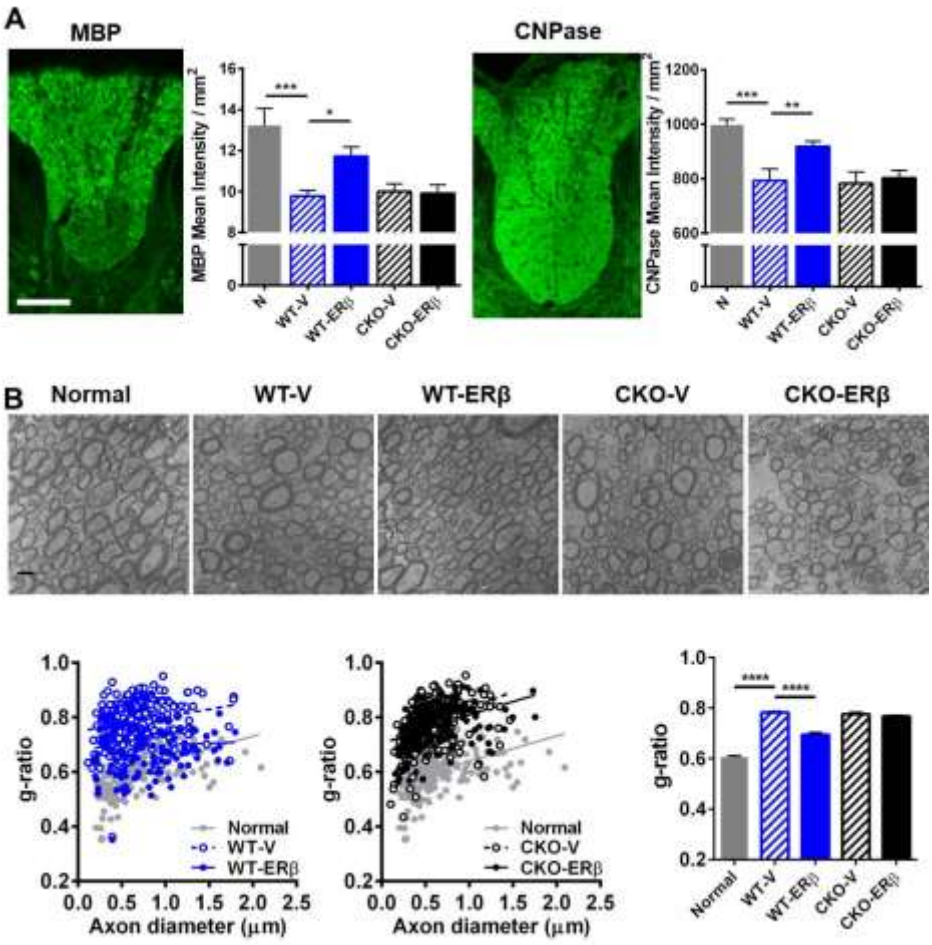

Figure 3.4 ERβ on CD11c^{+} cells is necessary for ERβ-ligand mediated myelin preservation and remyelination during EAE. (A) Representative images and quantitative analyses of MBP^{+} and CNPase^{+} mean intensity in dorsal white matter of the spinal cord. Scale bar, 100 μm. **(B)** Representative electron microscopy images of ultraresolution of axons and myelin thickness in the dorsal white matter of spinal cord. Myelin thickness in the WT and CKO EAE mice treated with vehicle and ERβ-ligand was measured using the g-ratio (axon diameter) / (axon + outer myelin diameter) and is shown in comparison with normal. Quantitative analysis showed that WT-ERβ mice had a decrease in g-ratio due to increased outer myelin diameter, while CKO-ERβ mice did not. Scale bar, 1 μm. *$P < 0.05$; **$P < 0.01$; ***$P < 0.001$; ****$P < 0.0001$. Data are representative of three repeated experiments.

3.2.5 ERβ activation on CD11c$^+$ cells had no quantitative effects on immune cells during EAE

Despite the beneficial effects of ERβ-ligand treatment on axons and myelin during EAE, there was no effect on quantitative levels of CD3$^+$ T cells, Iba1$^+$ globoid macrophages or Iba1$^+$ ramified microglia in spinal cord white matter (Figure 3.5), as described (Tiwari-Woodruff et al., 2007; Spence et al., 2013).

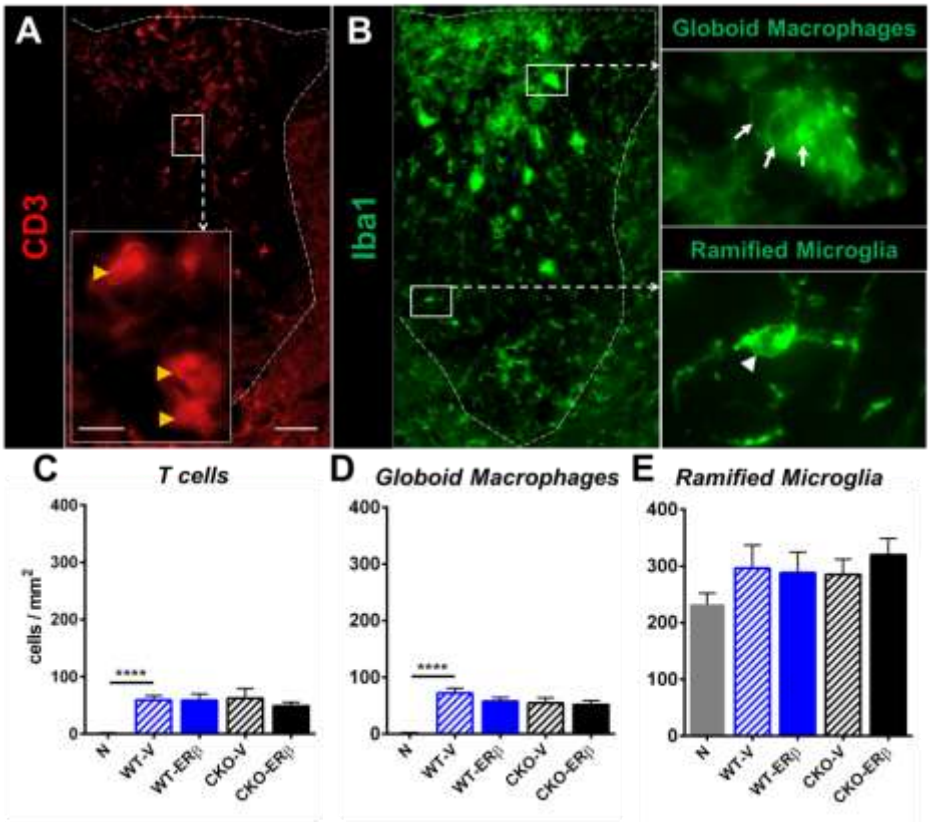

Figure 3.5 No quantitative effects on CNS resident and infiltrated immune cells. (A and B) Immunofluorescence images of spinal cord tissues stained with CD3 (red) and Iba1 (green). Dotted lines represent the area of dorsal white matter in the spinal cord. **(A)** CD3 staining of T cells in CNS (orange arrowhead) and **(B)** Iba1 staining of globoid macrophages (white arrow) and ramified microglia (white arrowhead). Scale bar, 50 μm and 5 μm (inset). Inset boxes are

40x images. Quantitative analysis of **(C)** infiltrated $CD3^+$ T cell, **(D)** $Iba1^+$ globoid macrophages in spinal cord white matter show that all EAE groups were increased compared to healthy controls, but not different from each other. **(E)** $Iba1^+$ ramified microglia cell numbers were no differences between groups. ****$P < 0.0001$.

3.2.6 ERβ activation on $CD11c^+$ cells has qualitative effects on CNS myeloid cells during EAE

However, there were qualitative effects of ERβ-ligand treatment on $Iba1^+$ myeloid cells. During EAE, vehicle treated WT EAE mice showed an increase in MHCII expression on $Iba1^+$ myeloid cells compared to healthy controls, and ERβ-ligand treatment abrogated this increase in MHCII. In contrast, this effect of ERβ-ligand treatment on $Iba1^+$ myeloid cells was lost in CKO EAE mice (Figure 3.6A,D). We then measured expression levels of pro-inflammatory inducible nitrogen oxide synthase (iNOS) and anti-inflammatory arginase-1 (Arg1), on $Iba1^+$ myeloid cells. We observed that iNOS expression on $Iba1^+$ myeloid cells was reduced in ERβ-ligand treated wild-type EAE mice compared to vehicle treated WT EAE mice, but this treatment effect did not occur in ERβ-ligand treated CKO EAE mice (Figure 3.6B,E). There was no effect on Arg1 expression (Figure 3.6C,F). Together, these results show that ERβ-ligand treatment reduced the pro-inflammatory phenotype of myeloid cells in the CNS during EAE, and this was mediated through direct effects of ERβ-ligand treatment on $CD11c^+$ cells.

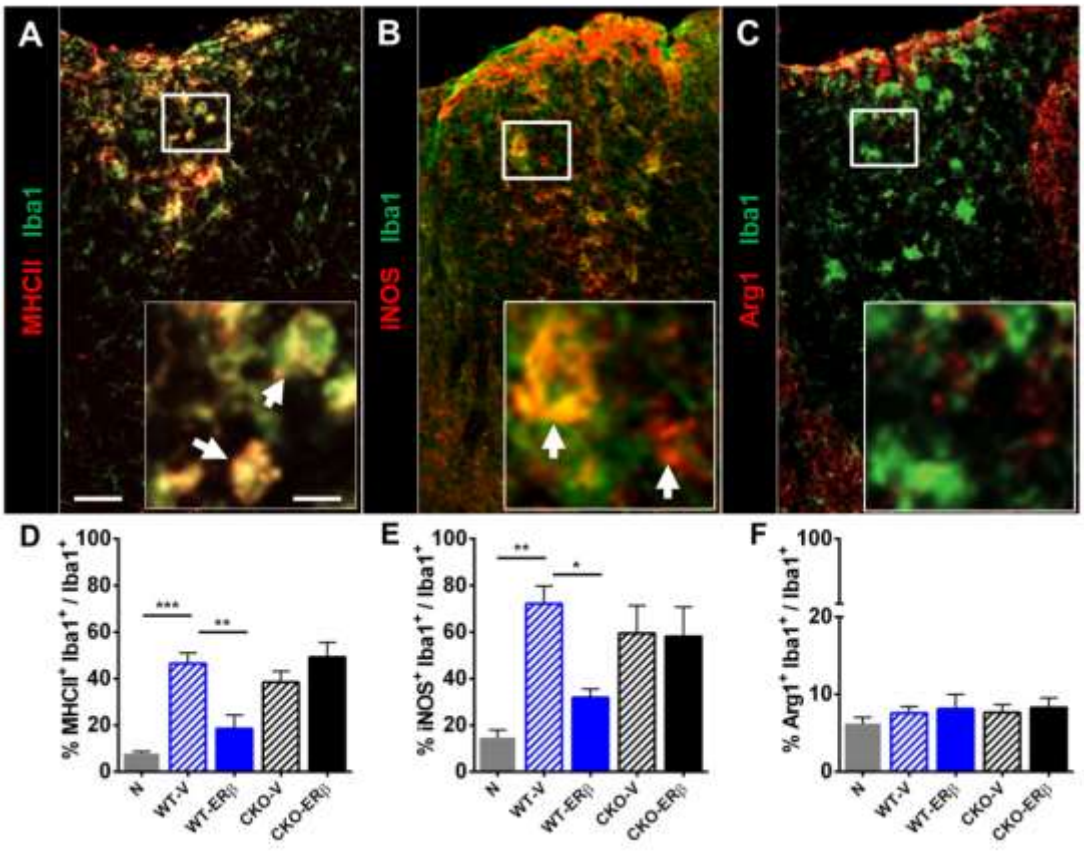

Figure 3.6 Qualitative effects of inflammatory markers on CNS resident and infiltrated Iba1$^+$ myeloid cells. (A) Representative images of spinal cord tissues stained with MHCII (red) and Iba1 (green), **(B)** iNOS (red) and Iba1 (green), and **(C)** Arg1 (red) and Iba1 (green). Scale bar, 50 μm and 10 μm (inset). Inset: white arrows indicate colocalization. **(D)** MHCII$^+$Iba1$^+$ myeloid cells were increased in vehicle treated WT EAE mice (WT-V) compared to healthy controls (N), while ERβ-ligand treated WT EAE mice (WT-ERβ) showed a reduction in percent MHCII$^+$Iba1$^+$ myeloid cells. In contrast, ERβ-ligand treated CKO EAE mice (CKO-ERβ) were no different from vehicle treated CKO EAE mice (CKO-V). (E) iNOS$^+$Iba1$^+$ myeloid cells were also reduced in ERβ-ligand treated WT EAE, but not in CKO EAE mice. **(F)** Arg1$^+$Iba1$^+$ myeloid cells were no differences between groups. *$P < 0.05$; **$P < 0.01$; ***$P < 0.001$. Data are representative of two repeated experiments.

3.2.7 ERβ signaling reduces pro-inflammatory phenotypes of CD11c$^+$ myeloid DC/MΦ during EAE

To characterize the direct effect of ERβ-ligand treatment on CD11c$^+$ microglia and CD11c$^+$ DC/MΦ in the CNS during EAE, we determined expression levels of iNOS, T-bet, CCR2, IL-10, Arg1 and YM-1 in FACS sorted CD11c$^+$ microglia and CD11c$^+$ myeloid DC/MΦ (Figure 3.7A) from the CNS of WT and CKO EAE mice treated with vehicle or ERβ-ligand. We found that pro-inflammatory iNOS and T-bet were reduced, while anti-inflammatory IL-10 was increased in CD11c$^+$ myeloid DC/MΦ from EAE mice treated with ERβ-ligand. In contrast, this ERβ-ligand treatment effect did not occur in CD11c$^+$ myeloid DC/MΦ from CKO mice (Figure 3.7B). Arg1 and YM-1 did not show significant changes. Interestingly, the ERβ-ligand treatment effect on iNOS, T-bet, and IL-10 observed in CD11c$^+$ myeloid DC/MΦ was not observed in CD11c$^+$ microglia. These results suggest that CD11c$^+$ myeloid DC/MΦ, not CD11c$^+$ microglia, are affected by ERβ-ligand treatment to reduce pro-inflammatory phenotypes *ex vivo* during EAE.

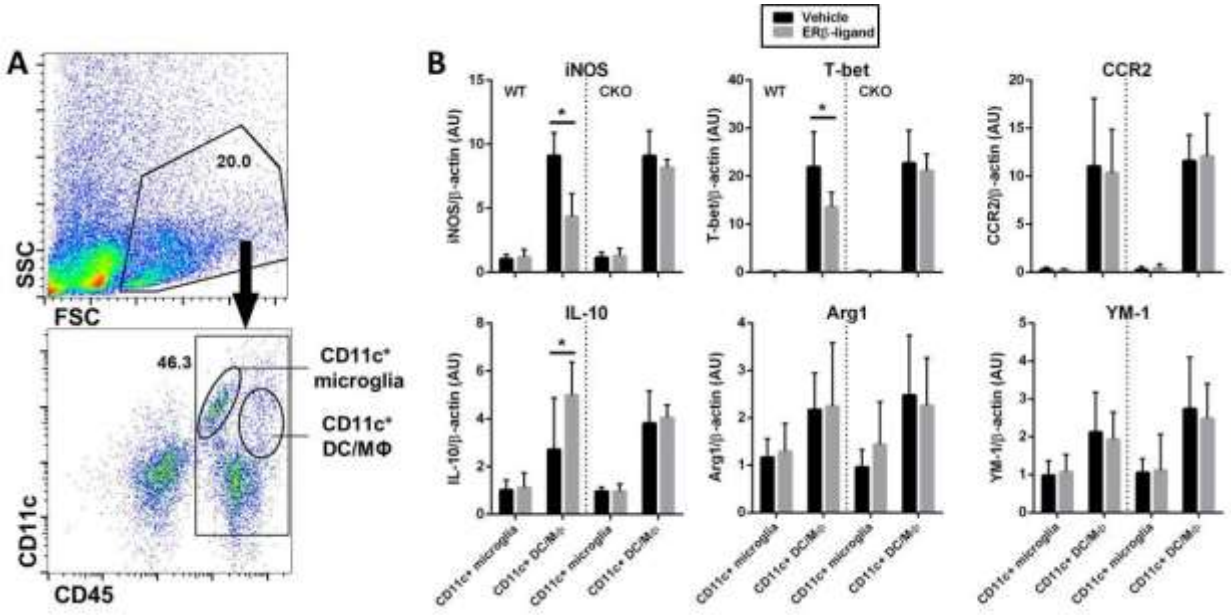

Figure 3.7 ERβ-ligand treatment effects on CD11c$^+$ microglia and CD11c$^+$ myeloid DC/MΦ cells gene expression. (A) Representative flow cytometry plots of isolated CNS mononuclear immune cells from a pool of two to four individual mice. CNS mononuclear immune cells were gated based on SSC and FSC (left), and subpopulations were identified using CD11c and CD45 staining (right). Cell populations labeled as CD11c$^+$ microglia, and CD11c$^+$ myeloid DC/MΦ were FACS sorted for mRNA isolation and quantitative PCR analysis. **(B)** Quantitative analysis of iNOS, T-bet, IL-10, CCR2, Arg1, and YM-1 mRNA expression levels of sorted CD11c$^+$ microglia and CD11c$^+$ myeloid DC/MΦ from WT EAE (left) and CKO EAE (right) mice treated with vehicle or ERβ-ligand. *$P < 0.05$. Data are from three separate experiments, with error bar representing variation between experiments.

3.2.8 ERβ activation on CD11c$^+$ microglia is not important for neuroprotection during EAE

Next, we determined whether direct effects of ERβ-ligand treatment on CD11c$^+$ cells during EAE *in vivo* were shown in resident microglia versus myeloid DC/MΦ. Studying these cell populations independently *in vivo* has been difficult since they share the same lineage (Ginhoux et al., 2010). The recent identification of microglia-specific markers now permits microglia-specific studies *in vitro* without contamination of peripherally derived myeloid cells; however, *in vivo* models are not yet available (Bennett et al., 2016).

To investigate which CD11c$^+$ population mediates the protective effects of ERβ-ligand treatment *in vivo*, we created CKO mice with ERβ deleted in one population, but not the other, using bone marrow chimeras. Bone marrow chimera experiments used C57BL/6J CD45.1 WT mice as donors to determine the reconstitution efficiency of CKO or WT recipient mice (CD45.2)

using flow cytometry with FITC-anti-CD45.2 and PE-anti-CD45.1 labeling of blood leucocytes. The reconstitution efficiency was ~95% (Figure 3.8). Bone marrow chimera (BMC) mice with the CKO of ERβ in $CD11c^+$ cells originating from the CNS ($CD11c^+$ microglia-CKO) were created by injecting CD45.1 WT donor bone marrow cells into irradiated WT versus CKO recipient mice (Figure 3.9A). We observed that chimeric mice with deletion of ERβ in CNS resident $CD11c^+$ microglia (WT→CKO) exhibited protection from clinical EAE with ERβ-ligand treatment, identical to that in chimeric wild-type (WT→WT) EAE mice (Figure 3.9B, Table 3.1). Neuropathology confirmed clinical EAE data, with ERβ-ligand treatment sparing $NF200^+$ axons and MBP^+ myelin and reducing βAPP^+ axons in both groups regardless of selective ERβ deletion in $CD11c^+$ microglia of recipients (Figure 3.9C–E). Lastly, ERβ-ligand treatment reduced MHCII expression in $Iba1^+$ myeloid cells in both WT→WT and WT→CKO EAE groups (Figure 3.9F) There was no effect on quantitative levels of immune cells in the CNS (Figure 3.11A–C). These results demonstrate that ERβ expression on CNS resident $CD11c^+$ microglia is not necessary for neuroprotective effects of ERβ-ligand treatment *in vivo* during EAE.

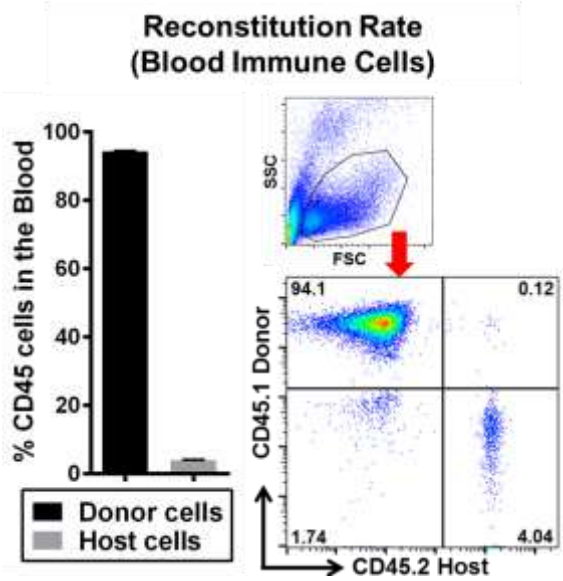

Figure 3.8. Reconstitution efficiency in BMC mice. Blood immune cells were stained with PE-CD45.1 and FITC-CD45.2 antibodies for flow cytometry analysis. Reconstitution rates were calculated based on the percentage donor versus host $CD45.1^+$ or $CD45.2^+$ cells among total $CD45^+$ blood immune cells. Shown is a representative experiment with reconstitution efficiency of 94.28 ± 0.23%.

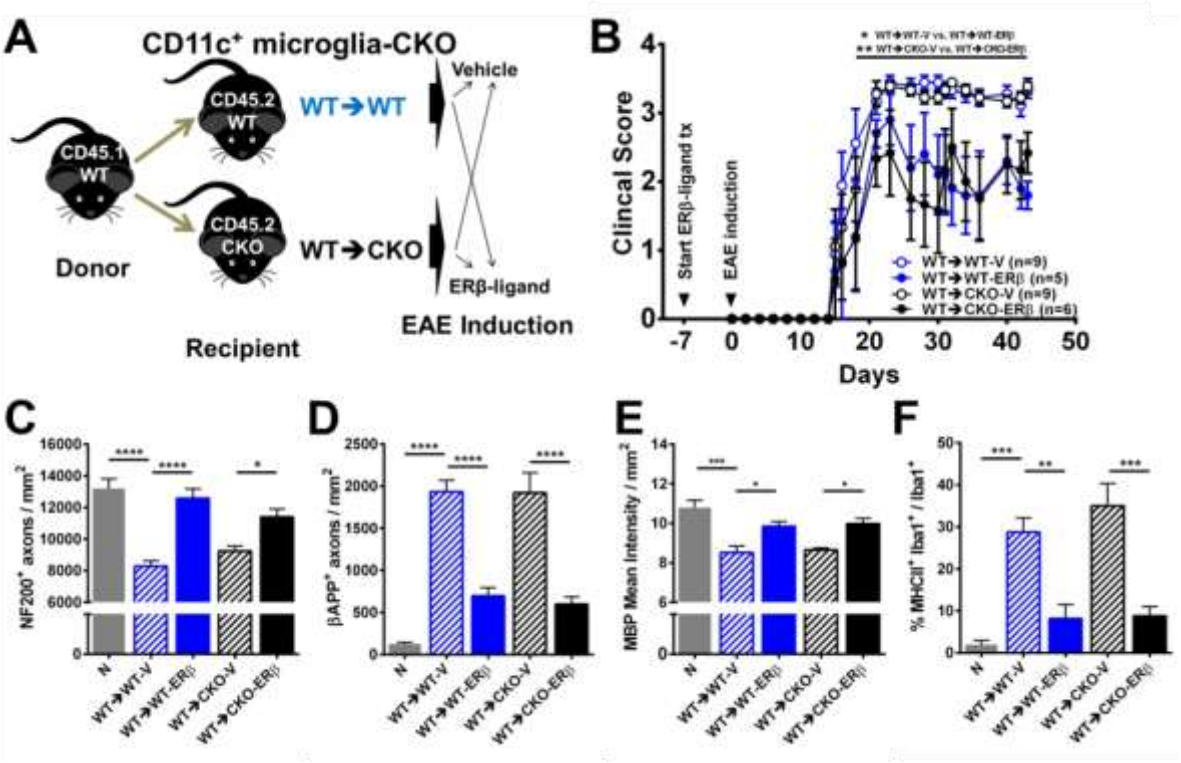

Figure 3.9 CD11c$^+$ microglial ERβ expression is not necessary for neuroprotection in EAE. **(A)** Diagram for creating CD11c$^+$ microglia-CKO using BMC. Briefly, CD45.1 wild-type mice were used as donors for bone marrow cells, and CD45.2 wild-type (WT→WT) or CKO (WT→CKO) were used as irradiated recipients. Each genotype was separated into two groups and received either vehicle or ERβ-ligand treatment (tx), EAE was induced, and mice were scored for EAE severity. **(B)** ERβ-ligand treated wild-type (WT→WT-ERβ, blue solid) EAE mice had significantly better scores compared to vehicle treated wildtype (WT→WT-V, blue clear) EAE mice. Similarly, ERβ-ligand treated CKO (WT→CKO-ERβ, black solid) EAE mice also had significantly better scores compared to vehicle treated conditional knockout (WT→CKO-V, black clear) EAE mice. Detailed EAE statistics are in Table 1. Quantitative analysis of **(C)** NF200$^+$ axonal count, **(D)** βAPP$^+$ axonal count, **(E)** MBP$^+$ myelin intensity, and **(F)** MHCII expression on Iba1$^+$ myeloid derived cells (percentage) in dorsal white matter of the

spinal cord. *P < 0.05; **P < 0.01; ***P < 0.001; ****P < 0.0001. Data are representative of two repeated experiments.

3.2.9 ERβ activation on CD11c$^+$ myeloid DC/MΦ is important for neuroprotection during EAE

Since CD11c$^+$ microglia were not the target of ERβ-ligand treatment *in vivo*, we next created CKO mice with ERβ deleted from CD11c$^+$ cells originating from the periphery (CD11c$^+$ myeloid DC/MΦ-CKO) by collecting donor bone marrow cells from CD45.2 WT or CKO mice and injecting them into irradiated CD45.1 WT recipient mice (Figure 3.10A). In contrast to the protection observed with ERβ-ligand treatment of chimeric WT (WT→WT) EAE mice, ERβ-ligand treatment was not protective in EAE mice with deletion of ERβ in CD11c$^+$ myeloid DC/MΦ (CKO→WT) (Figure 3.10B, Table 1). Neuropathological analyses of NF200$^+$ axons, βAPP$^+$ axons, and MBP$^+$ myelin confirmed that ERβ-ligand treatment mediated neuroprotective effects were lost in CD11c$^+$ myeloid DC/MΦ-CKO mice (Figure 3.10C–E). Also, ERβ-ligand treatment reduced MHCII expression in Iba1$^+$ myeloid cells in WT→WT EAE mice, whereas the protective effect was lost in the CKO→WT EAE mice (Figure 3.10F). There was no effect on quantitative levels of immune cells in the CNS (Figure 3.11D–F). Together, these results show that ERβ expression on CD11c$^+$ myeloid DC/MΦ mediates neuroprotective effects of ERβ-ligand treatment *in vivo* during EAE.

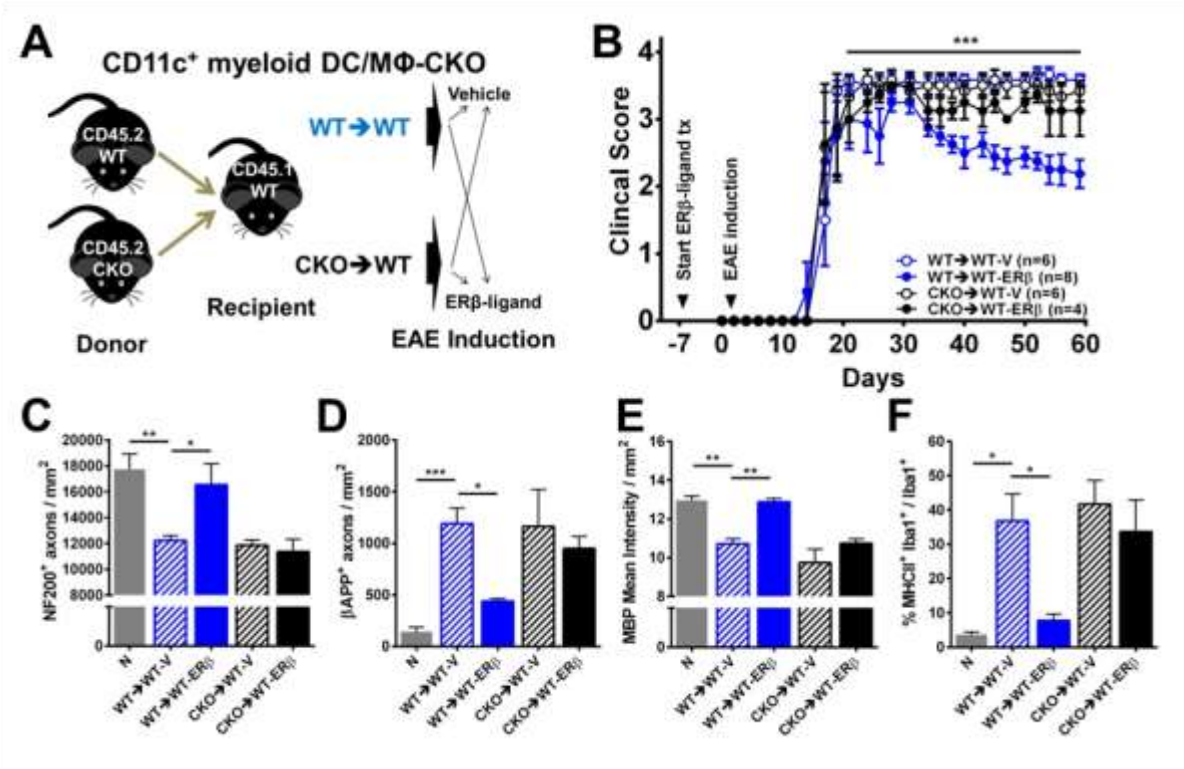

Figure 3.10 ERβ expression on CD11c$^+$ myeloid DC/MΦ is necessary for neuroprotection in EAE. (A) Diagram for creating CD11c$^+$ myeloid DC/MΦ-CKO using bone marrow chimeras. Briefly, CD45.2 wild-type (WT→WT) versus CKO (CKO→WT) mice were used as donors for bone marrow cells, and CD45.1 wild-type mice were used as irradiated recipients. Each genotype was separated into two groups and received either vehicle or ERβ-ligand treatment (tx), EAE was induced, and mice were scored for EAE severity. **(B)** ERβ-ligand treated wild-type (WT→WT-ERβ, blue solid) EAE mice had significantly better EAE scores compared to vehicle treated wild-type (WT→WT-V, blue open) EAE mice, whereas ERβ-ligand mediated protection did not occur in ERβ-ligand treated conditional knockout (CKO→WT-ERβ, black solid) compared to vehicle treated CKO (CKO→WT-V, black clear) EAE mice. Detailed EAE statistics are in Table 1. Quantitative analysis of **(C)** NF200$^+$ axonal count, **(D)** βAPP$^+$ axonal count, **(E)** MBP$^+$ myelin intensity, and **(F)** MHCII expression on Iba1$^+$ myeloid derived cells

(percentage) in dorsal white matter of the spinal cord. *P < 0.05; **P < 0.01; ***P < 0.001; ****P < 0.0001.

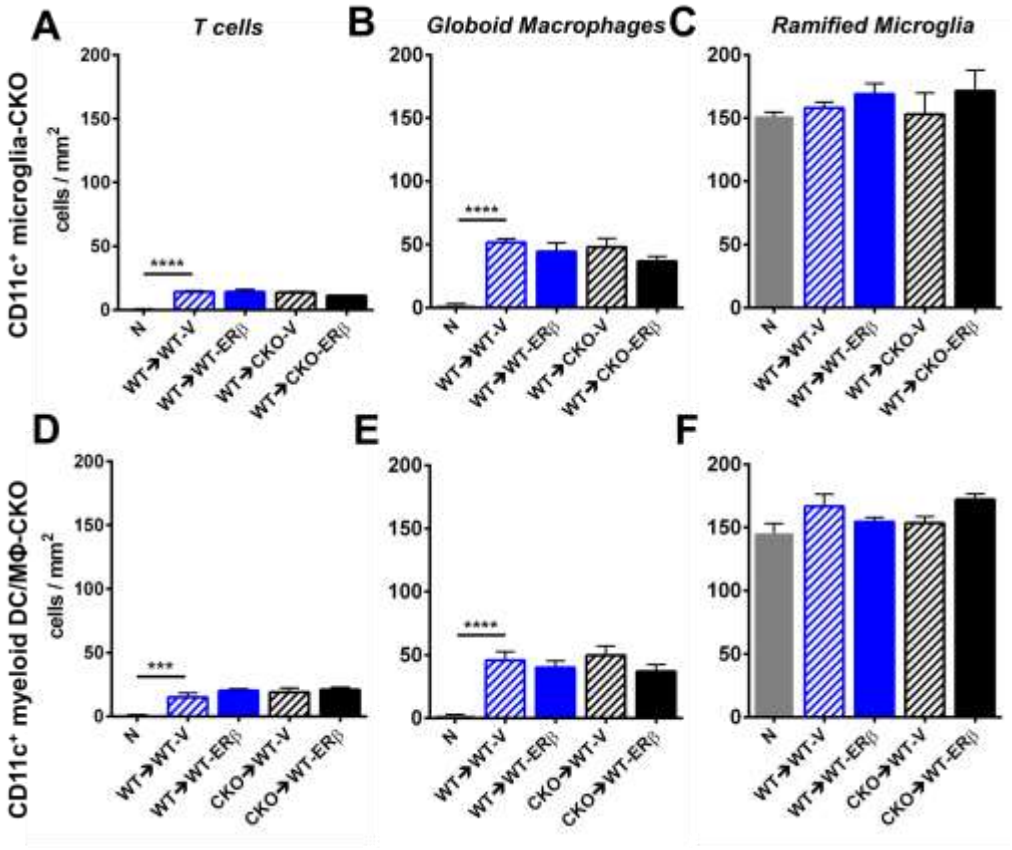

Figure 3.11. No quantitative effects on CNS resident and infiltrated immune cells in BMC EAE mice. Quantitative analysis of **(A and D)** infiltrated $CD3^+$ T cells and **(B and E)** $Iba1^+$ globoid macrophages in the spinal cord white matter of $CD11c^+$ microglia CKO and $CD11c^+$ myeloid DC/MΦ CKO EAE mice, respectively, showed that all EAE groups were increased compared to healthy controls, but no different from each other. **(C and F)** CNS resident $Iba1^+$ ramified microglia cell numbers in the spinal cord white matter were no differences between groups. ***P < 0.001; ****P < 0.0001.

3.2.10 ERβ activation on CD11c$^+$ cells is important for permitting oligodendrocyte maturation.

To understand whether ERβ-ligand treatment on CD11c$^+$ cells has an effect on oligodendrocytes, we investigated Olig2$^+$ oligodendrocyte lineage cell subpopulations using oligodendrocyte precursor cell (OPC) marker chondroitin sulphate proteoglycan (NG2), immature/mature oligodendrocyte marker adenomatous polyposis coli (CC1), and a mature marker glutathione S-transferase-pi (GSTπ) during EAE in WT and CKO mice (Figure 3.12A). The percentages of Olig2$^+$GSTπ$^+$ mature and Olig2$^+$CC1$^+$ immature/mature oligodendrocytes were reduced in WT EAE mice compared to normal controls, and ERβ-ligand treatment increased these cells in WT EAE mice. In contrast, ERβ-ligand treatment of EAE in CKO mice did not induce an increase in these oligodendrocyte subpopulations (Figure 3.12B,C) showing that ERβ-ligand acting on CD11c$^+$ cells was necessary for this effect. Olig2$^+$NG2$^+$ OPCs did not show changes with disease or with ERβ-ligand treatment (Figure 3.12D). Together, these results demonstrate that ERβ-ligand treatment increases immature/mature oligodendrocytes during EAE, suggesting that ERβ-ligands modulatory effects on inflammation are permitting oligodendrocyte maturation, as in CKO mice these beneficial effects no longer occur. To further examine effects of ERβ-ligand treatment on oligodendrocytes, we used mice with deletion of ERβ specifically in Olig1$^+$ oligodendrocyte lineage cells (OLCs).

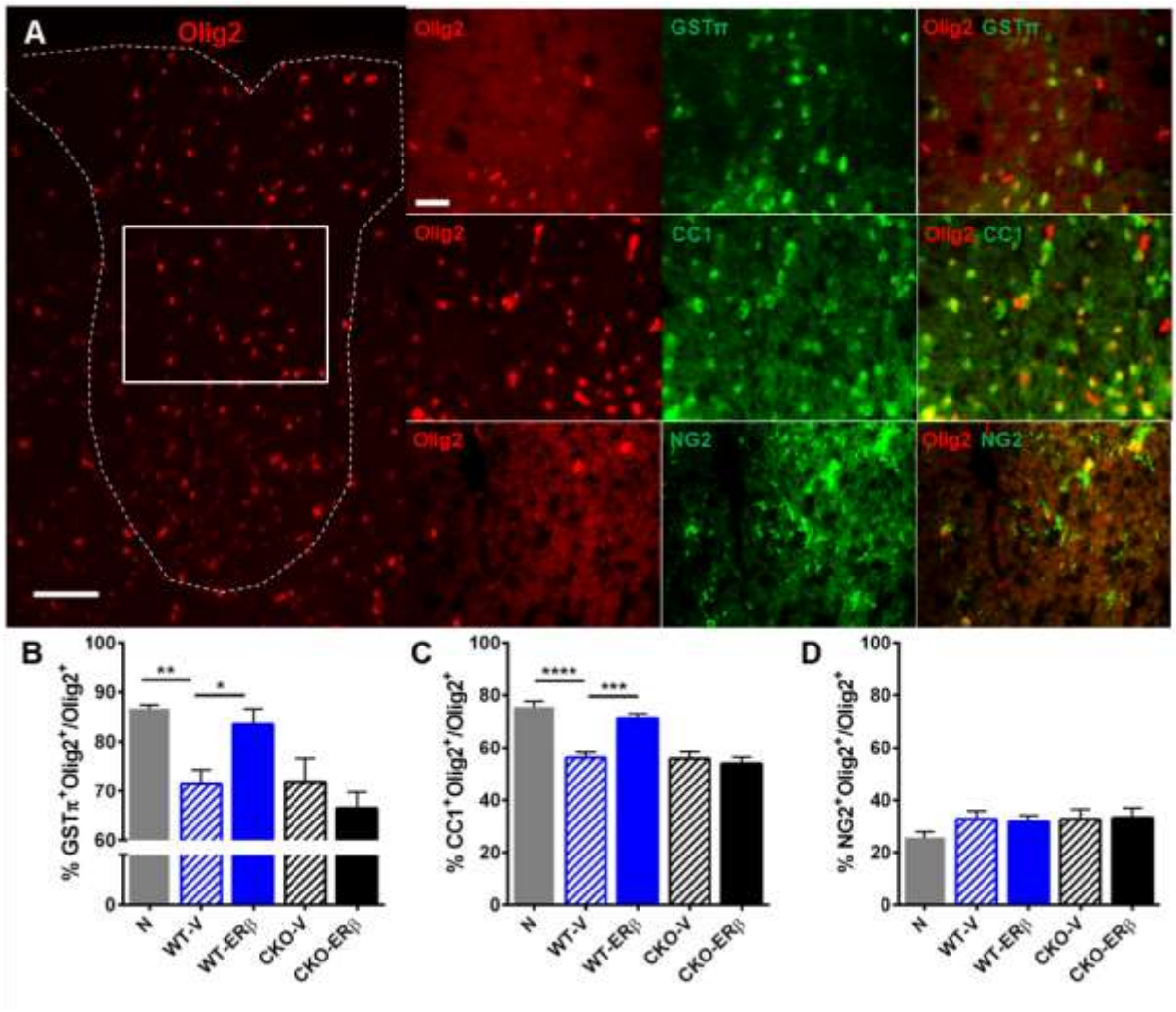

Figure 3.12 ERβ-ligand treatment acts on CD11c$^+$ cells to permit increases in mature oligodendrocytes during EAE. (A) Immunofluorescence images of spinal cord tissues stained with Olig2 (red), and co-stained with GSTπ (green), CC1 (green), and NG2 (green). On the left is a representative image of Olig2$^+$ oligodendrocyte lineage cells (OLC) in dorsal white matter of the spinal cord. On the right are representative images of each co-stain; Olig2-GSTπ (top), Olig2-CC1 (middle) and Olig2-NG2 (bottom). Scale bar, 50 μm (left) and 20 μm (right). The white box indicates the area where the co-stains were imaged. Quantitative analyses of **(B)** Olig2$^+$GSTπ$^+$ mature oligodendrocytes, **(C)** Olig2$^+$CC1$^+$ immature/mature oligodendrocytes, and **(D)** Olig2$^+$NG2$^+$ oligodendrocyte precursor cells, each in dorsal white matter of the spinal cord.

*P < 0.05; **P < 0.01; ***P < 0.001; ****P < 0.0001. Data are representative of two repeated experiments.

3.2.11 ERβ on Olig1$^+$ oligodendrocytes is necessary for ERβ-ligand mediated neuroprotection.

To further examine effects of ERβ-ligand treatment on oligodendrocytes, we used mice with a specific deletion of ERβ specifically in Olig1$^+$ OLCs. We crossed Olig1-cre mice with ERβ$^{fl/fl}$ mice to generate *Olig1*-cre$^+$;ERβ$^{fl/fl}$ mice (Olig1 CKO) and littermate controls *Olig1*-cre$^-$; ERβ$^{fl/fl}$ (Olig1-WT), then induced EAE and treated with ERβ-ligand or vehicle (Figure 3.13A). ERβ-ligand treated Olig1-WT EAE mice exhibited protection from EAE compared to vehicle treated Olig1-WT EAE mice. In contrast, Olig1-CKO EAE mice did not show clinical disease protection with ERβ-ligand treatment, thereby showing direct effects of ERβ-ligand treatment on Olig1$^+$ OLCs (Figure 3.13B, Table 1). Neuropathology of axons and myelin showed that the ERβ-ligand treatment mediated neuroprotective effects were lost in Olig1-CKO EAE mice (Figure 3.13B,C). In contrast, the immunomodulatory effect of ERβ-ligand treatment on MHCII expression on Iba1$^+$ myeloid cells was not lost in Olig1-CKO mice with EAE (Figure 3.13D), differing from how treatment effects on MHCII were lost in CD11c-CKO EAE mice (Figure 3.3A,D). Furthermore, ERβ-ligand treatment increased both the percentage of Olig2$^+$GSTp$^+$ mature oligodendrocytes and Olig2$^+$CC1$^+$ immature/mature oligodendrocytes during EAE in Olig1-WT mice, but both of these effects were lost in Olig1-CKO mice with EAE (Figure 3.13E). Together, these data show that direct effects of ERβ-ligand treatment on CD11c$^+$ cells and on Olig1$^+$ cells are both necessary for neuroprotection during EAE, for one without the other is not sufficient.

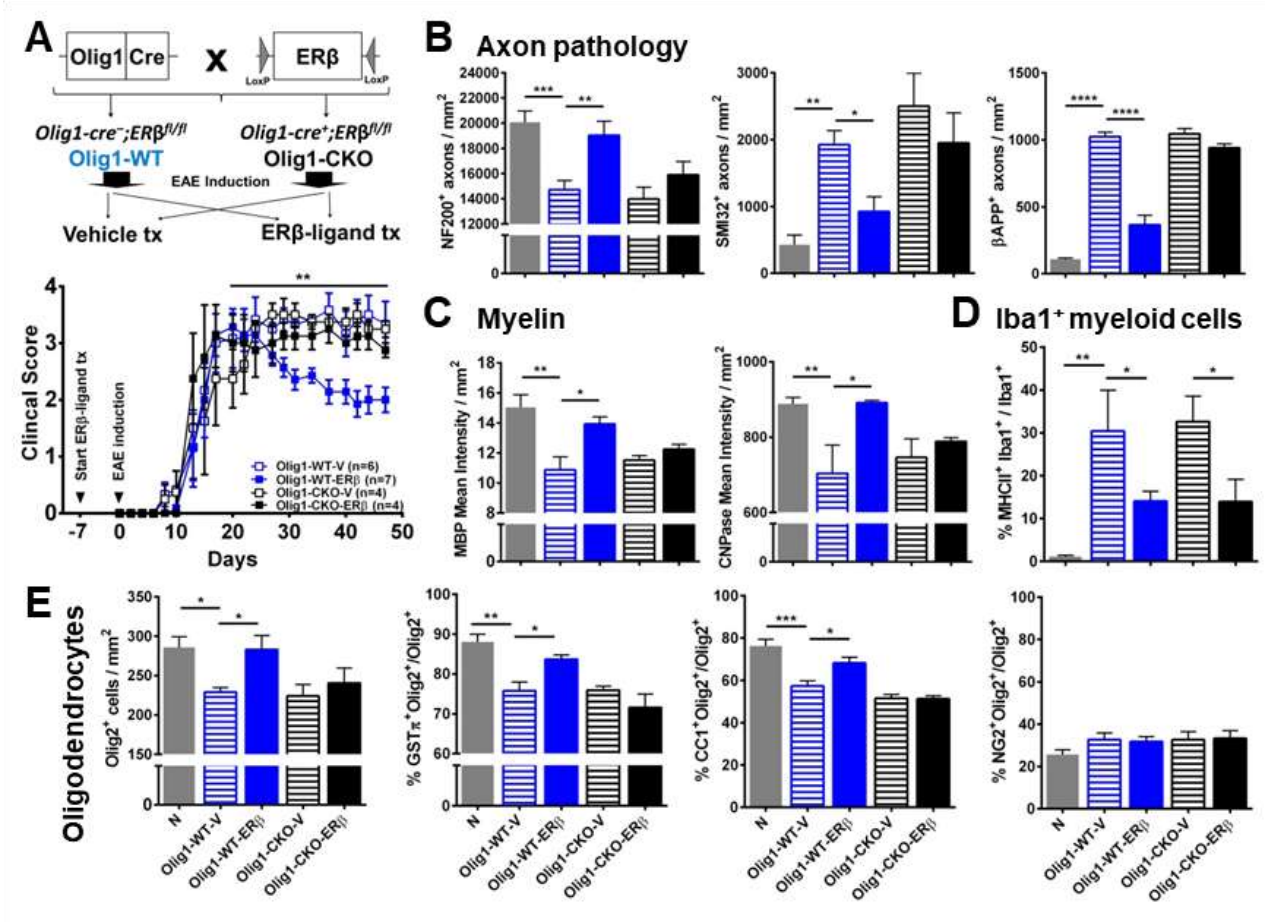

Figure 3.13 ERβ expression on Olig1$^+$ cells is necessary for neuroprotection in EAE. (A) Breeding scheme for creating wildtype (WT) and conditional knockout (CKO) mice of ERβ in Olig1$^+$ cells. Briefly, *Olig1*-Cre$^+$ mice were crossed with mice carrying an ERβ gene flanked by *loxP* sites (ERβ$^{fl/fl}$). Homozygous ERβ$^{fl/fl}$ mice without (Olig1-WT) or with (Olig1-CKO) Cre were generated. Each genotype was separated into two groups and received either vehicle or ERβ-ligand treatment (tx), EAE was induced and mice were scored for EAE severity as above. ERβ-ligand treated Olig1-WT EAE mice (Olig1-WT-ERβ, red) had significantly better clinical scores compared to vehicle treated Olig1-WT EAE mice (Olig1-WT-V, black). In contrast, ERβ-ligand mediated protection did not occur in ERβ-ligand treated Olig1-CKO EAE mice (Olig1-CKO-ERβ, green) when compared to vehicle treated Olig1-CKO EAE mice (Olig1-CKO-V,

blue). Detailed EAE statistics in Table 1. Quantitative analyses of **(B)** $NF200^+$, $SMI32^+$, and βAPP^+ axonal counts, **(C)** MBP^+ and $CNPase^+$ myelin intensity, and **(D)** $MHCII^+Iba1^+$ myeloid cells in dorsal white matter of the spinal cord. **(E)** Quantitative analyses of total $Olig2^+$ OLCs, and the percentage of subpopulations: $Olig2^+NG2^+$ oligodendrocyte precursor cells, $Olig2^+CC1^+$ immature/mature oligodendrocytes, and $Olig2^+GST\pi^+$ mature oligodendrocytes in dorsal white matter of the spinal cord. *P < 0.05; **P < 0.01; ***P < 0.001; ****P < 0.0001. Data are representative of three repeated experiments.

3.3 Discussion

Here we show for the first time that ERβ expressed in $CD11c^+$ cells plays an important role in mediating neuroprotection during EAE. When ERβ was specifically deleted from $CD11c^+$ cells, the protective effect of ERβ-ligand treatment was lost. We then used bone marrow chimeras to show that ERβ in peripherally derived $CD11c^+$ myeloid dendritic cells and macrophages was responsible, while ERβ in $CD11c^+$ microglia was not. We also found that ERβ in $Olig1^+$ OLCs can mediate direct neuroprotective effects during EAE. When effects of ERβ-ligand treatment on either myeloid dendritic cells and macrophages or OLCs were removed, treatment was no longer neuroprotective. Together these in vivo mechanistic studies show that effects on these two cells types are complementary. Direct effects on OLCs increase numbers of mature OLCs during EAE, but direct effects on $CD11c^+$ myeloid dendritic cells and macrophages are also needed to modulate the inflammatory microenvironment in the CNS and avoid an arrest in OLC maturation. These findings underscore the need for combination treatment strategies in EAE that both modulate the inflammatory microenvironment of myeloid dendritic cells and macrophages in the CNS and promote the maturation of oligodendrocytes.

Distinguishing between the effects of ERβ-ligand treatment on CNS resident microglia versus peripheral myeloid dendritic cells and macrophages has therapeutic implications, suggesting that ERβ signaling pathways in myeloid dendritic cells and macrophages are candidate targets. The majority of myeloid dendritic cells and macrophages in the CNS during EAE release pro-inflammatory cytokines and cause myelin and axonal damage. During EAE, the infiltrates are classified as $CD45^{hi}CD11c^{+}CD11b^{+}$ myeloid dendritic cells and macrophages with elevated levels of MHCII, IL-6, iNOS and other pro-inflammatory molecules (King et al., 2009; Vainchtein et al., 2014; Wlodarczyk et al., 2014). Recruitment of these cells through the CCL2-CCR2 axis has been shown to be critical for further recruitment of Th1/Th17 encephalitogenic cells and progression of chronic EAE (Dogan et al., 2008). When MHCII was ablated from these cells, this recruitment was prevented, and EAE was ameliorated (Greter et al., 2005; Clarkson et al., 2015). These reports are consistent with our findings that protection from EAE with ERβ-ligand treatment coincided with reductions in MHCII, iNOS, and T-bet, with an increase in IL-10, in $CD11c^{+}$ myeloid dendritic cells and macrophages in the CNS. That said, the infiltration of myeloid dendritic cells and macrophages is not always detrimental in EAE since they can perform phagocytosis to clear debris and secrete neurotrophic factors for recruitment, differentiation, and maturation of OPCs to facilitate remyelination (Miron et al., 2013; Rawji and Yong, 2013). However, direct ERβ activation on $CD11c^{+}$ myeloid dendritic cells and macrophages did not increase expression of ARG1 and YM-1 markers of this protective phenotype.

A limitation of our study is that bone marrow chimeras are imperfect and can be associated with the microglial pool being a mixed population of resident microglia and those which repopulate from the periphery after irradiation. This could confound interpretation of our

negative findings in Fig. 6 where deletion of ERβ in the $CD11c^+$ microglial population did not prevent ERβ-ligand induced disease protection. The protective effect of ERβ-ligand treatment might have remained in WT→CKO EAE mice if not all of the $CD11c^+$ microglia were devoid of ERβ due to repopulation. However, data in Figure 3.7, where effects of ERβ-ligand treatment on iNOS, T-bet, and IL-10 were found on the $CD11c^+$ myeloid dendritic cell and macrophage population, but not on the $CD11c^+$ microglial population, makes an effect of ERβ-ligand treatment acting on repopulating $CD11c^+$ microglial less likely. That said, our findings focusing on $CD11c^+$ cells do not rule out additional actions of ERβ in $CD11c^-$ microglia.

When ERβ-ligands were first shown to provide neuroprotection during late, but not early, EAE (Tiwari-Woodruff et al., 2007), it suggested that ERβ-ligand conferred protective effects that were unique from other previous EAE treatments, which reduced early EAE as a prelude to reducing late EAE. Translational studies then showed efficacy when ERβ-ligand treatment was started after EAE onset (Kim et al., 1999; Tiwari-Woodruff et al., 2007; Wisdom et al., 2013), together prompting investigations using cell-specific knockouts to assess neuroprotective mechanisms in vivo and laying the foundation for development of next generation oestrogen treatments to maximize ERβ-mediated neuroprotective efficacy, while minimizing ERα-mediated adverse effects, for treatment of neurodegenerative diseases (Nilsson et al., 2011; Paterni et al., 2014; Warner and Gustafsson, 2015). While various ERβ-ligands were protective in EAE, it remained unclear whether in vivo effects could occur directly through binding to ERβ expressed by immune cells. Studies included the classic ERβ-ligand DPN [with an β/α affinity of 70:1 (Meyers et al., 2001; Du et al., 2011)], indazole-Cl [β/α, 107:1 (De Angelis et al., 2005; Moore et al., 2014)], LY3201 [β/α, 19:1 (Richardson et al., 2007; Wu et al., 2013)], and AC-186 [β/α, 830:1 (McFarland et al., 2013; Itoh et al., 2017)]. Also, 5-androstene-3β,17β-diol (β/α, 4:1)

(Kuiper et al., 1997) reduced iNOS, IL-1β, IL-6 and IL-23 expression in cultured activated microglia and astrocytes through recruitment of inhibitory transcription factors to inflammatory promotors, and was protective in EAE, with this protection lost in global ERβ knockouts (Saijo et al., 2011). However, CKO studies of ERβ in astrocytes previously (Spence et al., 2013) and $CD11c^{+}$ microglia here did not show direct effects on these cells *in vivo* during EAE, underscoring important differences between *in vivo* versus *in vitro* studies of these cells. Here, we show direct effects *in vivo* of ERβ-ligand treatment on CNS infiltrated bone marrow derived myeloid DC/MΦ during EAE.

Investigations of neuroprotection induced by estrogen treatment can inform the development of other neuroprotective treatments. The optimal receptor for ligation during treatment, ERβ, has not only been identified, but it has also now been selectively deleted in neurons, astrocytes, oligodendrocytes, microglia and peripheral myeloid cells to determine functional effects *in vivo* during disease. This comprehensive approach has not been applied to any other neuroprotective treatment for any neurological disease. Other putative neuroprotective treatments have used cell-specific conditional knockouts in one, and rarely in two, CNS cell types. The comprehensive approach used with ERβ-ligand treatment permits critical insights herein regarding *in vivo* mechanisms of neuroprotection by contrasting effects in some cells (myeloid DC/MΦ and OLCs) with lack of effects in others (neurons, astrocytes, resident microglia). Specifically, the mechanism of neuroprotection during ERβ-ligand treatment in EAE involves a combination of effects on two developmentally different populations. ERβ ligation on myeloid DC/MΦ is immunomodulatory in the CNS microenvironment, while on OLCs enhances OPC differentiation and maturation to increase remyelination (Khalaj et al., 2013; Kumar et al., 2013; Lariosa-Willingham et al., 2016). The maturation of oligodendrocytes by ERβ-ligand

treatment during EAE cannot occur without immunomodulation of myeloid DC/MΦ in the CNS. Indeed, when each cell type ($CD11c^+$ or $Olig1^+$) is targeted for ERβ specific deletion independently, neuroprotective treatment effects are lost. Thus, each is necessary, but not sufficient. This emphasizes the importance of developing treatment strategies targeting not only for remyelination but also inhibition of pro-inflammatory bone marrow-derived DC/MΦ. Targeting ERβ signaling pathways in cells of these two distinct lineages may be ideally suited to achieve neuroprotection in multiple sclerosis and perhaps other neurodegenerative diseases.

3.4 Methods and materials

Animals Mice with ERβ selective deletion on $CD11c^+$ and $Olig1^+$ cells were generated by crossing transgenic mice that express Cre under the regulation of the *CD11c* promoter. C57BL/6J-Tg(*Itgax*-cre,EGFP)4097Ach/J mice (CD11c-cre) was purchased from Jackson Laboratory (Lu et al., 2002; Stranges et al., 2007), and crossed with C57BL/6J-$ERβ^{floxed/floxed}$ mice carrying a ERβ (*Esr2*) gene flanked by LoxP sites, a gift from Dr. Pierre Chambon, France (Antal et al., 2008). For the bone marrow chimera study, we used a C57BL/6J congenic strain B6.SJL-*Ptprc*a*Pepc*b/BoyJ (CD45.1) mice (Shen et al., 1985). Animals were maintained under standard conditions in a 12 h dark/12 h light cycle with access to food and water *ad libitum*. All procedures were done in accordance to the guidelines of the National Institutes of Health and the Chancellor's Animal Research Committee of the University of California, Los Angeles Office for the Protection of Research Subjects.

Surgery (ovariectomy) To eliminate the effects of circulating endogenous estrogens during the experiments, ovariectomy was performed in female mice when they were 4 to 5 weeks old. Mice

were anesthetized by inhalational anesthesia with isoflurane. Carprofen (1.2 mg/ml per animal, Zoetis) and 0.5 ml of saline were injected subcutaneously before the procedure. The fur above the lateral dorsal back was removed, and the skin was sterilized with betadine and alcohol scrubs. Bilateral incisions were made into the back. A hemostat was placed on the fallopian tubes, and the ovaries were removed. Muscle layer was closed with absorbable suture, and the skin layer was closed with wound clips. Amoxicillin (50 mg/ml, Virbac) was added to the water for 5 days for antibiotics (0.5 mg/ml water), and another dose of carprofen was given within 24 h following surgery. Wound clips were removed 7 days later. All procedures were approved by the Office of Animal Research Oversight and UCLA institutional animal care and use committee, known locally as the Chancellor's Animal Research Committee.

Experimental autoimmune encephalomyelitis induction and ERβ-ligand treatment Female mice were immunized subcutaneously with myelin oligodendrocyte glycoprotein (MOG), amino acids 35–55 (200 μg per mouse, Mimotopes) emulsified in Complete Freund's Adjuvant, supplemented with *Mycobacterium Tuberculosis* H37Ra (200 μg per mouse, Difco Laboratories), over two sites drained by left inguinal and auxiliary lymph nodes in a total volume of 0.1 ml per mouse (Day 0). Pertussis toxin (500 ng per mouse, List Biological Laboratories) was injected intraperitoneally on Day 0 and Day 2. On Day 7, a booster immunization was delivered over contralateral lymph nodes. Ages of female mice for EAE induction were 8 to 12 weeks. The animals were monitored daily for EAE signs based on a standard EAE 0–5 scale scoring system: 0, healthy; 1, complete loss of tail tonicity; 2, loss of righting reflex; 3, partial paralysis; 4, complete paralysis of one or both hind limbs; and 5, moribund (Kim et al., 2014). For ERβ-ligand treatment we used diarylpropionitrile (DPN). Treatment was initiated 1 week before EAE

induction. Briefly, DPN was dissolved in 100% EtOH and then mixed into 100% Miglyol® 812 (CREMER Oleo GmbH & Co. KG) at 1:9 ratio making the final EtOH concentration 10%, and given subcutaneously every other day at a dose of 8 mg/kg per day until the end of each experiment. Selectivity of DPN at this dose was shown using the sensitive off target outcome of uterine weight. All assessments were done in a blinded fashion with regards to knowledge of treatment randomization. For randomization of mice, after ovariectomy and before EAE induction, recovered healthy mice from each genotype were randomly assigned to treatment with Vehicle or ERβ-ligand. For blinding of drug treatment, third party concealment with color coded labeling of Vehicle or ERβ-ligand treatment syringes was done before treatment started for each experiment.

Histological preparation Mice were exposed to a lethal dose of isoflurane and perfused transcardially with ice-cold 1xPBS for 8 min, followed by 10% buffered formalin for 8 min. Spinal cords were dissected and stored in 10% buffered formalin for 12 h overnight, then submerged in 30% sucrose, 0.1% sodium azide, 1xPBS for 24 h at 4℃. A thoracic and lumbar portion of the spinal cords were cut and embedded in optical cutting temperature compound (OCT, Tissue Tek) and stored at -80℃ after flash frozen in an isopropanol bath chilled with liquid nitrogen. Tissues were cryosectioned at -25°C into 40 μm thick sections using a cryostat (Leica CM1860) and stored in 0.1% sodium azide, 1xPBS at 4℃ before used for immunofluorescence staining.

Immunofluorescence staining Spinal cord sections were washed thoroughly using 1xPBS with 0.1% TritonX-100 (PBSt) to remove residual sodium azide. In the case of anti-MBP staining,

tissue sections were incubated with 5% glacial acetic acid, 95% EtOH solution for 30 min at room temperature (RT) and then washed with 1xPBSt before blocking. For blocking, tissues were treated with 10% normal goat serum in 1xPBSt for 1 h at RT. Primary antibody and secondary antibody staining were done at appropriate concentrations with 2% normal goat serum, 1xPBSt for overnight at 4℃ and 1 h at RT, respectively. Primary antibodies: anti-ERβ 1:100 (ab3577, Abcam), anti-ERβ 1:500 (68-4, EMD Millipore), anti-EGFP 1:1000 (NB100-1700, Novus Biologicals), anti-NF200 1:750 (N4142, Sigma), anti-SMI32 1:1000 (NE1023, EMD Millipore), anti-βAPP 1:200 (51-2700, Thermo Fisher Scientific), anti-MBP 1:750 (MAB386, EMD Millipore), anti-CNPase 1:500 (MAB326R, EMD Millipore), anti-CD3 1:2000 (1F4, BD Biosciences), anti-Iba1 1:500 (sc-32725, Santa Cruz Biotechnology), anti-Iba1 1:10,000 (Wako Chemicals), anti-MHCII (I-A/I-E) 1:400 (M5/114.15.2, Biolegend), anti-iNOS 1:500 (AB5384, EMD Millipore), anti-Arg1 1:100 (BD Biosciences), anti-Olig2 1:1000 (AB9610, EMD Millipore), anti-Olig2 1:200 (MABN50, EMD Millipore), anti-NG2 1:500 (AB5320 EMD Millipore), anti-CC1 1:500 (OP80, Calbiochem), and anti-GSTπ 1:1000 (ADI-MSA-102, Enzo Life Sciences). Secondary antibodies: all secondary antibodies (1:1000) were produced from goat and the followings were used for staining the tissues: anti-rabbit-Cy3 (AP132C, EMD Millipore), anti-rabbit-DyLight® 649 (AP187SD, EMD Millipore), anti-mouse-DyLight® 649 (AP181SD, EMD Millipore), anti-rat-Cy3 (AP136C, EMD Millipore), and anti-rat-Cy5 (AB6565, Abcam). Nuclei were stained with DAPI at 1:5000 concentrations in 1xPBS. After serial washes sections were mounted onto slides (Superfrost® Plus, VWR) allowed to semi-dry, and coverslipped (24x60, Fisher Scientific) with fluoromount® G (SouthernBiotech) for confocal microscopy.

Confocal microscopy and image analysis Stained sections were examined and imaged using Olympus BX51 fluorescence microscope with a DP50 digital camera. Images were taken in stacks, 10x images were taken at 10–μm thickness with 2–μm stacks and 40x images were taken at 5–μm thickness with 1μm stacks. All images were taken and processed using the integrated software program Slidebook4.2 (Intelligent Imaging Innovations). ImageJ (NIH) was used to perform integration and analysis of images. All analyses were done in a blinded fashion with regards to knowledge of treatment randomization.

Electron Microscopy Mice were exposed to a lethal dose of isoflurane and perfused transcardially with ice-cold 1xPBS for 8 min, followed by 2.5% glutaraldehyde, 2% paraformaldehyde in 0.1M phosphate buffer, 0.9% sodium chloride (PBS) for 8 min. Thoracic portions of the spinal cords were dissected and post fixed for 2 hours at room temperature in the same fixative and stored at 4℃ until processing. Tissues were washed with PBS, post fixed in 1% OsO4 in ddH20 for 90 minutes on ice, dehydrated in a graded series of ethanol, treated with propylene oxide and infiltrated with Eponate 12TM (Ted Pella) overnight. Tissues were embedded in fresh Eponate and polymerized at 60℃ for 48 hours. Approximately 50-60 nm thick sections were cut on an RMC MT-X ultramicrotome and picked up on formvar coated copper grids. The sections were stained with uranyl acetate and lead citrate and examined on a JEOL 100CX electron microscope at 60kV. Images were collected on type 4489 EM film, and the negatives scanned to create digital files. Films (Kodak) were developed and scanned at high resolution. The analysis was done with ImageJ and g-ratio was used for the extent of remyelination on axons. g-ratio = (axon diameter) / (axon + outer myelin diameter).

CNS immune cell isolation and flow cytometry and cell sorting Animals were overdosed with isoflurane and perfused transcardially with 10 ml of 1xPBS within 2 min. Brain and spinal cords were collected into a 15 ml tube with 2 ml of 2% FBS in 1xPBS (FACS buffer). Collected CNS tissues were passed through 70 μm followed by 40 μm cell strainers to obtain single cell suspensions. Cells were centrifuged at 1500 rpm for 5 min at 4℃ and resuspended in 30% Percoll solution (GE Healthcare Biosciences). The resuspended solution was then layered onto 70% Percoll solution, carefully so that the two solutions do not mix, and centrifuged for 1500 rpm for 20 min at 4℃. After centrifugation mononuclear CNS immune cells were collected at the 70%:30% interface of Percoll solution and washed. Cells were stained with premixed combination of antibodies: APC-anti-CD11c (N418, BioLegend), PE-anti-CD45 (30-F11, Biolegend), PerCP/Cy5.5-anti-CD11b (M1/70, Biolegend), incubated for 30 min at 4℃ and washed thoroughly. For FACS sorting, cells were stained with premixed combination of antibodies: APC-anti-CD11c and PE-anti-CD45, and incubated for 30min at 4℃. Flow cytometry was performed using BD LSRFortessa cytometer and FACS sorting was performed using BD FACSAriaIII High-Speed Cell Sorter at the UCLA Jonsson Comprehensive Cancer Center (JCCC) and Center for AIDS Research Flow Cytometry Core Facility that is supported by National Institutes of Health awards P30 CA016042 and 5P30 AI028697, and by the JCCC, the UCLA AIDS Institute, the David Geffen School of Medicine at UCLA, the UCLA Chancellor's Office, and the UCLA Vice Chancellor's Office of Research. The analysis was performed with FlowJo software (Tree Star).

RNA isolation and quantitative PCR of sorted CD11c^{+} cells from the CNS FACS sorted cells were centrifuged at 2000 rpm for 5min at 4℃ and resuspended in TRI Reagent® (Zymo

Research). RNA was isolated using the Direct-zol™ RNA MiniPrep Plus kit (Zymo Research) according to manufacturer's instructions. cDNA was synthesized using the Tetro cDNA Synthesis kit (Bioline) according to manufacturer's instructions. Quantitative PCR was performed using PowerUp™ SYBR™ Green Master Mix (Thermo Fisher Scientific) on the Bio-Rad Opticon 2 qPCR / Peltier Thermal Cycler according to manufacturer's instruction. Primers are listed in Table 3. The efficiency of each set of primers was assessed by qPCR on a serial dilution of cDNA from spleen immune cells and was confirmed to be above 90%. All gene expression levels were normalized to levels of β-Actin using the ΔΔCt and expressed as fold change relative to $CD11c^+$ microglia cells sorted from vehicle treated WT EAE mice.

Primer list for quantitative PCR

Actβ (5′-GGCTCCTAGCACCATGAAGA-3′, 5′-ACTCCTGCTTGCTGATCCAC-3′)

Nos2 (5′-GTGACACACAGCGCTACAAC-3′, 5′-GATGGTCACATTCTGCTTCTGG-3′)

Tbx21 (5′-ATGCCAGGGAACCGCTTAT-3′, 5′-ATTGTTGGAAGCCCCCTTGT-3′)

Il-10 (5′-CAGTACAGCCGGGAAGACAA-3′, 5′- TGGCAACCCAAGTAACCCTTA-3′)

Ccr2(5′-CATCTGCAAAAACAAATCAAAGGA-3′, 5′-GACAAGGCTCACCATCATCG-3′)

Arg1 (5′-ACATTGGCTTGCGAGACGTA-3′, 5′-ATCGGCCTTTTCTTCCTTCCC-3′)

Chil3 (5′-GCAGAAGCTCTCCAGAAGCAAT-3′, 5′-TCCCTTCTATTGGCCTGTCCT-3′)

Esr2 (5′-ATTCTTCTCAAGCAGGTGGCCC-3′, 5′-TTGGATCTGGTGCAGCAAGG-3′)

Bone marrow chimera (BMC)

BM cell collection from donor mice: Cells were isolated from femurs and tibias of age-matched female donors. BM cells were subjected to T and B cells depletion by AutoMACS Magnetic Cell

Separator (Miltenyi Biotec). Briefly, cells were incubated with anti-CD90.2 and anti-CD19 Miltenyi Biotec microbeads at 1:9 dilutions in AutoMACS buffer solution for 15 min at 4℃. Cells were then washed with AutoMACS buffer, resuspended at a concentration of 1 x 10^8 cells per 500 μL, and passed through AutoMACS Magnetic Cell Separator columns using the "Deplete" program. Collected cells were washed and resuspended at the concentration of 1.5 x 10^7 cells per 0.2 mL per mouse in lactated Ringer's solution (Abbott Laboratories).

Preparation and irradiation of recipient mice. Female mice were first ovariectomized at 4 to 5 weeks old and rested 2 weeks for recovery, as described earlier. Mice used for BMC received sulfamethoxazole and trimethoprim (TMS, 0.5 mg/ml water) for antibiotics. The mice were then subjected to irradiation once with a dose of 850 rads using ^{137}Cesium source irradiator (Model MKI-68A, JL Shepherd) provided by the UCLA Center for AIDS Research Humanized Mouse Core, supported by National Institutes of Health (NIH) grant P30AI28697. Within 1 to 2 h, irradiated mice received BM cells collected from the donors via tail vein injections. After transplantation, animals were given TMS mixed in autoclaved water for 7 weeks.

Experimental autoimmune encephalomyelitis induction and drug treatment. Female mice were immunized subcutaneously with MOG peptide 35–55 emulsified in Complete Freund's Adjuvant, supplemented with *Mycobacterium Tuberculosis* H37Ra, over four sites drained by inguinal and auxiliary lymph nodes on both sides in a total volume of 0.1 ml per mouse and received one dose of pertussis toxin (500 ng per mouse, List Biological Laboratories) intraperitoneally on Day 0. Ages of female mice for EAE induction were 14 to 16 weeks due to the time needed for recovery from transplantation and reconstitution. ERβ-ligand was treated 1 week before induction, where healthy mice from each genotype were randomly assigned to treatment with Vehicle or ERβ-

ligand. Treatment was given subcutaneously every other day at a dose of 8 mg/kg per day until the end of each experiment.

Reconstitution Rate Mice were anesthetized by inhalational anesthesia with isoflurane and blood was drawn by retro-orbital puncture. Briefly, 100 ul of blood was collected using 0.5 M EDTA coated 50 μl microcapillary pipets (Kimble Glass). The collected blood was treated with anti-CD16/32 (93, BioLegend) for 10 min at RT for blocking; then cells were stained with a premixed combination of antibodies: PE-anti-CD45.1 (A20, Biolegend) and FITC-anti-CD45.2 (104, Biolegend), for 30 min at RT. Stained cells were subjected to RBC lysis/fixation buffer (Biolegend) and washed thoroughly for flow cytometry. Flow cytometry was performed using the BD LSRFortessa cytometer at the UCLA Jonsson Comprehensive Cancer Center (JCCC) and Center for AIDS Research Flow Cytometry Core Facility.

Statistical Analysis Statistical analyses of EAE experiments were evaluated using two-way ANOVA with Bonferroni's multiple comparison tests. This test was performed due to the existence of two variables, conditional knockout, and drug treatment. In addition, repeated measures were used to observe the treatment effects over time during EAE. Statistical analyses of neuropathological experiments were evaluated using one-way ANOVA with Bonferroni's multiple comparison tests, comparing treatment effects in two different transgenic groups. Data are presented as means ± s.e.m. Power calculations for EAE experiments were determined for sample size to reach $P < 0.05$ by Myung S. Sim, M.S. Dr.PH, in the Department of Medicine Statistic Core at UCLA. A minimum of five animals per EAE group was stated to provide statistical significance at a level of $P < 0.05$ using 95% power analysis, consistent with numbers

for EAE experiments in the field. Mice that never exhibited signs of EAE or died during an experiment were excluded, based on previously established criteria in the lab. Specifically, mice with EAE induced, but never exhibit signs of EAE, will be excluded from the study. In addition, mice that die during experiments will be excluded, due to inability to carry forward previous scores over time during repeated measures. This criterion was applied equally to all groups. Data distribution was assumed to be normal. All statistical analyses were performed using Prizm 6 (version 6.01) software (GraphPad, CA).

3.5 Bibilography

Antal MC, Krust A, Chambon P, Mark M. Sterility and absence of histopathological defects in nonreproductive organs of a mouse ERbeta-null mutant. Proc Natl Acad Sci USA 2008; 105: 2433–8.

Bailey SL, Schreiner B, McMahon EJ, Miller SD. CNS myeloid dendritic cells presenting endogenous myelin peptides ‘preferentially' polarize CD4+ T(H)-17 cells in relapsing EAE. Nat Immunol 2007; 8: 172–80.

Bennett ML, Bennett FC, Liddelow SA, Ajami B, Zamanian JL, Fernhoff NB., et al. New tools for studying microglia in the mouse and human CNS. Proc Natl Acad Sci USA 2016; 113: E1738–46.

Bulloch K, Miller MM, Gal-Toth J, Milner TA, Gottfried-Blackmore A, Waters EM., et al. CD11c/EYFP transgene illuminates a discrete network of dendritic cells within the embryonic, neonatal, adult, and injured mouse brain. J Comp Neurol 2008; 508: 687–710.

Clarkson BD, Walker A, Harris MG, Rayasam A, Sandor M, Fabry Z. CCR2-dependent dendritic cell accumulation in the central nervous system during early effector experimental

autoimmune encephalomyelitis is essential for effector T cell restimulation in situ and disease progression. J Immunol 2015; 194: 531–41.

De Angelis M, Stossi F, Carlson KA, Katzenellenbogen BS, Katzenellenbogen JA. Indazole estrogens: highly selective ligands for the oestrogen receptor beta. J Med Chem 2005; 48: 1132–44.

Dogan RN, Elhofy A, Karpus WJ. Production of CCL2 by central nervous system cells regulates development of murine experimental autoimmune encephalomyelitis through the recruitment of TNF- and iNOS-expressing macrophages and myeloid dendritic cells. J Immunol 2008; 180: 7376–84.

Du S, Sandoval F, Trinh P, Umeda E, Voskuhl R. Oestrogen receptor-beta ligand treatment modulates dendritic cells in the target organ during autoimmune demyelinating disease. Eur J Immunol 2011; 41: 140–50.

Ginhoux F, Greter M, Leboeuf M, Nandi S, See P, Gokhan S., et al. Fate mapping analysis reveals that adult microglia derive from primitive macrophages. Science 2010; 330: 841–5.

Greter M, Heppner FL, Lemos MP, Odermatt BM, Goebels N, Laufer T., et al. Dendritic cells permit immune invasion of the CNS in an animal model of multiple sclerosis. Nat Med 2005; 11: 328–34.

Itoh N, Kim R, Peng M, DiFilippo E, Johnsonbaugh H, MacKenzie-Graham A., et al. Bedside to bench to bedside research: oestrogen receptor beta ligand as a candidate neuroprotective treatment for multiple sclerosis. J Neuroimmunol 2017; 304: 63–71.

Itoh Y, Voskuhl RR. Cell specificity dictates similarities in gene expression in multiple sclerosis, Parkinson's disease, and Alzheimer's disease. PLoS One 2017; 12: e0181349.

Karman J, Ling C, Sandor M, Fabry Z. Initiation of immune responses in brain is promoted by local dendritic cells. J Immunol 2004; 173: 2353–61.

Khalaj AJ, Yoon J, Nakai J, Winchester Z, Moore SM, Yoo T., et al. Estrogen receptor (ER) beta expression in oligodendrocytes is required for attenuation of clinical disease by an ERbeta ligand. Proc Natl Acad Sci USA 2013; 110: 19125–30.

Kim RY, Hoffman AS, Itoh N, Ao Y, Spence R, Sofroniew MV., et al. Astrocyte CCL2 sustains immune cell infiltration in chronic experimental autoimmune encephalomyelitis. J Neuroimmunol 2014; 274: 53–61.

Kim S, Liva SM, Dalal MA, Verity MA, Voskuhl RR. Estriol ameliorates autoimmune demyelinating disease: implications for multiple sclerosis. Neurology 1999; 52: 1230–8.

King IL, Dickendesher TL, Segal BM. Circulating Ly-6C+ myeloid precursors migrate to the CNS and play a pathogenic role during autoimmune demyelinating disease. Blood 2009; 113: 3190–7.

Kuiper GG, Carlsson B, Grandien K, Enmark E, Haggblad J, Nilsson S., et al. Comparison of the ligand binding specificity and transcript tissue distribution of estrogen receptors alpha and beta. Endocrinology 1997; 138: 863–70.

Kumar S, Patel R, Moore S, Crawford DK, Suwanna N, Mangiardi M., et al. Estrogen receptor beta ligand therapy activates PI3K/Akt/mTOR signaling in oligodendrocytes and promotes remyelination in a mouse model of multiple sclerosis. Neurobiol Dis 2013; 56: 131–44.

Lariosa-Willingham KD, Rosler ES, Tung JS, Dugas JC, Collins TL, Leonoudakis D. A high throughput drug screening assay to identify compounds that promote oligodendrocyte differentiation using acutely dissociated and purified oligodendrocyte precursor cells. BMC Res Notes 2016; 9: 419.

Lelu K, Laffont S, Delpy L, Paulet PE, Perinat T, Tschanz SA., et al. Estrogen receptor alpha signaling in T lymphocytes is required for estradiol-mediated inhibition of Th1 and Th17 cell differentiation and protection against experimental autoimmune encephalomyelitis. J Immunol 2011; 187: 2386–93.

Lu QR, Sun T, Zhu Z, Ma N, Garcia M, Stiles CD., et al. Common developmental requirement for Olig function indicates a motor neuron/oligodendrocyte connection. Cell 2002; 109: 75–86.

Mackenzie-Graham AJ, Rinek GA, Avedisian A, Morales LB, Umeda E, Boulat B., et al. Estrogen treatment prevents gray matter atrophy in experimental autoimmune encephalomyelitis. J Neurosci Res 2012; 90: 1310–23.

McFarland K, Price DL, Davis CN, Ma JN, Bonhaus DW, Burstein ES., et al. AC-186, a selective nonsteroidal estrogen receptor beta agonist, shows gender specific neuroprotection in a Parkinson's disease rat model. ACS Chem Neurosci 2013; 4: 1249–55.

Mei F, Fancy SP, Shen YA, Niu J, Zhao C, Presley B., et al. Micropillar arrays as a high-throughput screening platform for therapeutics in multiple sclerosis. Nat Med 2014; 20: 954–60.

Meyers MJ, Sun J, Carlson KE, Marriner GA, Katzenellenbogen BS, Katzenellenbogen JA. Estrogen receptor-beta potency-selective ligands: structure-activity relationship studies of diarylpropionitriles and their acetylene and polar analogs. J Med Chem 2001; 44: 4230–51.

Miller SD, McMahon EJ, Schreiner B, Bailey SL. Antigen presentation in the CNS by myeloid dendritic cells drives progression of relapsing experimental autoimmune encephalomyelitis. Ann N Y Acad Sci 2007; 1103: 179–91.

Miron VE, Boyd A, Zhao JW, Yuen TJ, Ruckh JM, Shadrach JL., et al. M2 microglia and macrophages drive oligodendrocyte differentiation during CNS remyelination. Nat Neurosci 2013; 16: 1211–18.

Mishra MK, Yong VW. Myeloid cells - targets of medication in multiple sclerosis. Nat Rev Neurol 2016; 12: 539–51.

Moore SM, Khalaj AJ, Kumar S, Winchester Z, Yoon J, Yoo T., et al. Multiple functional therapeutic effects of the estrogen receptor beta agonist indazole-Cl in a mouse model of multiple sclerosis. Proc Natl Acad Sci USA 2014; 111: 18061–6.

Morales LB, Loo KK, Liu HB, Peterson C, Tiwari-Woodruff S, Voskuhl RR. Treatment with an estrogen receptor alpha ligand is neuroprotective in experimental autoimmune encephalomyelitis. J Neurosci 2006; 26: 6823–33.

Nilsson S, Koehler KF, Gustafsson JA. Development of subtype-selective estrogen receptor-based therapeutics. Nat Rev Drug Discov 2011; 10: 778–92.

Paharkova-Vatchkova V, Maldonado R, Kovats S. Estrogen preferentially promotes the differentiation of CD11c+ CD11b(intermediate) dendritic cells from bone marrow precursors. J Immunol 2004; 172: 1426–36.

Paterni I, Granchi C, Katzenellenbogen JA, Minutolo F. Estrogen receptors alpha (ERalpha) and beta (ERbeta): subtype-selective ligands and clinical potential. Steroids 2014; 90: 13–29.

Prodinger C, Bunse J, Kruger M, Schiefenhovel F, Brandt C, Laman JD., et al. CD11c-expressing cells reside in the juxtavascular parenchyma and extend processes into the glia limitans of the mouse nervous system. Acta Neuropathol 2011; 121: 445–58.

Prokai L, Nguyen V, Szarka S, Garg P, Sabnis G, Bimonte-Nelson HA., et al. The prodrug DHED selectively delivers 17beta-estradiol to the brain for treating estrogen-responsive disorders. Sci Transl Med 2015; 7: 297ra113.

Rawji KS, Yong VW. The benefits and detriments of macrophages/microglia in models of multiple sclerosis. Clin Dev Immunol 2013; 2013: 948976.

Richardson TI, Dodge JA, Durst GL, Pfeifer LA, Shah J, Wang Y., et al. Benzopyrans as selective estrogen receptor beta agonists (SERBAs). Part 3: synthesis of cyclopentanone and cyclohexanone intermediates for C-ring modification. Bioorg Med Chem Lett 2007; 17: 4824–8.

Saijo K, Collier JG, Li AC, Katzenellenbogen JA, Glass CK. An ADIOL-ERbeta-CtBP transrepression pathway negatively regulates microglia-mediated inflammation. Cell 2011; 145: 584–95.

Samantaray S, Matzelle DD, Ray SK, Banik NL. Physiological low dose of estrogen-protected neurons in experimental spinal cord injury. Ann N Y Acad Sci 2010; 1199: 86–9.

Shen FW, Saga Y, Litman G, Freeman G, Tung JS, Cantor H., et al. Cloning of Ly-5 cDNA. Proc Natl Acad Sci USA 1985; 82: 7360–3.

Spence RD, Hamby ME, Umeda E, Itoh N, Du S, Wisdom AJ., et al. Neuroprotection mediated through estrogen receptor-{alpha} in astrocytes. Proc Natl Acad Sci USA 2011; 108: 8867–72.

Spence RD, Voskuhl RR. Neuroprotective effects of estrogens and androgens in CNS inflammation and neurodegeneration. Front Neuroendocrinol 2012; 33: 105–15.

Spence RD, Wisdom AJ, Cao Y, Hill HM, Mongerson CR, Stapornkul B., et al. Estrogen mediates neuroprotection and anti-inflammatory effects during EAE through ERalpha

signaling on astrocytes but not through ERbeta signaling on astrocytes or neurons. J Neurosci 2013; 33: 10924–33.

Srinivasan K, Friedman BA, Larson JL, Lauffer BE, Goldstein LD, Appling LL., et al. Untangling the brain's neuroinflammatory and neurodegenerative transcriptional responses. Nat Commun 2016; 7: 11295.

Stranges PB, Watson J, Cooper CJ, Choisy-Rossi CM, Stonebraker AC, Beighton RA., et al. Elimination of antigen-presenting cells and autoreactive T cells by Fas contributes to prevention of autoimmunity. Immunity 2007; 26: 629–41.

Suzuki S, Brown CM, Wise PM. Neuroprotective effects of estrogens following ischemic stroke. Front Neuroendocrinol 2009; 30: 201–11.

Tiwari-Woodruff S, Morales LB, Lee R, Voskuhl RR. Differential neuroprotective and anti-inflammatory effects of estrogen receptor (ER)alpha and ERbeta ligand treatment. Proc Natl Acad Sci USA 2007; 104: 14813–8.

Uchoa MF, Moser VA, Pike CJ. Interactions between inflammation, sex steroids, and Alzheimer's disease risk factors. Front Neuroendocrinol 2016; 43: 60–82.

Vainchtein ID, Vinet J, Brouwer N, Brendecke S, Biagini G, Biber K., et al. In acute experimental autoimmune encephalomyelitis, infiltrating macrophages are immune activated, whereas microglia remain immune suppressed. Glia 2014; 62: 1724–35.

Warner M, Gustafsson JA. Estrogen receptor beta and Liver X receptor beta: biology and therapeutic potential in CNS diseases. Mol Psychiatry 2015; 20: 18–22.

Wisdom AJ, Cao Y, Itoh N, Spence RD, Voskuhl RR. Estrogen receptor-beta ligand treatment after disease onset is neuroprotective in the multiple sclerosis model. J Neurosci Res 2013; 91: 901–8.

Wlodarczyk A, Cedile O, Jensen KN, Jasson A, Mony JT, Khorooshi R., et al. Pathologic and protective roles for microglial subsets and bone marrow- and blood-derived myeloid cells in central nervous system inflammation. Front Immunol 2015; 6: 463.

Wlodarczyk A, Lobner M, Cedile O, Owens T. Comparison of microglia and infiltrating CD11c(+) cells as antigen presenting cells for T cell proliferation and cytokine response. J Neuroinflammation 2014; 11: 57.

Wu WF, Tan XJ, Dai YB, Krishnan V, Warner M, Gustafsson JA. Targeting estrogen receptor beta in microglia and T cells to treat experimental autoimmune encephalomyelitis. Proc Natl Acad Sci USA 2013; 110: 3543–8.

CHAPTER 4

Estrogen acts on oligodendrocytes to upregulate cholesterol synthesis genes during remyelination in the cuprizone and EAE models

4.1 Introduction

Multiple sclerosis (MS) is an autoimmune disease of the central nervous system (CNS), characterized by demyelination, axonal damage, and synaptic loss. Current treatments for MS are immunomodulatory, effective in reducing relapses, but not in repairing disabilities. New treatment strategies targeting oligodendrocytes to promote remyelination are needed to improve disabilities (Lopez Juarez et al., 2016; Plemel et al., 2017).

Remyelination is a natural process that repairs myelin and provides axonal protection in the CNS. In MS patients, remyelination is insufficient and progressive neurodegeneration occurs (Franklin, 2002; Franklin and Ffrench-Constant, 2008; Stankoff et al., 2016). Lack of remyelination in MS is related to the inability of oligodendrocyte progenitor cells (OPCs) to differentiate into mature myelinating oligodendrocytes (Wolswijk, 1998; Chang et al., 2002). This deficit is in part due to the hostile CNS microenvironment that inhibits OPC differentiation, such as pro-inflammatory cytokines and chemokines (Chew et al., 2005; Moore et al., 2015), leucine rich repeat and immunoglobin-like domain-containing protein 1 (LINGO1) (Mi et al., 2005), and chondroitin sulfate proteoglycans (CSPGs) (Back et al., 2005). Thus, successful remyelination in MS requires both intrinsic factors promoting oligodendrocyte maturation and myelination, as well as extrinsic factors modulating inflammation, as one without the other may not be sufficient. Indeed, we previously reported that treatment with the estrogen receptor beta (ERβ)-ligand, diarylpropionitrile (DPN), enhanced remyelination in the animal model of MS,

experimental autoimmune encephalomyelitis (EAE), through both direct and indirect effects on oligodendrocytes. Specifically, ERβ-ligand treatment promoted oligodendrocyte maturation and remyelination by directly targeting ERβ on oligodendrocytes. ERβ-ligand also acted directly on $CD11c^+$ myeloid dendritic cells and macrophages to reduce the pro-inflammatory CNS microenvironment (Kim et al., 2018).

Molecular mechanisms of intrinsic processes within oligodendrocytes during ERβ-ligand treatment warrant further study since this may reveal new therapeutic pathways to target. EAE is the most widely used animal model to study MS. However, there is limited remyelination in EAE, thereby preventing the study of molecular mechanisms in oligodendrocytes during remyelination. Here we use the cuprizone diet-induced demyelination mouse model to explore molecular mechanisms in oligodendrocytes during remyelination. In this model, toxic reversible demyelination is associated with oligodendrocyte death induced by cuprizone diet. Remyelination occurs following cuprizone withdrawal and switch to normal diet. Unlike the EAE model, there is minimal infiltration of blood derived immune cells, with inflammation limited primarily to glial activation (Matsushima and Morell, 2001).

Recent progress in the study of oligodendrocytes using cell isolation and high throughput sequencing techniques has yielded valuable insights into how oligodendrocytes and their subpopulations are regulated during developmental myelination (Zhang et al., 2014; Moyon et al., 2016). However, the oligodendrocyte specific transcriptome during remyelination has not been elucidated. Here, for the first time, we use RiboTag technology to determine oligodendrocyte specific gene expression during remyelination after chronic demyelination in the cuprizone model. RiboTag technology uses the Cre-Lox recombination system to generate transgenic mice expressing hemagglutinin (HA)-tagged ribosomes in specific cell types (Sanz et al., 2009;

Anderson et al., 2016; Itoh et al., 2018). Olig1-RiboTag mice permit the isolation of oligodendrocyte specific transcripts from whole tissue samples, with RNA sequencing and analysis revealing intrinsic mechanisms that oligodendrocytes use during remyelination in vivo in the adult CNS during injury. Finally, we extended the RiboTag approach to determine intrinsic mechanisms within oligodendrocytes during remyelination induced by ERβ-ligand treatment in both the chronic cuprizone and EAE models.

4.2 Results

4.2.1 Oligodendrocyte specific RNA isolation from Olig1-RiboTag mice

To investigate oligodendrocyte specific transcriptome changes in vivo, we used the RiboTag technology (Sanz et al., 2009; Anderson et al., 2016; Itoh et al., 2018). As illustrated in Figure 4.1A, we crossed Olig1-Cre mice with RiboTag mice (Olig1-RiboTag) to generate mice expressing HA-tagged ribosomal protein only in oligodendrocyte lineage cells. Anti-HA antibody immunoprecipitation (IP) permitted isolation of oligodendrocyte lineage cell specific ribosome associated transcripts. When tissues from specific brain regions were used, this technology allowed isolation of actively translated mRNA in a cell-specific and region-specific manner (Itoh et al., 2018). Here, we focused on white matter tissues from the corpus callosum (CC) and optic nerve (ON) to validate the specificity of HA labeling in the white matter of Olig1-RiboTag mice. Validation was carried out by using immunofluorescence and quantitative PCR (qPCR). Double immunolabelling showed co-localization of HA with the oligodendrocyte marker GSTπ. No HA co-localization was observed with other cell specific markers, namely GFAP for astrocytes, NF200 for neurons and Iba1 for microglia (Figure 4.1B, D). By qPCR, we confirmed enrichment of oligodendrocyte specific genes *Plp*, *Ugt8a*, and *Pdgfrα* in HA-IP RNA

samples versus input RNA samples, whereas astrocyte gene *Aldhl1l*, neuronal genes *Syp* and *Gap43*, and microglia genes *Tmem119* and *Aif1* were de-enriched (Figure 4.1C, E). These results collectively validated the RiboTag technology as a valuable tool to isolate oligodendrocyte specific RNAs from white matter of Olig1-RiboTag mice.

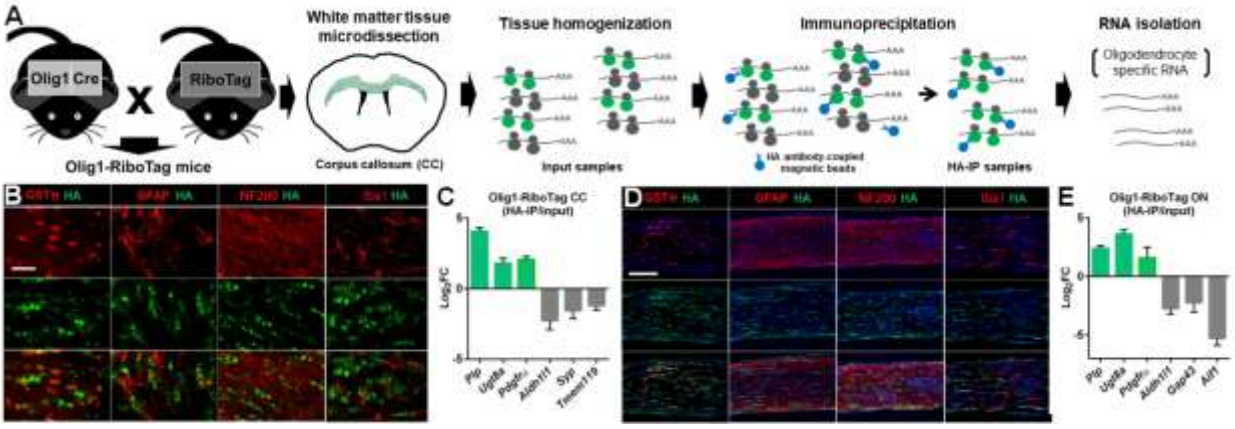

Figure 4.1 Isolation and validation of oligodendrocyte specific transcripts from Olig1-RiboTag mice. (A) Experimental strategy to isolate oligodendrocyte specific RNA from corpus callosum (CC) of Olig1-RiboTag mouse. **(B and D)** Representative images from corpus callosum (B) and optic nerve (ON) (D) of Olig1-RiboTag mice validating the specificity of HA expression in oligodendrocytes. Immunofluorescence staining for HA showed co-localization with the oligodendrocyte marker GSTπ and non-colocalization with the astrocyte marker GFAP, neuronal marker NF200, and microglial marker Iba1. Scale bar, 20μm for (B) and 50μm for (D). **(C and E)** qPCR results comparing HA-IP RNA samples versus input RNA samples from corpus callosum (C) and optic nerve (E) of Olig1-RiboTag mice showed enrichment of oligodendrocyte genes (*Plp*, *Ugt8a*, and *Pdgfrα*) and de-enrichment of astrocyte (*Aldh1l1)*, neuronal (*Syp or Gap43*), and microglial (*Tmem119 or Aif1*) genes.

4.2.2 Remyelination after chronic demyelination in the cuprizone diet-induced model

To understand molecular mechanisms in oligodendrocytes during remyelination we used the cuprizone mouse model. First, we identified a time course that entails both chronic demyelination and axonal damage. We tested two different cuprizone exposure time points, 6 weeks (6w) and 9 weeks (9w), each followed by a recovery period on normal diet for 3 weeks (6w+3w and 9w+3w, respectively). Mice receiving normal diet for the duration of the entire experiment were used as normal controls (N). Immunofluorescence was performed on brain sections to assess myelin (myelin basic protein, MBP; Figure 4.2A, B), oligodendrocytes ($CC1^+$ and $GST\pi^+$ oligodendrocytes; Figure 4.2C, D), and axonal damage (βAPP and SMI32; Figure 4.2E, F) in the corpus callosum. Demyelination, oligodendrocyte loss, and axonal damage were more pronounced in the corpus callosum of mice receiving cuprizone diet for 9 weeks than in those receiving it for 6 weeks (Figure 4.2A-F). During the 3 week recovery period, remyelination occurred to a lesser degree in 9w+3w mice compared to 6w+3w mice. Interestingly, MBP intensity level was significantly lower in 9w+3w mice, but not in 6w+3w mice, each as compared to controls (N), providing a critical window for further remyelination to occur with treatment using 9w+3w, but not 6w+3w time course (Figure 4.2B). Axonal damage after the 3 week recovery period was also more pronounced in the 9w+3w mice than in 6w+3w mice as compared to normal controls (N) (Figure 4.2E-F). Together, these results showed that 9 weeks of cuprizone diet feeding caused demyelination and axonal damage that is not fully restored with normal diet. Thus, the 9w+3w time course can be used to investigate therapeutic strategies to enhance remyelination and prevent axonal loss during chronic disease and was used herein.

We first assessed known oligodendrocyte specific gene expression in Olig1-RiboTag mice using this more chronic time course. We collected oligodendrocyte specific transcripts from

normal (N), 9w and 9w+3w mice and performed qPCR to measure myelin specific genes. Expression levels of myelin protein genes *Mbp*, *Mag*, *Plp*, and *Mog*, were significantly reduced in 9w mice when compared to normal controls (N). As expected, a significant increase in the expression levels of these genes was observed in 9w+3w mice, as compared to 9w mice (Figure 4.2G). These results confirmed that we were able to detect oligodendrocyte specific gene expression changes during cuprizone diet-induced chronic demyelination and remyelination in Olig1-RiboTag mice.

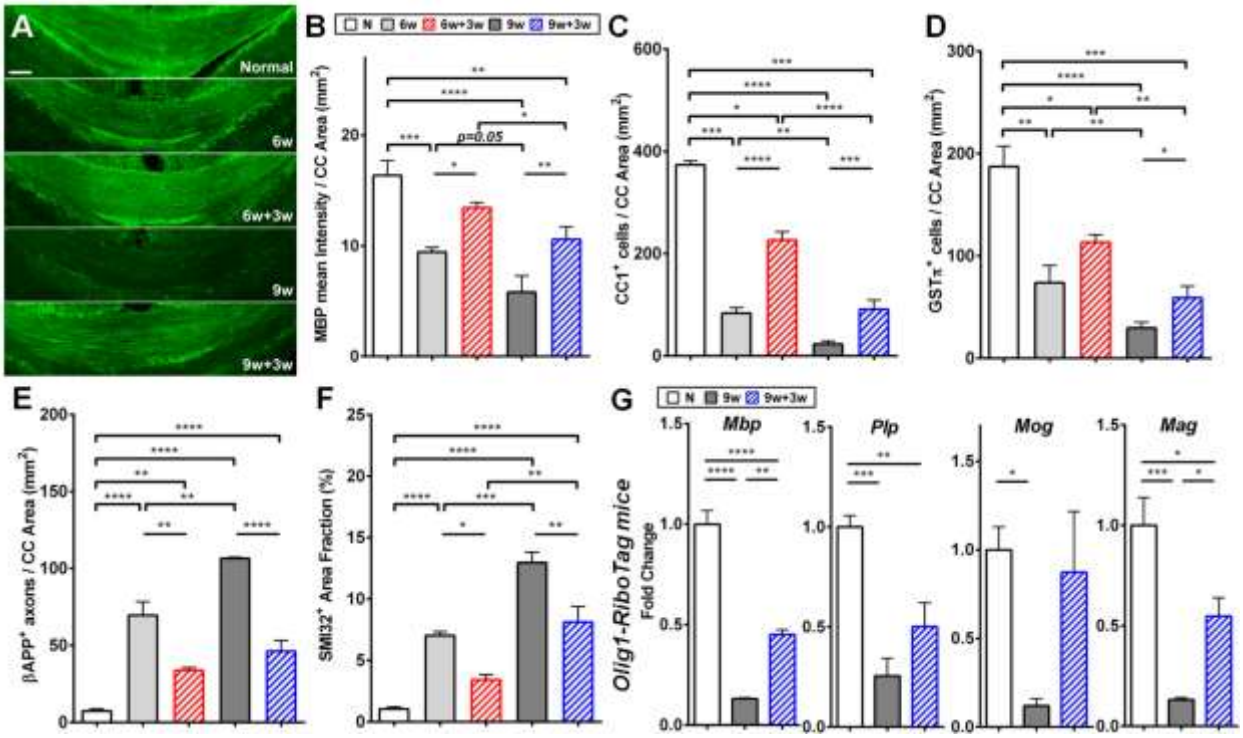

Figure 4.2 Time course of remyelination after chronic demyelination in the cuprizone model. (A) Representative images of corpus callosum sections stained for MBP. Scale bar, 100µm. Normal = normal controls; 6w = mice fed with cuprizone diet for 6 weeks; 6w+3w = mice fed with cuprizone for 6 weeks and normal diet for 3 weeks; 9w = mice fed with cuprizone diet for 9 weeks; 9w+3w = mice fed with cuprizone for 9 weeks and normal diet for 3 weeks. **(B-**

F) Quantitative analyses of MBP intensity (B), immature/mature $CC1^+$ and mature $GST\pi^+$ oligodendrocyte populations (C and D, respectively), and axonal damage βAPP^+ axons and $SMI32^+$ area (E and F, respectively) in the corpus callosum (CC). **(G)** Oligodendrocyte specific expression levels of *Mbp*, *Plp*, *Mog*, and *Mag* myelin genes from Olig1-RiboTag mice. Myelin genes were significantly reduced in mice fed with cuprizone diet for 9 weeks (9w) compared to normal controls (N), and were increased in mice fed with cuprizone for 9 weeks followed by normal diet for 3 weeks (9w+3w). *P < 0.05; **P < 0.01; ***P < 0.001; ****P < 0.0001.

4.2.3 Dominance of enrichment of cholesterol synthesis pathways during remyelination after chronic demyelination

We used the 9+3 week time course in Olig1-RiboTag mice to perform high throughput sequencing of oligodendrocyte ribosome associated transcripts. Briefly, we collected corpus callosum tissues from mice receiving 9 weeks of cuprizone diet (9w) and mice receiving 9 weeks of cuprizone diet followed by 3 weeks of normal diet (9w+3w). Oligodendrocyte specific transcripts isolated from corpus callosum tissue homogenates were used for RNA-sequencing (Figure 4.3A). We performed canonical pathway analysis of differentially expressed oligodendrocyte specific genes between 9w and 9w+3w mice. There were 2459 differentially expressed genes, FDR < 0.1. During recovery (9w+3w) cholesterol synthesis pathways (superpathway of cholesterol biosynthesis, cholesterol biosynthesis I, II and III) dominated as the top four upregulated pathways, whereas neuroinflammatory pathways were among the most downregulated pathways (Figure 4.3B). A heat map of individual genes showed that all 19 cholesterol synthesis genes were upregulated (red) in 9w+3w mice (Figure 4.3C).

We confirmed the up-regulation of cholesterol synthesis pathway genes during remyelination by performing qPCR on oligodendrocyte specific transcripts isolated from corpus callosum of a different set of Olig1-RiboTag mice. As illustrated in Figure 4.4A, we investigated three cholesterol synthesis genes encoding for important enzymes in cholesterol synthesis, namely 3-hydroxy-3-methylglutaryl-CoA synthase1 (*Hmgcs1*), farnesyl diphosphate synthase (*Fdps*), and farnesyl-diphosphate farnesyltransferase 1 (*Fdft1*). We found that 9w+3w mice had significantly increased *Hmgcs1*, *Fdps*, and *Fdft1* gene expression levels (Figure 4.4B). We then confirmed increased expression of *Hmgcs1*, *Fdps*, and *Fdft1* at the protein level, by performing immunofluorescence on tissues obtained from wildtype mice. Double immunolabelling for HMGCS1, FDPS, or FDFT1 with oligodendrocyte immature/mature marker CC1 showed a significant increase of cholesterol synthesis protein expression in $CC1^+$ oligodendrocytes in the corpus callosum of 9w+3w mice (Figure 4.4C-E). Together, these results show that oligodendrocytes upregulate cholesterol synthesis gene expression during remyelination after chronic demyelination.

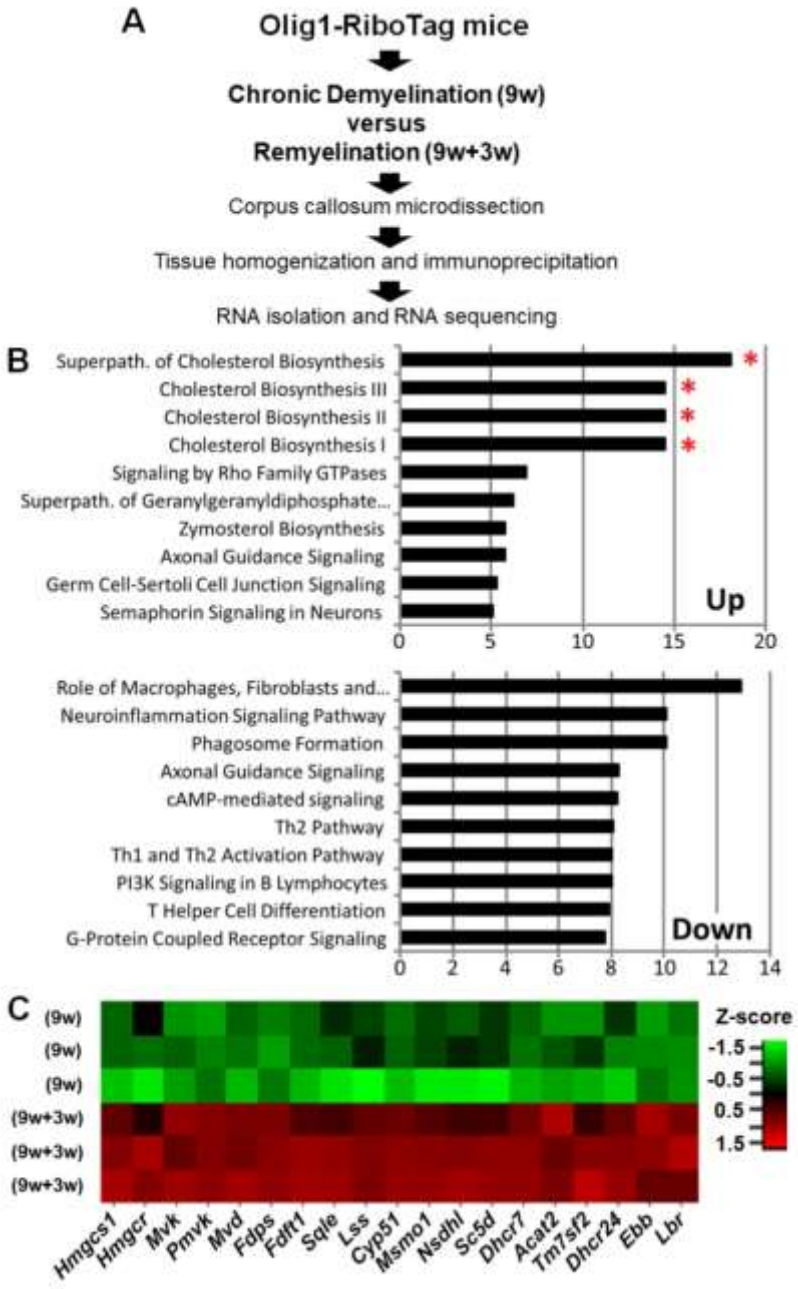

Figure 4.3 Oligodendrocyte specific transcriptome changes during remyelination after chronic demyelination. (A) Experimental scheme to study oligodendrocyte specific transcriptomes in corpus callosum tissue of mice fed with cuprizone diet for 9 weeks (9w) versus mice fed with cuprizone for 9 weeks followed by normal diet for 3 weeks (9w+3w) using the Olig1-RiboTag mice. **(B)** Principal component analysis of 9w (gray) and 9w+3w (blue) mice

showed a clear separation of gene expression patterns between the two groups. **(C)** Top ten upregulated and downregulated canonical pathways from differentially expressed oligodendrocyte genes comparing 9w+3w to 9w mice. Red asterisks (*) indicates cholesterol synthesis pathways as top four upregulated pathways in 9w+3w mice. **(D)** Heat map showed upregulation (red) of multiple cholesterol synthesis pathways genes in 9w+3w mice.

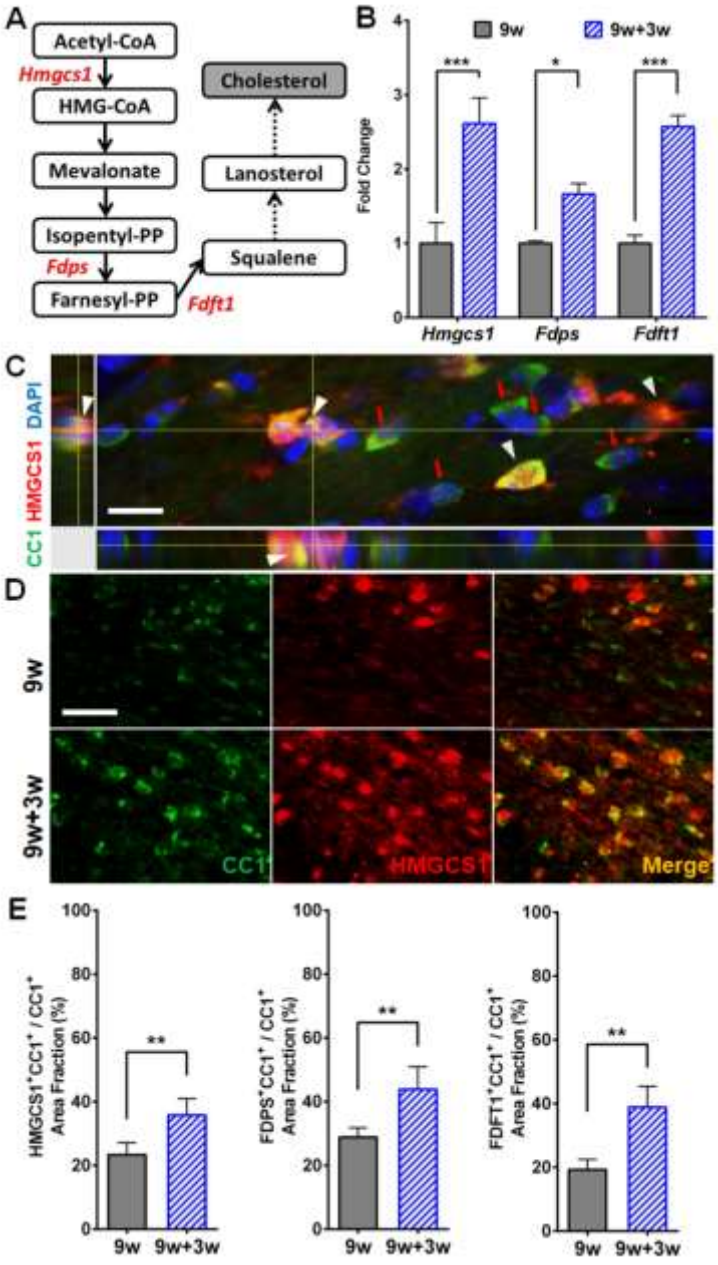

Figure 4.4 Validation of upregulated cholesterol synthesis genes in oligodendrocytes during remyelination. (A) Summary of cholesterol synthesis pathway and genes of interest (*Hmgcs1, Fdps, and Fdft1;* in red). **(B)** qPCR results of oligodendrocyte specific *Hmgcs1*, *Fdps*, and *Fdft1* mRNA expression levels showed that cholesterol synthesis pathway genes were upregulated in 9w+3w mice. **(C)** Orthogonal view of immunofluorescence image co-stained for HMGCS1 (red) and CC1 (green) in the corpus callosum. DAPI represents nuclear stain. Arrowheads indicate $HMGCS1^{+}CC1^{+}$ oligodendrocytes. Red arrows indicate $HMGCS1^{-}CC1^{+}$ oligodendrocytes. Scale bar, 10 μm. **(D)** Representative images of HMGCS1 (red) and CC1 (green) co-stained corpus callosum from 9w mice (top row) and 9w+3w mice (bottom row). Scale bar, 50μm. **(E)** Cholesterol synthesis protein expression in $CC1^{+}$ oligodendrocytes measured by area fraction (%); HMGCS1 (left), FDPS (middle), and FDFT1 (right). 9w+3w mice showed an increase in cholesterol synthesis protein expression in $CC1^{+}$ oligodendrocytes. *P < 0.05; **P < 0.01; ***P < 0.001.

4.2.4 ERβ-ligand treatment enhances remyelination and increases oligodendrocytes during remyelination in the cuprizone diet-induced model

In a previous study, we showed that the beneficial effects of ERβ-ligand treatment on remyelination and clinical disease protection in EAE were directly mediated through ERβ on $Olig1^{+}$ oligodendrocytes (Kim et al., 2018). However, molecular mechanisms within oligodendrocytes remained unclear. Here, we asked whether ERβ-ligand treatment could further enhance remyelination in the chronic cuprizone model with a critical window of room for improvement. We used C57BL/6 wildtype mice of four groups: 1) 9w mice, 2) 9w+3w mice receiving vehicle treatment (9w+3w/Veh), 3) 9w+3w mice receiving ERβ-ligand treatment

(9w+3w/ERβ) and 4) normal control mice receiving normal diet for the entire experiment (N). We assessed myelin sheath thickness in the corpus callosum of each experimental group using electron microscopy (EM) to evaluate the degree of demyelination and remyelination (Figure 4.5A). Myelin thickness was quantified using the g-ratio (axon diameter divided by the myelin + axon diameter). The 9w mice showed increased g-ratio compared to normal controls, confirming a significant decrease in myelin thickness during chronic demyelination. Also as expected, 9w+3w/Veh mice showed reduced g-ratio compared to the 9w mice, indicative of increased myelin sheath thickness during natural remyelination. Interestingly, 9w+3w/ERβ mice exhibited a further significant reduction in g-ratio, showing an increase in myelin sheath thickness close to that of normal controls (Figure 4.5B, C). These results showed that ERβ-ligand treatment enhanced remyelination in the chronic cuprizone model.

To investigate whether ERβ-ligand treatment was acting directly on oligodendrocytes, we crossed Olig1-cre mice with $ERβ^{fl/fl}$ mice to obtain mice with conditional knockout of ERβ in $Olig1^{+}$ cells (*Olig1*-cre^{+};$ERβ^{fl/fl}$, Olig1-CKO) and wildtype littermates (*Olig1*-cre^{-};$ERβ^{fl/fl}$, Olig1-WT). We then used the 9+3 week time course to induce chronic demyelination (9w) and remyelination (9w+3w). We assessed remyelination in the four groups: Olig1-WT mice treated with 1) vehicle (9w+3w/Veh WT), or 2) ERβ-ligand (9w+3w/ERβ WT) and Olig1-CKO mice treatment with 3) vehicle (9w+3w/Veh CKO) or 4) ERβ-ligand (9w+3w/ERβ CKO). Mice fed normal diet for the duration of the entire experiment were used as normal controls (N). We assessed myelin integrity by measuring MBP intensity in the corpus callosum using immunofluorescence. Consistent with EM results, 9w+3w/ERβ WT mice revealed a further significant increase in MBP intensity when compared to 9w+3w/Veh WT mice (Figure 4.5D, E). In contrast, the beneficial effect of ERβ-ligand treatment on remyelination was no longer seen in

9w+3w/ERβ CKO mice compared to 9w+3w/Veh CKO mice (Figure 4.5E and Table 4.1). In addition, when we extended the remyelination phase from 3 weeks to 6 weeks of normal diet, with or without ERβ-ligand treatment, each following the 9 weeks of cuprizone diet (9w+6w), myelin intensity in WT mice receiving ERβ-ligand treatment was again significantly increased compared to vehicle treated mice, whereas in the CKO mice no effect was seen (Table 4.1).

We investigated whether ERβ-ligand treatment has direct effects on mature oligodendrocytes. We assessed mature GSTπ^+ oligodendrocyte and immature/mature CC1$^+$ populations in the corpus callosum of each experimental group by double immunolabelling for GSTπ or CC1 with pan-oligodendrocyte (all oligodendrocyte lineage cells, OLCs) marker Olig2 (Figure 4.5F-I). We observed a significant decrease in the percentage of both GSTπ^+ and CC1$^+$ oligodendrocytes in 9w mice compared to normal controls (N). During remyelination, ERβ-ligand treatment significantly increased the percentage of both GSTπ^+ and CC1$^+$ cells in 9w+3w/ERβ WT compared to 9w+3w/Veh WT mice. This protective effect was lost in 9w+3w/ERβ CKO mice when compared to 9w+3w/Veh CKO mice (Figure 4.5G, I). These results demonstrate that ERβ-ligand treatment enhances remyelination and oligodendrocyte maturation, with these beneficial effects mediated by direct effects on ERβ in Olig1$^+$ oligodendrocytes.

We then determined whether ERβ-ligand treatment has direct effects on OPCs. We assessed OPC populations in the corpus callosum by double immunolabelling for the OPC marker NG2 and OLC marker Olig2 (Figure 4.5J). In keeping with previous studies (Mason et al., 2000; Matsushima and Morell, 2001), we detected a significant increase in the percentage of NG2$^+$ OPCs during demyelination in 9w mice compared to normal controls (N), suggesting ongoing recruitment of OPCs in demyelinated corpus callosum areas. During remyelination, the percentage of NG2$^+$ OPCs significantly dropped in 9w+3w/Veh WT compared to 9w mice.

Interestingly, ERβ-ligand treatment increased the percentage of $NG2^+$ OPCs in 9w+3w/ERβ WT mice when compared to 9w+3w/Veh WT mice. In the 9w+3w CKO mice, ERβ-ligand treatment did not affect $NG2^+$ OPCs, indicating that ERβ activation in $Olig1^+$ oligodendrocytes can increase OPCs during remyelination after chronic demyelination (Figure 4.5K).

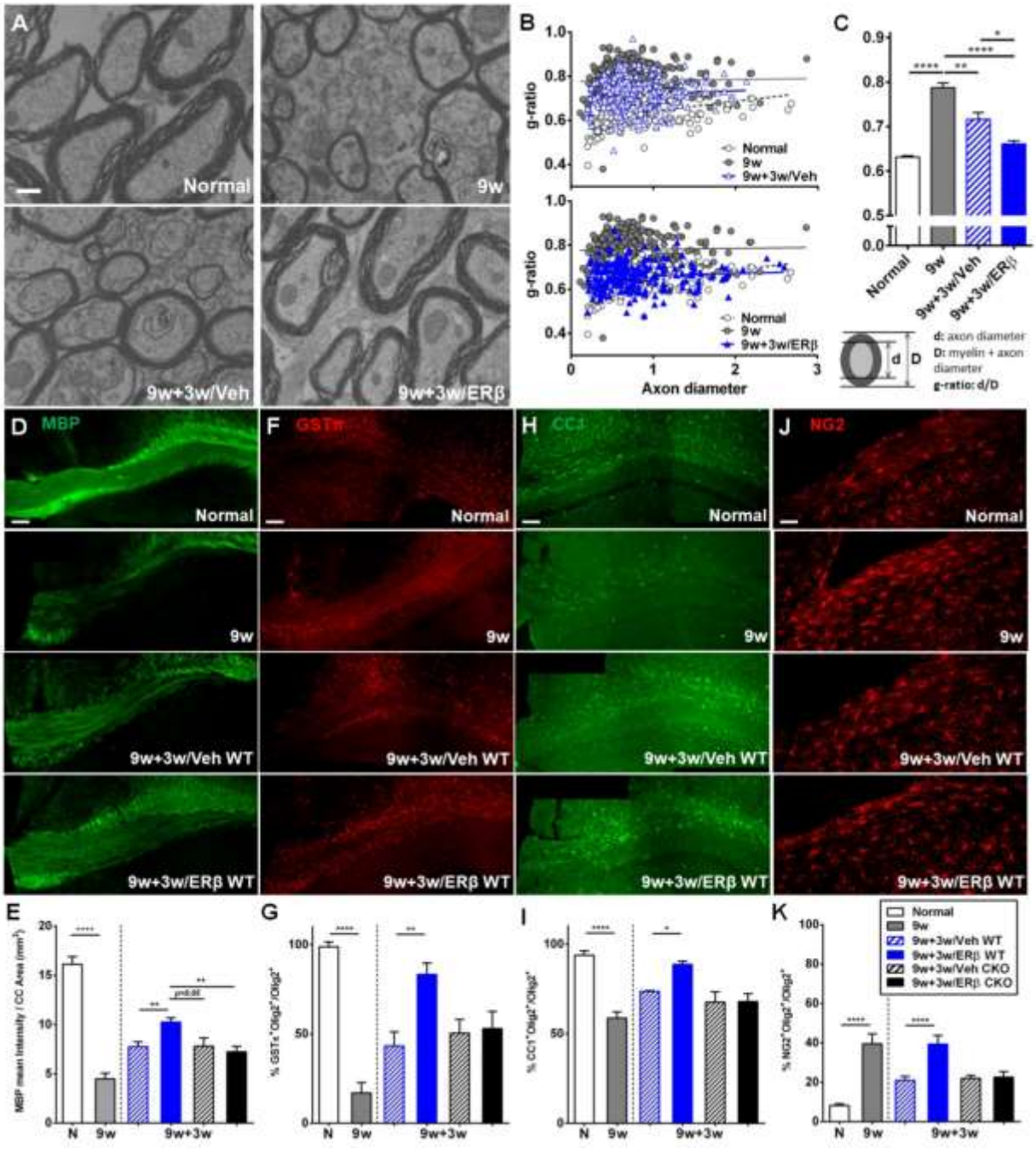

Figure 4.5 ERβ-ligand treatment during the remyelination phase of the cuprizone model further enhances remyelination and increases mature oligodendrocytes and OPCs. (A) Representative electron microscopy images of ultra-resolution axons and myelin in the corpus callosum of normal controls (N), mice fed with cuprizone diet for 9 weeks (9w), mice fed with cuprizone for 9 weeks and receiving vehicle treatment during 3 week recovery period (9w+3w/Veh), and mice fed with cuprizone for 9 weeks and receiving ERβ-ligand treatment during 3 week recovery period (9w+3w/ERβ). Scale bar, 0.5μm. **(B)** Plots of g-ratio versus axon diameter for 9w+3w/Veh (top) and 9w+3w/ERβ (bottom) mice compared to 9w mice and normal controls (N), with a linear function. **(C)** Quantitative analysis showed that 9w mice had increased g-ratio compared to normal controls (N) indicative of demyelination. Vehicle treated (9w+3w/Veh) mice showed a decrease in g-ratio compared to 9w mice indicative of remyelination. ERβ-ligand treated (9w+3w/ERβ) mice showed a further significant decrease in g-ratio indicative of enhanced remyelination. **(D, F, H, J)** Representative images of MBP^+ stained myelin (D), $GST\pi^+$ mature oligodendrocytes (F), $CC1^+$ immature/mature oligodendrocytes (H), and $NG2^+$ OPCs (J) in the corpus callosum. Scale bars, 100 μm. Normal controls (N), mice fed with cuprizone diet for 9 weeks (9w), 9w+3w Olig1-WT mice treated with vehicle (9w+3w/Veh WT) or ERβ-ligand (9w+3w/ERβ WT), and 9w+3w Olig1-CKO mice treated with vehicle (9w+3w/Veh CKO) or ERβ-ligand (9w+3w/ERβ CKO). **(E, G, I, K)** Quantitative analysis of MBP mean intensity (E), and percentage analyses of $GST\pi^+$ mature oligodendrocytes (G), $CC1^+$ immature/mature oligodendrocytes (I), and $NG2^+$ OPCs (K) showed that ERβ-ligand treated 9w+3w/ERβ WT mice had more myelin, mature oligodendrocytes, and OPCs compared to vehicle treated 9w+3w/Veh WT mice, whereas ERβ-ligand treatment had no

effect in Olig1 conditional knockout (CKO) mice (9w+3w/Veh CKO versus 9w+3w/ERβ CKO). *P < 0.05; **P < 0.01; ****P < 0.0001.

		MBP Mean intensity (Vehicle vs ERβ-ligand)						Mean Difference	Standard Error	P value
Ex. 1	9w+3w	Veh WT	n=4	7.46	ERβ WT	n=10	10.25	-2.790	0.699	0.0047
		Veh CKO	n=4	7.80	ERβ CKO	n=5	7.24	0.560	0.932	> 0.9999
	9w+6w	Veh WT	n=5	9.26	ERβ WT	n=5	12.68	-3.420	1.082	0.0389
		Veh CKO	n=5	9.24	ERβ CKO	n=4	9.60	-0.360	1.148	> 0.9999
Ex. 2	9w+3w	Veh WT	n=5	11.72	ERβ WT	n=5	13.40	-1.679	0.284	0.0002
		Veh CKO	n=5	11.18	ERβ CKO	n=4	12.04	-0.859	0.302	0.0734
	9w+6w	Veh WT	n=4	13.91	ERβ WT	n=6	17.41	-3.497	0.777	0.0022
		Veh CKO	n=5	13.84	ERβ CKO	n=5	14.30	-0.463	0.762	> 0.9999
Ex. 3	9w+6w	Veh WT	n=4	15.35	ERβ WT	n=3	19.11	-3.762	1.082	0.0223
		Veh CKO	n=3	16.88	ERβ CKO	n=4	15.46	1.419	1.082	> 0.9999

Table 4.1 Mean MBP intensity, Mean difference, standard errors and significance levels for each comparison in all experiments. Repeated measures two-way ANOVA, with Bonferroni's multiple comparisons test. Wildtype vehicle treated (Veh WT) versus ERβ ligand treated (ERβ WT) and conditional knockout vehicle treated (Veh CKO) versus ERβ ligand treated (ERβ CKO). 9w+3w = mice fed with cuprizone for 9 weeks and normal diet for 3 weeks; 9w+6w = mice fed with cuprizone for 9 weeks and normal diet for 6 weeks.

4.2.5 No effects of ERβ-ligand treatment on microglia and reactive astrocytes during remyelination

In the cuprizone model, microglia cells and astrocytes become activated during demyelination (Matsushima and Morell, 2001; Skripuletz et al., 2013; Gudi et al., 2014). Here, we determined whether ERβ-ligand treatment modulated microglia and astrocyte reactivity by assessing activation of $Iba1^+$ microglia and $GFAP^+$ astrocytes by double-immunolabelling with major histocompatibility class II (MHCII). We observed a significant increase in the percentage of

MHCII expressing microglia and astrocytes in 9w mice compared to normal controls (N) and a significant reduction during remyelination in 9w+3w mice, but no effect of ERβ-ligand treatment (Figure 4.6).

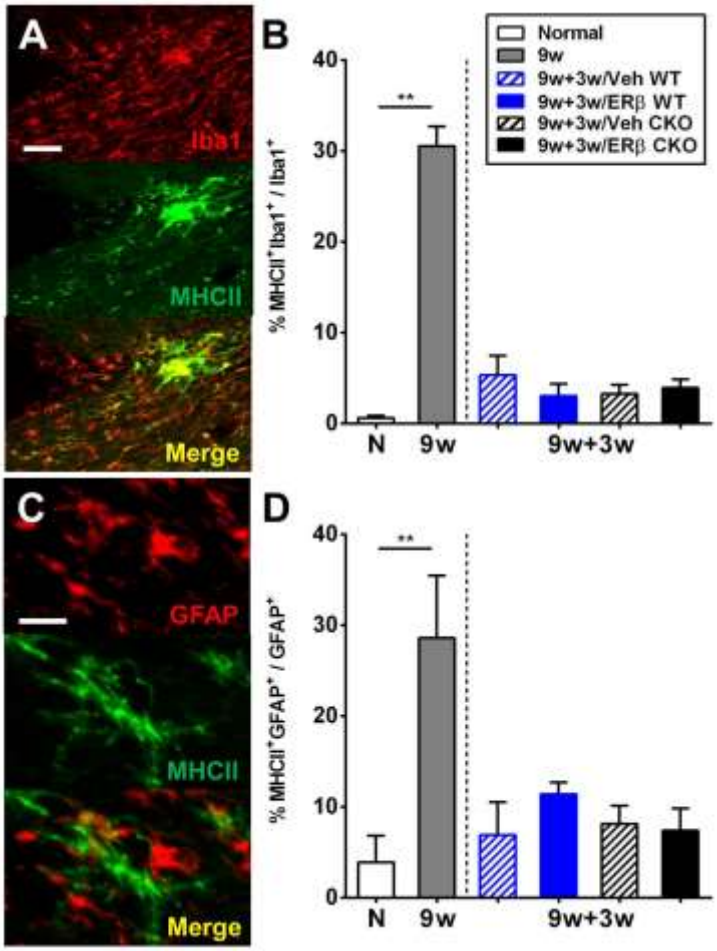

Figure 4.6 ERβ-ligand treatment has no effect on microglia and reactive astrocytes during remyelination. (A) Representative images of Iba1 (red) microglia cells and MHCII (green) stained corpus callosum. Merged images show the co-localization of Iba1 and MHCII (yellow). Scale bar, 50 μm **(B)** Quantitative analysis of $MHCII^{+}Iba1^{+}$ double positive among $Iba1^{+}$ microglia cells. **(C)** Representative images of GFAP (red) reactive astrocytes and MHCII (green) stained corpus callosum. Merged images show the co-localization of GFAP and MHCII (yellow).

Scale bar, 50 μm **(D)** Quantitative analysis of $MHCII^+GFAP^+$ double positive among $GFAP^+$ reactive astrocytes. ** $p<0.01$.

4.2.6 ERβ-ligand treatment upregulates cholesterol synthesis pathway genes in oligodendrocytes

Since we had found an increase in cholesterol synthesis pathways during natural remyelination with normal diet, we next determined whether ERβ-ligand treatment further increased cholesterol synthesis gene expression in oligodendrocytes during remyelination after chronic demyelination using Olig1-RiboTag mice. Briefly, we collected oligodendrocyte specific transcripts from the corpus callosum of 9w+3w/Veh and 9w+3w/ERβ Olig1-RiboTag mice and assessed the expression level of cholesterol synthesis genes by qPCR (Figure 4.7A). We found that ERβ-ligand treatment increased *Hmgcs1*, *Fdps*, and *Fdft1* expression levels in oligodendrocytes from 9w+3w/ERβ compared to 9w+3w/Veh mice (Figure 4.7B). Gene expression was confirmed at the protein level by immunofluorescence in Olig1-WT and Olig1-CKO mice (Figure 4.7C-E). Double immunolabelling for HMGCS1 or FDPS with CC1 revealed a significant increase in cholesterol synthesis protein expression in $CC1^+$ oligodendrocytes in the corpus callosum of 9w+3w/ERβ WT mice compared to 9w+3w/Veh WT mice. In contrast, we did not observe this effect in 9w+3w/ERβ CKO versus 9w+3w/Veh CKO mice (Figure 4.7D, E). Together, these findings demonstrate that ERβ-ligand treatment increases cholesterol synthesis pathways in oligodendrocytes during remyelination and that these effects are mediated by direct effects on ERβ in $Olig1^+$ oligodendrocytes.

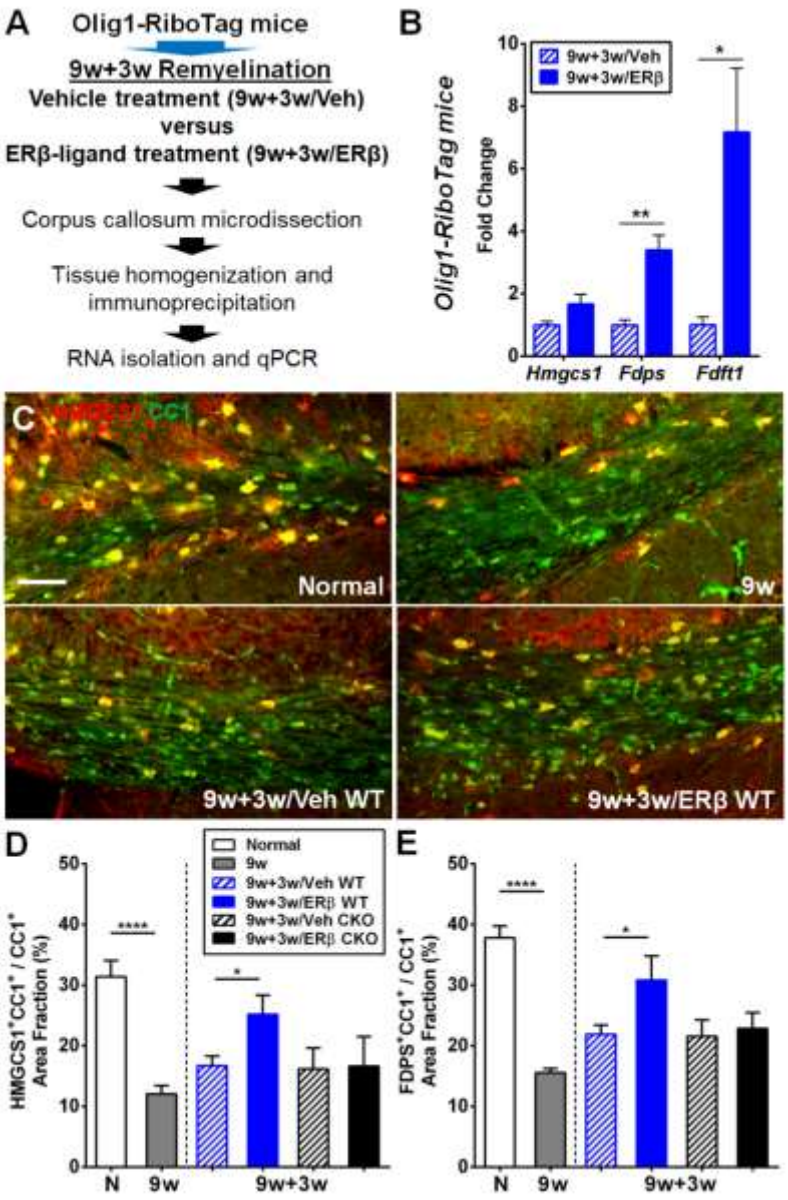

Figure 4.7 ERβ-ligand treatment during the remyelination phase of the cuprizone model further increases cholesterol synthesis gene expression in oligodendrocytes. (A) Experimental scheme to study oligodendrocyte specific gene expression in corpus callosum tissues during remyelination in vehicle treated (9w+3w/Veh) versus ERβ-ligand treated (9w+3w/ERβ) Olig1-RiboTag mice. **(B)** qPCR for oligodendrocyte specific *Hmgcs1*, *Fdps*, and *Fdft1* mRNA expression levels showed that cholesterol synthesis pathway genes were

upregulated with ERβ-ligand treatment in ERβ-ligand treated (9w+3w/ERβ) Olig1-RiboTag mice. **(C)** Representative images of HMGCS1 (red) and CC1 (green) co-stained corpus callosum sections obtained from normal controls (N), 9w, 9w+3w/Veh WT, and 9w+3w/ERβ WT mice. Scale bar, 100μm. **(D and E)** Cholesterol synthesis protein expression in $CC1^+$ oligodendrocytes measured by area fraction (%); HMGCS1 (D) and FDPS (E). In Olig1-WT mice, 9w+3w/ERβ WT mice showed increased expression of cholesterol synthesis proteins compared to 9w+3w/Veh WT mice, whereas ERβ-ligand treatment had no effect in Olig1-CKO mice (9w+3w/Veh CKO versus 9w+3w/ERβ CKO). *P < 0.05; **P < 0.01; ****P < 0.0001.

4.2.7 ERβ-ligand treatment increases cholesterol synthesis pathway gene expression in oligodendrocytes during remyelination in EAE

EAE is the most widely used model of MS and is characterized by adaptive immune responses with infiltration of peripheral immune cells, glial activation, demyelination, and axonal damage. Here, we extended our investigation of ERβ-ligand treatment in the cuprizone model to the EAE model. First, we showed by EM that ERβ-ligand treatment induced remyelination in dorsal white matter of the spinal cord in EAE mice, as we previously described (Kim et al., 2018). Specifically, EAE mice treated with vehicle showed a significant increase in g-ratio compared to normal controls (N), confirming a significant reduction in myelin thickness with disease. In contrast, ERβ-ligand treatment compared to vehicle treatment of EAE showed a significant reduction in g-ratio, indicating remyelination (Figure 4.8).

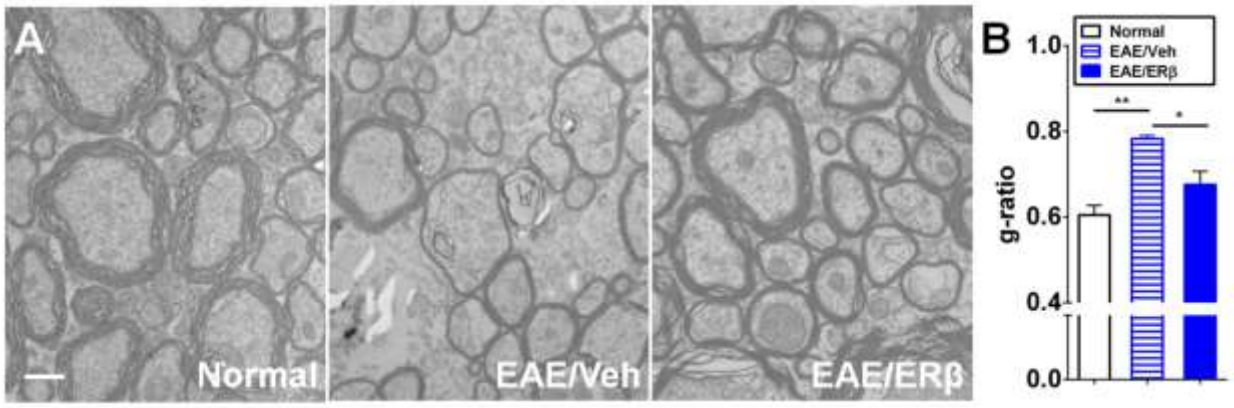

Figure 4.8 ERβ-ligand treatment induces remyelination during EAE. (A) Representative electron microscopy images of ultra-resolution axons and myelin in the spinal cord normal controls (N), WT EAE mice treatment with Vehicle (WT EAE-Veh) and WT EAE mice treated with ERβ-ligand (WT-EAE-ERβ) during EAE. Scale bar, 0.5μm. **(B)** Quantitative analysis showing that WT EAE-Veh mice had increased g-ratio compared to normal controls (N) indicating demyelination. WT-EAE-ERβ showed a significant decrease in g-ratio compared to WT EAE-Veh indicating remyelination. *P < 0.05; **P < 0.01.

Next, we induced EAE in Olig1-WT (EAE WT) and Olig1-CKO (EAE CKO) mice and treated with ERβ-ligand or vehicle. ERβ-ligand treated EAE WT mice (EAE/ERβ WT) showed protection from EAE clinical disease compared to vehicle treated EAE WT mice (EAE/Veh WT). In contrast, ERβ-ligand treated EAE CKO mice (EAE/ERβ CKO) did not show clinical disease protection when compared to vehicle treated EAE CKO mice (EAE/Veh CKO) (Figure 4.9A). MBP staining intensity in dorsal white matter of the spinal cord was higher in EAE/ERβ WT mice compared to EAE/Veh WT mice, while this protective effect was not observed in EAE/ERβ CKO mice (Figure 4.9B, C). Furthermore, ERβ-ligand treatment increased the number of $Olig2^+$ OLCs and $GST\pi^+$ mature oligodendrocytes during EAE in EAE/ERβ WT mice compared to

EAE/Veh WT, and both effects were lost in EAE CKO mice (Figure 4.9D-F). Together these data show direct effects of ERβ-ligand treatment on Olig1^{+} oligodendrocytes in mediating clinical protection, inducing remyelination, and increasing mature oligodendrocytes. Finally, we investigated whether cholesterol synthesis pathway genes were upregulated in oligodendrocytes in EAE during ERβ-ligand treatment induced remyelination. A significant increase in cholesterol synthesis protein expression (HMGCS1 and FDPS) was observed in CC1^{+} oligodendrocytes of EAE/ERβ WT mice when compared to EAE/Veh WT mice. In contrast, EAE/ERβ CKO mice did not show this increase (Figure 4.9G-I). Together, these results show that ERβ-ligand treatment induces remyelination in EAE that involves increased cholesterol synthesis gene expression in oligodendrocyte lineage cells that is mediated by direct effects of ERβ-ligand treatment on these cells.

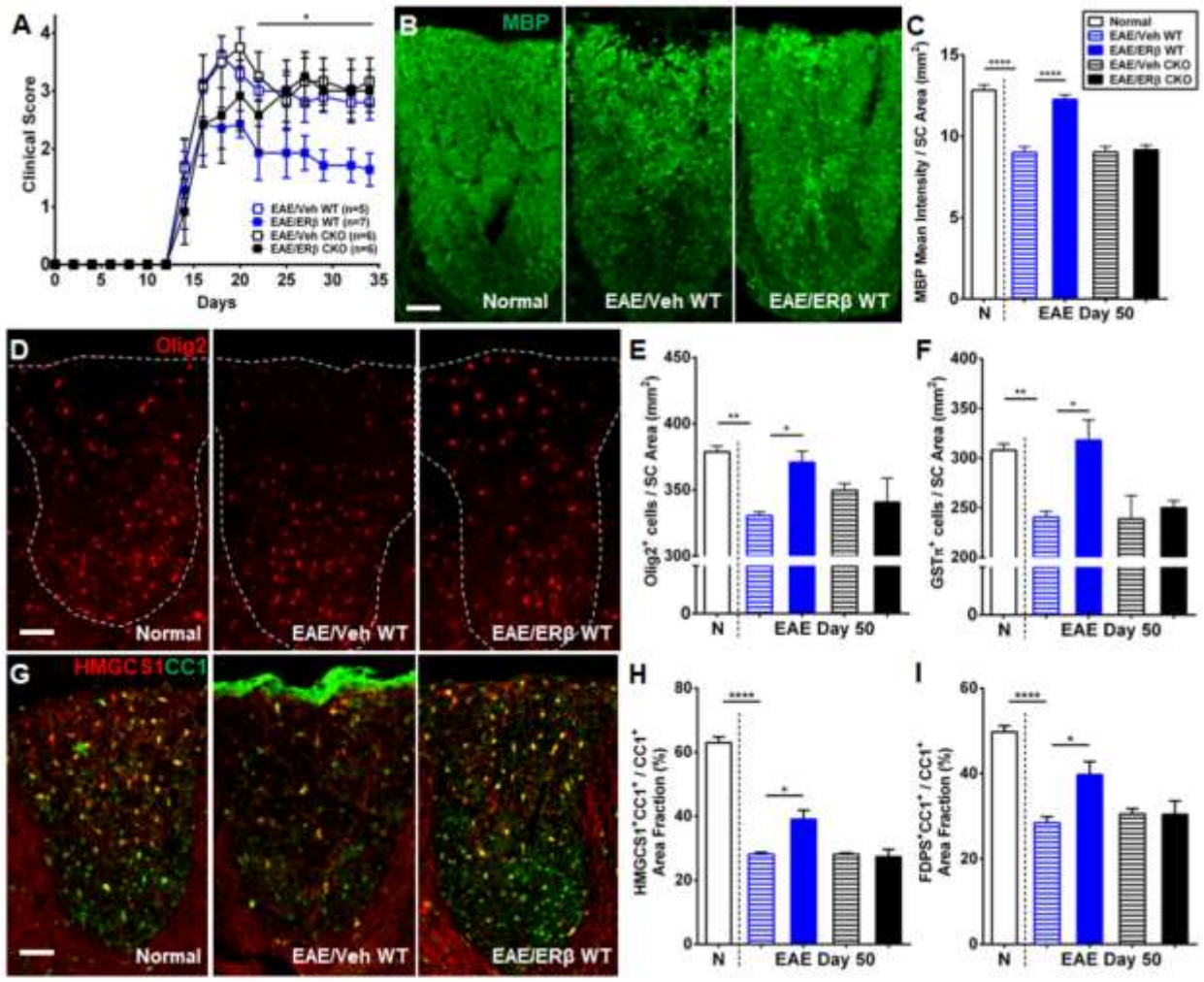

Figure 4.9 ERβ-ligand treatment during EAE. (A) EAE clinical disease scores show that, in Olig1-WT mice, EAE/ERβ WT mice (blue solid) had significantly less severe EAE scores compared to EAE/Veh WT mice (blue clear), whereas there was no difference in EAE clinical score in ERβ conditional knock out mice; EAE/ERβ CKO mice (black solid) versus EAE/Veh CKO mice (black clear). **(B)** Representative images of MBP (green) stained dorsal white matter of spinal cord from Normal, EAE/Veh WT, and EAE/ERβ WT mice. Scale bar, 100μm. **(C)** Quantitative analysis of MBP intensity during EAE shows that ERβ-ligand treatment preserved myelin in EAE/ERβ WT mice compared to EAE/Veh WT, whereas this effect was abolished in EAE CKO mice (EAE/ERβ CKO versus EAE/Veh CKO). **(D)** Representative images of Olig2

(red) stained dorsal white matter of spinal cord from Normal, EAE/Veh WT, and EAE/ERβ WT mice. Scale bar, 100μm. **(E and F)** Quantitative analysis of $Olig2^+$ oligodendrocyte lineage cells (OLCs) (E) and $GST\pi^+$ mature oligodendrocytes (F). ERβ-ligand treated EAE/ERβ WT mice had significantly increased OLCs and mature oligodendrocytes compared to vehicle treated EAE/Veh WT mice, whereas ERβ-ligand treatment had no effect in EAE CKO mice (EAE/ ERβ CKO versus EAE/Veh CKO). **(G)** Representative images of HMGCS1 (red) and CC1 (green) co-stained dorsal white matter of spinal cord from Normal, EAE/Veh WT, and EAE/ERβ WT mice. Scale bar, 100μm. **(H and I)** Cholesterol synthesis protein expression in $CC1^+$ oligodendrocytes measured by area fraction (%); HMGCS1 (H) and FDPS (I). EAE/ERβ WT mice showed increased expression of cholesterol synthesis proteins compared to EAE/Veh WT mice, whereas ERβ-ligand treatment did not show this effect in EAE CKO mice (EAE/ ERβ CKO versus EAE/Veh CKO). *P < 0.05; **P < 0.01; ****P < 0.0001.

4.3 Discussion

Here we applied RiboTag technology to the cuprizone mouse model to investigate oligodendrocyte specific gene expression changes during remyelination after chronic demyelination *in vivo*. We showed that oligodendrocytes upregulate cholesterol synthesis pathway genes during remyelination. Moreover, for the first time, we identified ERβ-ligand as a treatment able to increase oligodendrocyte maturation and enhance cholesterol synthesis gene expression in oligodendrocytes to promote remyelination by signaling directly through ERβ on oligodendrocytes. These findings were validated in two distinct mouse models of MS, namely cuprizone and EAE.

Cholesterol is a rate limiting factor for CNS myelination during development (Saher et al., 2011). Since peripheral cholesterol does not cross the blood brain barrier (BBB), de novo synthesis of cholesterols by CNS cells is essential for myelination. Previous studies have shown that cholesterol synthesis in oligodendrocytes has an essential role in regulating myelin gene expression and in facilitating OPCs differentiation through PI3K/Akt/mTOR signaling (Wahl et al., 2014; Mathews and Appel, 2016). On the other hand, ablation of genes within the cholesterol synthesis pathway or inhibition of cholesterol synthesis by pharmacological interventions (such as statins) in vivo, led to hypomyelination associated with deficits in myelin gene and protein expression during development (Saher et al., 2005; Smolders et al., 2010; Mathews et al., 2014).

In the adult brain, the majority of cholesterol (about 80%) is found in the myelin sheath (Norton and Poduslo, 1973). Recent evidence suggests that cholesterol synthesis dysregulation may be a significant contributor to MS and EAE pathology (van de Kraats et al., 2014; Zhornitsky et al., 2016; Lavrnja et al., 2017; Itoh et al., 2018). Interestingly, clinical trials using cholesterol lowering drugs, statins (3-hydroxy-3-methyl glutaryl coenzyme A reductase), showed protection in MS patients(Vollmer et al., 2004; Togha et al., 2010). However, such clinical trials of statins entail anti-inflammatory properties, not only effects on CNS cholesterol metabolism. Other studies reported that treatment with statins has detrimental or no effects on MRI disease activity or clinical relapses (Birnbaum et al., 2008; Sorensen et al., 2011; Kamm et al., 2012). The adverse effects are thought to be due to statins impairing remyelination (Klopfleisch et al., 2008) or inducing the formation of abnormal myelin-like membrane sheath (Maier et al., 2009). These studies suggest that, rather than inhibiting cholesterol synthesis, CNS cells require cholesterol as a biological substrate to provide neuroprotection and enhance remyelination during disease. Therefore, increasing cholesterol availability and de novo cholesterol synthesis in

CNS cell types may serve as a treatment strategy for neuroprotection. Interestingly, recent treatment studies targeting cholesterol metabolism and transport have shown neuroprotective effects and enhancement of remyelination in the cuprizone and EAE mouse models of MS (Berghoff et al., 2017; Chevalier and Rosenberger, 2017; Itoh et al., 2018).

De novo cholesterol synthesis in the brain is not mutually exclusive to oligodendrocytes as it occurs in other cell types, such as neurons and astrocytes. However, after the early brain developmental phase oligodendrocytes reduce their de novo synthesis of cholesterols and start relying on astrocyte-derived lipids (Mauch et al., 2001; Funfschilling et al., 2007; Camargo et al., 2017). Here, we reported for the first time that in the cuprizone model oligodendrocytes upregulate de novo cholesterol synthesis during remyelination after chronic demyelination. We also observed that during remyelination the number of OPCs was reduced, but the number of mature oligodendrocytes and myelin integrity increased. In agreement with previous evidence (Moyon et al., 2015), our data strongly suggest that after chronic demyelination newly formed OPCs revert to an immature state, typical of an early developmental phase, increase de novo cholesterol synthesis and mature into myelinating oligodendrocytes. Notably, during development, fetal oligodendrocytes are exposed to high levels of estradiol and estriol from the mother's blood. Therefore, we asked whether estrogen modulates oligodendrocyte ability to make myelin. Interestingly, we found that ERβ-ligand treatment during remyelination increased the number of OPCs, increased oligodendrocyte maturation, enhanced oligodendrocyte de novo cholesterol synthesis, and increased remyelination compared to the naturally remyelinated control group. Most importantly, ERβ conditional knockout mice showed that these effects were directly mediated through ERβ-ligand acting on oligodendrocytes.

Finally, we investigated the mechanisms of ERβ-ligand treatment in the EAE model and found increased expression of cholesterol synthesis genes in mature oligodendrocytes, accompanied by enhanced oligodendrocyte maturation and remyelination. In conclusion, this study suggests that in both the cuprizone model and EAE, ERβ-ligand treatment recapitulates developmental myelination, a time when fetal oligodendrocytes are exposed to high levels of estradiol and estriol and are actively synthesizing cholesterols to make myelin. Complementary to a previous study focusing on astrocytes (Itoh et al., 2018), this study focuses on oligodendrocytes provides further evidence that a cell specific transcriptomics approach can offer valuable insights into in vivo mechanisms of actions for the development of neuroprotective treatments in complex neurodegenerative diseases.

4.4 Methods and materials

Animals All mice used in this study were young adult females (age 8-12 weeks) on a C57BL/6 background. Olig1-RiboTag mice: B6;129S4-Olig1tm1(cre)Rth/J (Olig1-cre) mice and B6N.129-Rpl22tm1.1Psam/J (RiboTag) mice were purchased from Jackson Laboratory (Lu et al., 2002; Sanz et al., 2009). The two transgenic mice were crossed to obtain homozygote mice of Olig1-cre and RiboTag (Olig1-RiboTag), expressing HA-tagged ribosomal protein RPL22 in $Olig1^{+}$ oligodendrocyte lineage cells. Olig1-ERβ mice: C57BL/6J-ERβfloxed/floxed mice were a gift from Dr. Pierre Chambon, France (Antal et al., 2008) and were crossed with B6;129S4-Olig1tm1(cre)Rth/J (Olig1-cre) mice to obtain mice with ERβ selective deletion in $Olig1^{+}$ oligodendrocyte lineage cells. Animals were maintained under standard conditions in a 12 h dark/12 h light cycle with access to food and water ad libitum. All procedures were done in accordance to the guidelines of the National Institutes of Health and the Chancellor's Animal

Research Committee of the University of California, Los Angeles Office for the Protection of Research Subjects.

Cuprizone model and ERβ-ligand treatment Young adult female mice (age 8-10 weeks) were fed with 0.2% bis-(cyclohexanone)-oxaldihydrazone (cuprizone) diet (TD.140803, Harlan Teklad) for 6 weeks or 9 weeks to induce demyelination, followed by a 3 week recovery period on global 18% protein rodent control diet (TD.00588, Harlan Teklad) to induce natural remyelination. For ERβ-ligand treatment we used diarylpropionitrile (DPN, Tocris) as described (Kim et al., 2018). DPN was first dissolved in 100% EtOH and then diluted at 1:9 ration in 100% Miglyol® 812 (CREMER Oleo GmbH & Co. KG), reducing the final EtOH concentration to 10%. ERβ-ligand treatment was given during the 3 week normal diet period through subcutaneous injections every other day at a dose of 8 mg/kg per day until the end of the experiment. For randomization, after cuprizone diet feeding, mice were randomly assigned to treatment with Vehicle or ERβ-ligand for 3 weeks while on normal diet. For blinding of drug treatment, third party concealment with color coded labeling of Vehicle or ERβ-ligand treatment syringes was done before treatment started for each experiment.

Experimental autoimmune encephalomyelitis model and ERβ-ligand treatment Female mice (age 8-12 weeks) were immunized subcutaneously with myelin oligodendrocyte glycoprotein (MOG), amino acids 35–55 (200 μg per mouse, Mimotopes) emulsified in Complete Freund's Adjuvant, supplemented with Mycobacterium Tuberculosis H37Ra (200 μg per mouse, Difco Laboratories), over two sites drained by left inguinal and auxiliary lymph nodes in a total volume of 0.1 ml per mouse (Day 0). Pertussis toxin (500 ng per mouse, List Biological Laboratories)

was injected intraperitoneally on Day 0 and Day 2. On Day 7, a booster immunization was delivered over contralateral lymph nodes. The animals were monitored daily for EAE signs based on a standard EAE 0–5 scale scoring system: 0, healthy; 1, complete loss of tail tonicity; 2, loss of righting reflex; 3, partial paralysis; 4, complete paralysis of one or both hind limbs; and 5, moribund (Kim et al., 2014). ERβ-ligand treatment was initiated 1 week before EAE induction and given through subcutaneous injections every other day at a dose of 8 mg/kg per day until the end of the experiment. ERβ-ligand treatment preparation and randomization were done using the same method mentioned above.

Surgery (Ovariectomy) To eliminate the effects of circulating endogenous estrogens during the experiments, ovariectomy was performed in female mice (age - 5 weeks). Mice were anesthetized by inhalational anesthesia with isoflurane. Carprofen (1.2 mg/ml per animal, Zoetis) and 0.5 ml of saline were injected subcutaneously before the procedure. The fur above the lateral dorsal back was removed, and the skin was sterilized with betadine and alcohol scrubs. Bilateral incisions were made into the back. A hemostat was placed on the fallopian tubes, and the ovaries were removed. Muscle layer was closed with absorbable suture, and the skin layer was closed with wound clips. Amoxicillin (50 mg/ml, Virbac) was added to the water for 5 days for antibiotics (0.5 mg/ml water), and another dose of carprofen was given within 24 h following surgery. Wound clips were removed 7 days later as described (Kim et al., 2018). All procedures were approved by the Office of Animal Research Oversight and UCLA institutional animal care and use committee, known locally as the Chancellor's Animal Research Committee.

Co-immunoprecipitation (anti-HA antibody) and RNA isolation Mice were exposed to a lethal dose of isoflurane and transcardially perfused with ice-cold 1X PBS for 4 min, followed by perfusion with ice-cold 1% paraformaldehyde-1X PBS for 4 min. Corpus callosum and optic nerve tissues were collected, snap-frozen in liquid nitrogen and stored at -80℃. Frozen tissues were homogenized on ice using the Dounce Homogenizer with freshly made homogenization buffer containing: 50mM Tris-HCl (Invitrogen) pH 7.5, 100mM KCl (Fisher scientific), 12mM MgCl2 (Fisher Scientific), 1% Nonidet P-40 (Roche), 1mM DTT (Sigma-Aldrich), 1x Proteinase Inhibitors (Sigma-Aldrich), 200 Units/mL RNAsin (Promega), 100ug/mL cycloheximide (Sigma-Aldrich), and 1mg/mL heparin (Sigma-Aldrich). The homogenates were then centrifuged at 16,000g, 4 ℃ for 15 min. The supernatant was collected and incubated with pre-washed anti-HA conjugated magnetic beads (Pierce) overnight on a rotating wheel at 4 ℃. After removal of the supernatant, the magnetic beads were washed 3 times with high salt buffer containing: 50 mM Tris pH 7.5, 300 mM KCl, 12 mM MgCl2, 1% Nonidet P-40, 1 mM DTT, 100 g/mL cycloheximide. Then, 25 µl of proteinase K (4 mg/ml; Zymo Research) was added to the samples and incubated in a 55℃ water bath for 30 minutes. After incubation, 300 µl Tri-reagent was added, and the Direct-zol™ RNA MiniPrep Plus kit (Zymo Research) was used for RNA isolation according to manufacturer's instructions. RNA quantity and quality were measured using NanoDrop 1000 spectrophotometer (Thermo Scientific) and Agilent 2100 Bioanalyzer with pico chip, respectively as described (Itoh et al., 2018).

Library synthesis and high throughput RNA sequencing Double-stranded cDNA and the sequencing library were made using the Kapa RNA Kit Full kit. The workflow consisted of fragmentation of double stranded cDNA, end repair to generate blunt ends, A-tailing, adaptor

ligation, and PCR amplification. Barcoded adaptors were used for multiplexing samples in one lane. Sequencing was performed on Illumina HiSeq 3000 for a pair read 75 runs as described (Itoh et al., 2018). These procedures were performed in the UCLA Jonsson Comprehensive Cancer Center Clinical Microarray Core Facility.

RNA sequencing analysis Statistical analyses and production of figures were performed in R (R Core Team, 2018, http://www.R-project.org/). Qualities of raw sequence data were examined using FastQC (http://www.bioinformatics.babraham.ac.uk/projects/fastqc/), and Trimmomatic was used for cleaning. R package "QuasR" was used for the read alignment to the mouse genome (mm10) followed by the counting at the gene level. To visualize the relationship between samples, the principal component analysis was performed. We assumed read counts followed a negative binomial distribution and constructed generalized linear models based on this negative binomial distribution assumption. Differentially expressed genes between mice receiving cuprizone diet for 9 weeks (9w) and mice receiving cuprizone diet for 9 weeks and normal diet for 3 weeks (9w+3w) were identified using R package "edgeR." False discovery rate (FDR) of 0.1 was used as a threshold of differentially expressed genes. Canonical pathway enrichment analysis was performed for differentially expressed genes (FDR<0.1) in each tissue using Ingenuity Pathway Analysis (QIAGEN, Redwood City, www.qiagen.com/ingenuity) as described (Itoh et al., 2018).

Quantitative RT-PCR (qPCR) cDNA was synthesized using the Tetro cDNA Synthesis kit (Bioline) according to the manufacturer's instructions. qPCR was performed using PowerUp™ SYBR™ Green Master Mix (Thermo Fisher Scientific) on the Bio-Rad Opticon 2 qPCR / Peltier

Thermal Cycler. See table for primer information. The efficiency of each set of primers was assessed by qPCR on a serial dilution of cDNA from CNS tissues and was confirmed to be above 90%. All gene expression levels were normalized to levels of β-Actin by using the standard curve method and expressed as fold change.

Primer list for quantitative PCR

mouse *Actβ* (5′-GGCTCCTAGCACCATGAAGA-3′, 5′-ACTCCTGCTTGCTGATCCAC-3′)

mouse *Plp* (5′-CCGACAAGTTTGTGGGCATC-3′, 5′-TACATTCTGGCATCAGCGCA-3′)

mouse *Ugt8a* (5′-GCCGAAGGACGCGCTAT-3′, 5′-CAAGGCCGATGCTAGTGTCT-3′)

mouse *Pdgfrα* (5′-GTTGTGAGGCTGGTGGAGG-3′, 5′-GTTGTGAGGCTGGTGGAGG-3′)

mouse *Aldhl1l* (5′-GGCTCCTAGCACCATGAAGA-3′, 5′-ACTCCTGCTTGCTGATCCAC-3′)

mouse *Syn* (5′-GGGCCAATGATGGACTTCCT-3′, 5′-GCCTGTCTCCTTGAACACGA-3′)

mouse *Tmem119* (5′-CTTCACCCAGAGCTGGTTCC-3′, 5′-GGGAAGAGGCTGAAGAACCC-3′)

mouse *Mbp* (5′-GGAAGGCAGGTGATGGTTGA-3′, 5′-ACACTGGAGGGCAAACACTC-3′)

mouse *Mog* (5′-GGAAGGCAGGTGATGGTTGA-3′, 5′-GCTCCAGGAAGACACAACCA-3′)

mouse *Mag* (5′-GGTGTTGAGGGAGGCAGTTG-3′, 5′-CGTTGTCTGCTAGGCAAGCA-3′)

mouse *Hmgcs1* (5′-ATGGGGCTCGTGCATAGTAA-3′, 5′-ACTCTCAGTGCTCCCCGTTA-3′)

mouse *Fdps* (5′-GCACTGACATCCAGGACAAC-3′, 5′-AGCCACTTTTTCTGGGTCCT-3′)

mouse *Fdft1* (5′-TCCCTGACGTCCTCACCTAC-3′, 5′-CCCCTTCCGAATCTTCACTA-3′)

Histological preparation Mice were exposed to a lethal dose of isoflurane and perfused transcardially with ice-cold 1xPBS for 8 min, followed by 10% buffered formalin for 8 min. Brains, spinal cords, and optic nerves were dissected and stored in 10% buffered formalin

overnight at 4℃, then submerged in 30% sucrose, 0.1% sodium azide, 1xPBS for 24 h at 4℃.

Tissues were embedded in optical cutting temperature compound (OCT, Tissue Tek) and stored at -80℃ after flash freezing in an isopropanol bath chilled with liquid nitrogen. Tissues were cryosectioned at -25°C into 40 μm thick (brain and spinal cord) and 10 μm thick (optic nerve) sections using a cryostat (Leica CM1860) and stored in 0.1% sodium azide, 1xPBS at 4℃ before used for immunofluorescence staining.

Immunofluorescence staining Brain (between bregma -2 to 0), spinal cord (thoracic region) and optic nerve sections were washed thoroughly using 1xPBS with 0.1% TritonX-100 (PBSt). Tissue sections were incubated with 5% glacial acetic acid, 95% EtOH solution for 30 min at room temperature (RT) and then washed with 1xPBSt before blocking. For blocking, tissues were treated with 10% normal goat serum (NGS) in 1xPBSt for 1 h at RT. Primary and secondary antibody stainings were done at appropriate concentrations with 2% NGS, 1xPBSt for overnight at 4℃ and 1 h at RT, respectively. Primary antibodies: anti-HA 1:500 (16B12, Biolegend), anti-GSTπ 1:1000 (ADI-MSA-102, Enzo Life Sciences), anti-GFAP 1:1000 (Z0334, Dako), anti-NF200 1:750 (N4142, Sigma), anti-Iba1 1:10,000 (Wako Chemicals), anti-MBP 1:750 (MAB386, EMD Millipore), anti-CC1 1:500 (OP80, Calbiochem), anti-βAPP 1:200 (51-2700, Thermo Fisher Scientific), anti-SMI32 1:1000 (NE1023, EMD Millipore), anti-HMGCS1 1:500 (PA5-29488, ThermoFisher), anti-FDPS 1:500 (PA5-28228, ThermoFisher), anti-FDFT1 1:500 (ab109723, Abcam), anti-MHCII (I-A/I-E) 1:400 (M5/114.15.2, Biolegend), anti-Olig2 1:1000 (AB9610, EMD Millipore), anti-Olig2 1:200 (MABN50, EMD Millipore), anti-NG2 1:500 (AB5320 EMD Millipore), and anti-Sox2 1:100 (ab79351, Abcam). Secondary antibodies: all secondary antibodies (1:1000) were produced from goat and the followings were used for

staining the tissues: anti-rabbit-Cy3 (AP132C, EMD Millipore), anti-rabbit-DyLight® 649 (AP187SD, EMD Millipore), anti-mouse-DyLight® 649 (AP181SD, EMD Millipore), anti-rat-Cy3 (AP136C, EMD Millipore), and anti-rat-Cy5 (AB6565, Abcam). Nuclei were stained with DAPI at 1:5000 concentrations in 1xPBS. After serial washes, sections were mounted onto slides (Superfrost® Plus, VWR), allowed to semi-dry, and coverslipped (24x60, Fisher Scientific) with fluoromount® G (SouthernBiotech) for confocal microscopy as described (Kim et al., 2018).

Confocal microscopy and image analysis Stained sections were examined and imaged using Olympus BX51 fluorescence microscope with a DP50 digital camera. Images were taken in stacks, 10x images were taken at 8-10 μm thickness with 2 μm stacks and 40x images were taken at 5-6 μm thickness with 1 μm stacks. All images were taken and processed using the integrated software program Slidebook4.2 (Intelligent Imaging Innovations). ImageJ (NIH) was used to perform integration and analysis of images. All analyses were done in a blinded fashion with regards to knowledge of treatment randomization as described (Kim et al., 2018).

Electron Microscopy Mice were exposed to a lethal dose of isoflurane and perfused transcardially with ice-cold 1xPBS for 8 min, followed by 2.5% glutaraldehyde, 2% paraformaldehyde in 0.1M phosphate buffer, 0.9% sodium chloride (PBS) for 8 min. Corpus callosum region of the brain and thoracic portions of the spinal cords were dissected and post fixed for 2 hours at room temperature in the same fixative and stored at 4℃ until processing. Tissues were washed with PBS, post fixed in 1% OsO4 in ddH20 for 90 minutes on ice, dehydrated in a graded series of ethanol, treated with propylene oxide and infiltrated with resin Eponate 12 (Ted Pella) overnight. Tissues were embedded in fresh Eponate and polymerized at

60℃ for 48 hours. Approximately 50-60 nm thick sections were cut on an RMC MT-X ultramicrotome and picked up on formvar coated copper grids. The sections were stained with uranyl acetate and lead citrate and examined on a JEOL 100CX electron microscope at 60kV. Images were collected on type 4489 EM film, and the negatives scanned to create digital files. Films (Kodak) were developed and scanned at high resolution. The analysis was done with ImageJ and g-ratio was used for the extent of remyelination on axons. g-ratio = (axon diameter) / (axon + outer myelin diameter) as described (Kim et al., 2018).

Statistical Analysis Statistical analyses of immunofluorescence experiments to establish the disease model (Figure 2A-F) were evaluated using one-way ANOVA with Bonferroni's multiple comparison tests. Statistical analyses of qPCR results (Figure 2G, Figure 4B, and Figure 6B) were evaluated using unpaired two-tailed t-tests (Student's t-tests) or one-way ANOVA with Bonferroni's multiple comparison tests. Statistical analyses of immunofluorescence experiments regarding validation of cholesterol synthesis gene expression (Figure 4D) were evaluated using unpaired two-tailed t-tests (Student's t-tests). Statistical analyses of immunofluorescence experiments regarding ERβ-ligand treatment studies (Figures 5-8) were evaluated using two-way ANOVA with Bonferroni's multiple comparison tests for comparing treatment effects in two different transgenic groups, and one-way ANOVA with Bonferroni's multiple comparison tests for normal controls or chronic demyelination (9w) versus other groups. Data are presented as means ± S.E.M.. Power calculations for the experiments were determined for sample size to reach $P < 0.05$ by Myung S. Sim, M.S. Dr.PH, in the Department of Medicine Statistic Core at UCLA. A minimum of 4-5 animals per group was stated to provide statistical significance at a level of $P < 0.05$ using 95% power analysis, consistent with numbers used in the field. Data

distribution was assumed to be normal. All statistical analyses were performed using Prizm 6 (version 6.01) software (GraphPad, CA).

4.5 Bibilography

Anderson MA, Burda JE, Ren Y, Ao Y, O'Shea TM, Kawaguchi R, et al. Astrocyte scar formation aids central nervous system axon regeneration. Nature 2016; 532(7598): 195-200.

Antal MC, Krust A, Chambon P, Mark M. Sterility and absence of histopathological defects in nonreproductive organs of a mouse ERbeta-null mutant. Proc Natl Acad Sci U S A 2008; 105(7): 2433-8.

Back SA, Tuohy TM, Chen H, Wallingford N, Craig A, Struve J, et al. Hyaluronan accumulates in demyelinated lesions and inhibits oligodendrocyte progenitor maturation. Nat Med 2005; 11(9): 966-72.

Berghoff SA, Gerndt N, Winchenbach J, Stumpf SK, Hosang L, Odoardi F, et al. Dietary cholesterol promotes repair of demyelinated lesions in the adult brain. Nat Commun 2017; 8: 14241.

Birnbaum G, Cree B, Altafullah I, Zinser M, Reder AT. Combining beta interferon and atorvastatin may increase disease activity in multiple sclerosis. Neurology 2008; 71(18): 1390-5.

Camargo N, Goudriaan A, van Deijk AF, Otte WM, Brouwers JF, Lodder H, et al. Oligodendroglial myelination requires astrocyte-derived lipids. PLoS Biol 2017; 15(5): e1002605.

Chang A, Tourtellotte WW, Rudick R, Trapp BD. Premyelinating oligodendrocytes in chronic lesions of multiple sclerosis. N Engl J Med 2002; 346(3): 165-73.

Chevalier AC, Rosenberger TA. Increasing acetyl-CoA metabolism attenuates injury and alters spinal cord lipid content in mice subjected to experimental autoimmune encephalomyelitis. J Neurochem 2017; 141(5): 721-37.

Chew LJ, King WC, Kennedy A, Gallo V. Interferon-gamma inhibits cell cycle exit in differentiating oligodendrocyte progenitor cells. Glia 2005; 52(2): 127-43.

Franklin RJ. Why does remyelination fail in multiple sclerosis? Nat Rev Neurosci 2002; 3(9): 705-14.

Franklin RJ, Ffrench-Constant C. Remyelination in the CNS: from biology to therapy. Nat Rev Neurosci 2008; 9(11): 839-55.

Funfschilling U, Saher G, Xiao L, Mobius W, Nave KA. Survival of adult neurons lacking cholesterol synthesis in vivo. BMC Neurosci 2007; 8: 1.

Gudi V, Gingele S, Skripuletz T, Stangel M. Glial response during cuprizone-induced de- and remyelination in the CNS: lessons learned. Front Cell Neurosci 2014; 8: 73.

Hoffmann SA, Hos D, Kuspert M, Lang RA, Lovell-Badge R, Wegner M, et al. Stem cell factor Sox2 and its close relative Sox3 have differentiation functions in oligodendrocytes. Development 2014; 141(1): 39-50.

Itoh N, Itoh Y, Tassoni A, Ren E, Kaito M, Ohno A, et al. Cell-specific and region-specific transcriptomics in the multiple sclerosis model: Focus on astrocytes. Proc Natl Acad Sci U S A 2018; 115(2): E302-E9.

Kamm CP, El-Koussy M, Humpert S, Findling O, von Bredow F, Burren Y, et al. Atorvastatin added to interferon beta for relapsing multiple sclerosis: a randomized controlled trial. J Neurol 2012; 259(11): 2401-13.

Kim RY, Hoffman AS, Itoh N, Ao Y, Spence R, Sofroniew MV, et al. Astrocyte CCL2 sustains immune cell infiltration in chronic experimental autoimmune encephalomyelitis. J Neuroimmunol 2014; 274(1-2): 53-61.

Kim RY, Mangu D, Hoffman AS, Kavosh R, Jung E, Itoh N, et al. Oestrogen receptor β ligand acts on CD11c+ cells to mediate protection in experimental autoimmune encephalomyelitis. Brain 2018; 141(1): 132-47.

Klopfleisch S, Merkler D, Schmitz M, Kloppner S, Schedensack M, Jeserich G, et al. Negative impact of statins on oligodendrocytes and myelin formation in vitro and in vivo. J Neurosci 2008; 28(50): 13609-14.

Lavrnja I, Smiljanic K, Savic D, Mladenovic-Djordjevic A, Tesovic K, Kanazir S, et al. Expression profiles of cholesterol metabolism-related genes are altered during development of experimental autoimmune encephalomyelitis in the rat spinal cord. Sci Rep 2017; 7(1): 2702.

Lopez Juarez A, He D, Richard Lu Q. Oligodendrocyte progenitor programming and reprogramming: Toward myelin regeneration. Brain Res 2016; 1638(Pt B): 209-20.

Lu QR, Sun T, Zhu Z, Ma N, Garcia M, Stiles CD, et al. Common developmental requirement for Olig function indicates a motor neuron/oligodendrocyte connection. Cell 2002; 109(1): 75-86.

Maier O, De Jonge J, Nomden A, Hoekstra D, Baron W. Lovastatin induces the formation of abnormal myelin-like membrane sheets in primary oligodendrocytes. Glia 2009; 57(4): 402-13.

Mason JL, Jones JJ, Taniike M, Morell P, Suzuki K, Matsushima GK. Mature oligodendrocyte apoptosis precedes IGF-1 production and oligodendrocyte progenitor accumulation and differentiation during demyelination/remyelination. J Neurosci Res 2000; 61(3): 251-62.

Mathews ES, Appel B. Cholesterol Biosynthesis Supports Myelin Gene Expression and Axon Ensheathment through Modulation of P13K/Akt/mTor Signaling. J Neurosci 2016; 36(29): 7628-39.

Mathews ES, Mawdsley DJ, Walker M, Hines JH, Pozzoli M, Appel B. Mutation of 3-hydroxy-3-methylglutaryl CoA synthase I reveals requirements for isoprenoid and cholesterol synthesis in oligodendrocyte migration arrest, axon wrapping, and myelin gene expression. J Neurosci 2014; 34(9): 3402-12.

Matsushima GK, Morell P. The neurotoxicant, cuprizone, as a model to study demyelination and remyelination in the central nervous system. Brain Pathol 2001; 11(1): 107-16.

Mauch DH, Nagler K, Schumacher S, Goritz C, Muller EC, Otto A, et al. CNS synaptogenesis promoted by glia-derived cholesterol. Science 2001; 294(5545): 1354-7.

Mi S, Miller RH, Lee X, Scott ML, Shulag-Morskaya S, Shao Z, et al. LINGO-1 negatively regulates myelination by oligodendrocytes. Nat Neurosci 2005; 8(6): 745-51.

Moore CS, Cui QL, Warsi NM, Durafourt BA, Zorko N, Owen DR, et al. Direct and indirect effects of immune and central nervous system-resident cells on human oligodendrocyte progenitor cell differentiation. J Immunol 2015; 194(2): 761-72.

Moyon S, Dubessy AL, Aigrot MS, Trotter M, Huang JK, Dauphinot L, et al. Demyelination causes adult CNS progenitors to revert to an immature state and express immune cues that support their migration. J Neurosci 2015; 35(1): 4-20.

Moyon S, Huynh JL, Dutta D, Zhang F, Ma D, Yoo S, et al. Functional Characterization of DNA Methylation in the Oligodendrocyte Lineage. Cell Rep 2016; 15(4): 748-60.

Norton WT, Poduslo SE. Myelination in rat brain: changes in myelin composition during brain maturation. J Neurochem 1973; 21(4): 759-73.

Plemel JR, Liu WQ, Yong VW. Remyelination therapies: a new direction and challenge in multiple sclerosis. Nat Rev Drug Discov 2017; 16(9): 617-34.

Saher G, Brugger B, Lappe-Siefke C, Mobius W, Tozawa R, Wehr MC, et al. High cholesterol level is essential for myelin membrane growth. Nat Neurosci 2005; 8(4): 468-75.

Saher G, Quintes S, Nave KA. Cholesterol: a novel regulatory role in myelin formation. Neuroscientist 2011; 17(1): 79-93.

Sanz E, Yang L, Su T, Morris DR, McKnight GS, Amieux PS. Cell-type-specific isolation of ribosome-associated mRNA from complex tissues. Proc Natl Acad Sci U S A 2009; 106(33): 13939-44.

Skripuletz T, Hackstette D, Bauer K, Gudi V, Pul R, Voss E, et al. Astrocytes regulate myelin clearance through recruitment of microglia during cuprizone-induced demyelination. Brain 2013; 136(Pt 1): 147-67.

Smolders I, Smets I, Maier O, vandeVen M, Steels P, Ameloot M. Simvastatin interferes with process outgrowth and branching of oligodendrocytes. J Neurosci Res 2010; 88(15): 3361-75.

Sorensen PS, Lycke J, Eralinna JP, Edland A, Wu X, Frederiksen JL, et al. Simvastatin as add-on therapy to interferon beta-1a for relapsing-remitting multiple sclerosis (SIMCOMBIN study): a placebo-controlled randomised phase 4 trial. Lancet Neurol 2011; 10(8): 691-701.

Stankoff B, Jadasz JJ, Hartung HP, Kury P, Zalc B, Lubetzki C. Repair strategies for multiple sclerosis: challenges, achievements and perspectives. Curr Opin Neurol 2016; 29(3): 286-92.

Togha M, Karvigh SA, Nabavi M, Moghadam NB, Harirchian MH, Sahraian MA, et al. Simvastatin treatment in patients with relapsing-remitting multiple sclerosis receiving interferon beta 1a: a double-blind randomized controlled trial. Mult Scler 2010; 16(7): 848-54.

van de Kraats C, Killestein J, Popescu V, Rijkers E, Vrenken H, Lutjohann D, et al. Oxysterols and cholesterol precursors correlate to magnetic resonance imaging measures of neurodegeneration in multiple sclerosis. Mult Scler 2014; 20(4): 412-7.

Vollmer T, Key L, Durkalski V, Tyor W, Corboy J, Markovic-Plese S, et al. Oral simvastatin treatment in relapsing-remitting multiple sclerosis. Lancet 2004; 363(9421): 1607-8.

Wahl SE, McLane LE, Bercury KK, Macklin WB, Wood TL. Mammalian target of rapamycin promotes oligodendrocyte differentiation, initiation and extent of CNS myelination. J Neurosci 2014; 34(13): 4453-65.

Wolswijk G. Chronic stage multiple sclerosis lesions contain a relatively quiescent population of oligodendrocyte precursor cells. J Neurosci 1998; 18(2): 601-9.

Zhang Y, Chen K, Sloan SA, Bennett ML, Scholze AR, O'Keeffe S, et al. An RNA-sequencing transcriptome and splicing database of glia, neurons, and vascular cells of the cerebral cortex. J Neurosci 2014; 34(36): 11929-47.

Zhao C, Ma D, Zawadzka M, Fancy SP, Elis-Williams L, Bouvier G, et al. Sox2 Sustains Recruitment of Oligodendrocyte Progenitor Cells following CNS Demyelination and Primes Them for Differentiation during Remyelination. J Neurosci 2015; 35(33): 11482-99.

Zhornitsky S, McKay KA, Metz LM, Teunissen CE, Rangachari M. Cholesterol and markers of cholesterol turnover in multiple sclerosis: relationship with disease outcomes. Mult Scler Relat Disord 2016; 5: 53-65.

CHAPTER 5

General Conclusion, Limitations and Future Directions

In this dissertation, I aimed to understand the treatment effects of ER-specific ligands on neuroprotection and remyelination in mouse models of multiple sclerosis (MS). Both ERα and ERβ ligands have distinct and significant neuroprotective benefits in the CNS during disease. Despite ERα-ligands beneficial effects in the CNS, it is unfortunate to know that chronic treatment in humans could have adverse effects such as breast and uterine cancer, and increased risk for cardiovascular diseases. For this reason, our lab focuses on using approaches targeting the downstream effects of ERα-ligand mediated neuroprotection to find alternative treatment strategies for MS.

Previous studies from our lab showed that ERα-ligands are anti-inflammatory and act directly through astrocytes in the CNS for its neuroprotective effects. Specifically, CCL2 expression was significantly reduced in astrocytes when EAE mice were treated with ERα-ligand, whereas the removal of ERα from astrocytes reversed this effect showing a direct relationship between the two molecules. One study found that by simply deleting an upstream transcription factor of CCL2, NFκB, in astrocytes provided protection during EAE. However, whether deletion of CCL2 alone from astrocytes will reverse EAE clinical disease course remained unknown. In Chapter 2, I found that deletion of CCL2 from astrocytes provided disease protection late in EAE. Further neuropathological assessment showed that astrocyte CCL2 plays an essential role in sustaining inflammation during chronic EAE, as its deletion in astrocytes reduced infiltrating immune cells and dampened diffuse inflammation by activated microglia and astrocytes in white and gray matter of the CNS. These results suggested that targeted modulation

of CCL2 may reduce inflammation in the CNS during disease. Altogether, this research approach to investigate downstream targets of ERα-ligand treatment effects during EAE provided critical insights into alternative treatment strategies for neuroprotection.

Interestingly, in the previous study from our lab showed that chemokine CCL7 expression from astrocytes was also significantly reduced with ERα-ligand treatment during EAE. Studying the functional significance of astrocyte specific CCL7 was limited due to the difficulty of obtaining a CCL7 floxed mouse model that will enable to generate a conditional knockout of CCL7 on astrocytes. The floxed model is still unavailable, but similar to CCL2, CCL7 is also known to attract monocytes and macrophages and bind to the receptor for CCL2, CCR2. Therefore, it would be interesting to investigate the direct role of CCL7 expression from astrocytes during EAE, as it may provide additional insights for developing treatment strategies for MS.

Another method to develop alternative treatment strategies for MS is using other ER-specific ligands. Our lab mainly focuses on ligands that bind ERβ with minimal binding to ERα. Currently developed and tested ERβ-ligands are safe, with minimum toxic effects showing with chronic treatment in MS patients, such as estriol, a pregnancy hormone and a moderate ERβ-ligand. Neuroprotective effects of ERβ-ligands are known to modulate inflammation and increase oligodendrocyte maturation and myelination. However, direct mechanisms of ERβ-ligands in providing neuroprotection in the CNS during disease remains poorly understood. In Chapter 3, I used mice with targeted deletion of ERβ on $CD11c^+$ immune cells (myeloid dendritic cells and macrophages, DC/MΦ) and $Olig1^+$ oligodendrocytes to investigate the mechanisms of ERβ-ligand mediated neuroprotective effects. First, I assessed the mechanisms of ERβ-ligand treatment effects on $CD11c^+$ cells during EAE and found that ERβ-ligand treatment

modulated CD11c$^+$ myeloid DC/MΦs by reducing pro-inflammatory iNOS and T-bet expression, but increasing anti-inflammatory IL-10 expression. These effects led to a reduction of pro-inflammatory responses from Iba1$^+$ microglia and macrophages in the CNS microenvironment and subsequently permitted oligodendrocyte maturation and remyelination. Together, these findings suggested that ERβ on CD11c$^+$ myeloid DC/MΦ is essential in mediating ERβ-ligand treatment effects during EAE. Next, I assessed the mechanisms of ERβ-ligand treatment on Olig1$^+$ oligodendrocytes in EAE. Treatment of ERβ-ligand during EAE enhanced oligodendrocyte maturation and remyelination, and these effects were mediated through ERβ on Olig1$^+$ oligodendrocytes. In conclusion, I found that ERβ on both cell types were important in mediating neuroprotection, but when each cell type (CD11c$^+$ or Olig1$^+$) was targeted for ERβ specific deletion the neuroprotective treatment effects were lost. This suggested each is necessary, but not sufficient (Figure 5.1).

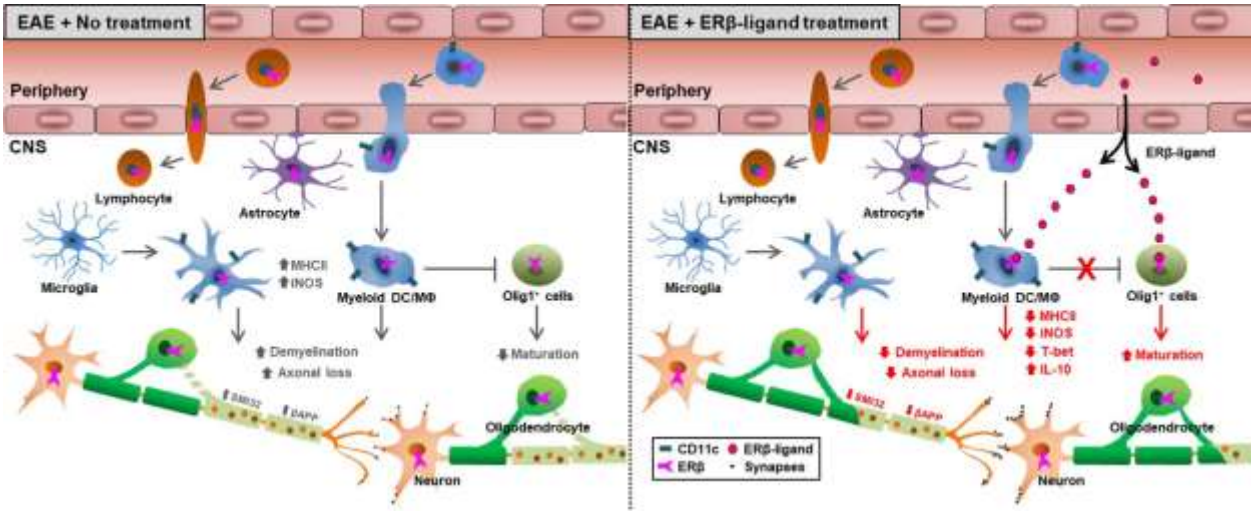

Figure 5.1 Mechanisms of ERβ-ligand treatment effects during EAE. During EAE, there is infiltration of lymphocytes and myeloid derived dendritic cells and macrophages (myeloid DC/MΦ), and activation of microglia cells in the CNS. Infiltrated and activated immune cells

initiate pro-inflammatory responses inducing demyelination, axonal damage and synaptic loss. Also, maturation of oligodendrocytes is blocked by inhibitory molecules in the CNS. With ERβ-ligand treatment, $CD11c^+$ myeloid DC/MΦ reduces pro-inflammatory responses and reverses inflammation block on oligodendrocyte maturation. Also, $Olig1^+$ oligodendrocytes enhance maturation and remyelination leading to protection from demyelination, axonal damage, and synaptic loss. Interestingly, when either cell type (myeloid DC/MΦ or oligodendrocytes) was targeted for ERβ deletion, neuroprotective effects of ERβ-ligand treatment were lost. Thus, actions of ERβ-ligand treatment on each cell type were necessary.

Unquestionably, remyelination by oligodendrocytes is the most warranted process in MS. However, in MS, this process is insufficient leading to further neurodegeneration and disability accumulation. Using the EAE model, I was able to describe the detailed mechanisms of ERβ-ligand treatment effects mediated through $CD11c^+$ myeloid DC/MΦs, but not through $Olig1^+$ oligodendrocytes. The EAE model uses a profound immune response mediated induction method making it challenging to investigate the specific mechanisms of remyelination in oligodendrocytes. In addition, remyelination rarely occurs. Therefore, I proposed to investigate the mechanisms of remyelination in oligodendrocytes and study ERβ-ligand treatment effects during remyelination using the cuprizone diet-induced demyelination model. I also used RiboTag technology to overcome the limitation of isolating CNS cell specific transcripts without using *ex vivo* manipulations. The utilization of RiboTag technology allowed the isolation of oligodendrocyte specific ribosome associated transcripts *in vivo*. In Chapter 4, I investigated the natural process of remyelination in oligodendrocytes by comparing oligodendrocyte specific transcriptomes between the remyelination and chronic demyelination phases via RNA-seq. The

results showed that cholesterol synthesis pathways, important for myelin membrane formation and axon ensheathment, were among the top upregulated pathways, and neuroinflammatory pathways, characteristics of oligodendrocytes during demyelination, were among the top downregulated. The significantly up or down regulated oligodendrocyte specific genes and pathways during remyelination are subjected for future investigations and in the plans to be used as targets for developing treatment strategies for enhancing remyelination during disease.

The increase in cholesterol synthesis pathways caught our attention as all four pathways were among the top 5 significantly upregulated pathways (Figure 4.3). I further validated that the pathway genes and found that they were increased in oligodendrocytes during remyelination in different sets of mice by qPCR and immunofluorescence. Then, I investigated whether ERβ-ligand treatment during remyelination had an effect on cholesterol synthesis in oligodendrocytes. I found that ERβ-ligand treatment enhances remyelination and increases oligodendrocytes (OPCs and mature) during remyelination in the cuprizone model. Most importantly, I found that cholesterol synthesis genes in mature oligodendrocytes were increased compared to non-treated natural remyelination mice. All these effects of ERβ-ligand treatment were mediated through ERβ expressed on $Olig1^{+}$ oligodendrocytes.

The goal for my thesis work was to obtain a comprehensive understanding of ERβ-ligand treatment effects on neuroprotection during disease. Therefore, I sought to investigate whether the effects of ERβ-ligand treatment on oligodendrocytes during remyelination in the cuprizone model were observed in the EAE model. Despite, having limited remyelination occurring in the model, its immune response driven disease induction and progression best represents the human disease. In addition to all the beneficial effects of ERβ-ligand treatment mediated through $Olig1^{+}$ oligodendrocytes during EAE (Chapter 3), I have observed that cholesterol synthesis genes were

increased in mature oligodendrocytes during EAE, and that this too was mediated through ERβ expressed on Olig1^{+} oligodendrocytes (Figure 4.9 and Figure 5.2).

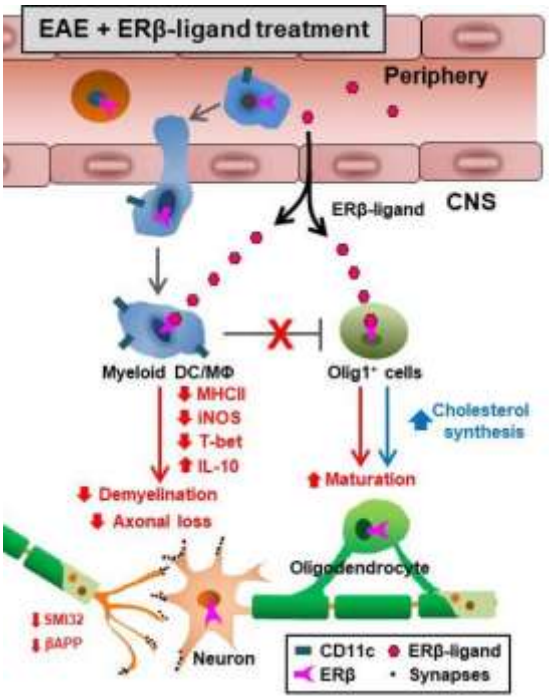

Figure 5.2 Mechanisms of ERβ-ligand treatment effects during EAE with insights from an investigation in the cuprizone model. An investigation using the cuprizone model gave crucial insights regarding the mechanisms of ERβ-ligand treatment effects through oligodendrocytes to increase maturation and enhance remyelination during EAE. Important transcriptional regulation oligodendrocytes experience during natural remyelination after chronic demyelination, upregulation of cholesterol synthesis, was increased with ERβ-ligand treatment during remyelination in the cuprizone model and during EAE.

We obtained critical insights by using two different disease models of MS to investigate the mechanisms of ERβ-ligand treatment effects on neuroprotection during disease. However, we also obtained results that were disagreeing. In Chapter 4, I observed that ERβ-ligand treatment

increased the OPCs during remyelination in the cuprizone model (Figure 4.5J, K). To determine what drove this effect, I assessed the expression levels of OPC specific genes, *Sox2, Sox9, Nkx2.2* and *Pdgfrα* in oligodendrocyte specific transcripts isolated from different sets of Olig1-RiboTag mice (Figure 5.3A). I found that *Sox2* gene expression was significantly increased in 9w+3w/ERβ compared to 9w+3w/Veh. No changes were observed in the expression level of other genes (Figure 5.3B). Next, I validated Sox2 expression at the protein level following ERβ-ligand treatment in both cuprizone and EAE mouse models and further investigated whether this effect was directly mediated through ERβ on $Olig1^+$ oligodendrocytes.

In the chronic cuprizone model, immunofluorescence for Sox2 revealed that in normals, Sox2 expressing cells neatly lined up along the subventricular zone (SVZ) where neural stem cells reside. During chronic demyelination (9w) and remyelination (9w+3w), $Sox2^+$ cells were found within the corpus callosum area (Figure 5.3C), suggesting that Sox2 expressing cells migrate to areas where demyelination has occurred. Double immunolabelling assessed Sox2 expression in $Olig2^+$ OLC and $NG2^+$ OPCs (Figure 5.3D, E). During demyelination, a significant increase in the percentage of $Sox2^+Olig2^+$ OLCs and $Sox2^+NG2^+$ OPCs in 9w mice was observed compared to normal controls (N). During remyelination, 9w+3w/Veh WT exhibited a decrease in the percentage of $Sox2^+Olig2^+$ OLCs and $Sox2^+NG2^+$ OPCs compared to 9w mice. However, ERβ-ligand treatment increased the percentage of both populations in 9w+3w/ERβ WT mice when compared to 9w+3w/Veh WT mice. In contrast, this effect was no longer observed in 9w+3w CKO mice (Figure 5.3F), indicating that the effect on Sox2 expression was mediated by direct effects on ERβ in $Olig1^+$ oligodendrocytes. Given previous evidence that Sox2 plays a role in OPC recruitment, maintenance, and differentiation after demyelination, these results suggested that ERβ-ligand treatment acts directly on oligodendrocytes during the

remyelination in the cuprizone model to maintain the OPC population by increasing expression of Sox2.

When I extended the investigation to EAE and assessed Sox2 expression in OPCs, I found no changes in $Sox2^{+}Olig2^{+}$ OLCs and $Sox2^{+}NG2^{+}$ OPCs with ERβ-ligand treatment in either EAE/ERβ WT mice or EAE/ERβ CKO mice (Figure 5.3G). These results showed that ERβ-ligand treatment increases Sox2 expression in OPCs through a direct effect on ERβ of $Olig1^{+}$ cells in the cuprizone model, but not in the EAE model. Thus, either factors in the cuprizone model are permissive, or factors in the EAE model are inhibitory, to the ability of ERβ ligand treatment on increasing Sox2 expression in OPCs. This example of discordant provided us a perspective that investigations of drug treatment effects in one particular disease model could provide critical insights and valuable understanding of its molecular mechanisms; however, the appreciated lesson could also be a model specific effect that is not necessarily a direct effect from the drug in the overall disease.

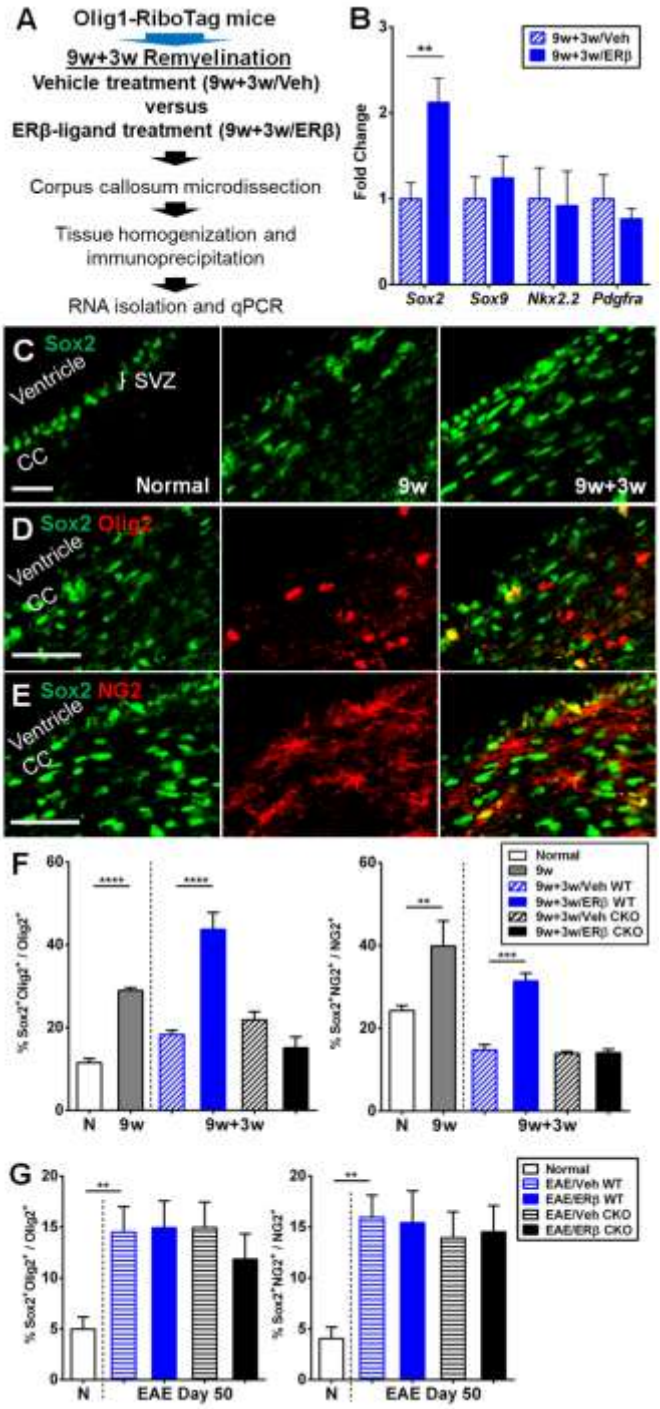

Figure 5.3 ERβ-ligand treatment increases Sox2 expression in OPCs in the cuprizone model, but not in the EAE model. (A) Experimental scheme to study oligodendrocyte specific gene expression in the corpus callosum tissues of Olig1-RiboTag mice during remyelination in vehicle treated (9w+3w/Veh) versus ERβ-ligand treated (9w+3w/ERβ). **(B)** qPCR results of OPC

specific developmental gene expression during remyelination in 9w+3w/Veh versus 9w+3w/ERβ Olig1-RiboTag mice. Gene expression of *Sox2* was increased in 9w+3w/ERβ compared to 9w+3w/Veh in Olig1-RiboTag mice, whereas *Sox9*, *Nkx2.2*, or *Pdgfrα* showed no changes. (**C)** Immunofluorescence images of Sox2 expression in the corpus callosum of normal controls (N), mice fed with cuprizone diet for 9 weeks (9w); mice fed with cuprizone for 9 weeks and normal diet for 3 weeks (9w+3w). Scale bar, 50μm. **(D and E)** Representative image of Olig2 (D, red) and NG2 (E, red) co-stained with Sox2 (green) in the corpus callosum. Scale bar, 50μm. **(F)** Quantitative analyses of $Sox2^{+}Olig2^{+}$ OLCs and $NG2^{+}Olig2^{+}$ OPCs showed that 9w+3w/ERβ WT mice had increased number of cells compared to 9w+3w/Veh WT mice, whereas ERβ-ligand treatment had no effect in 9w+3w Olig1-CKO mice (9w+3w/Veh CKO versus 9w+3w/ERβ CKO). **(G)** Quantitative analyses of $Sox2^{+}Olig2^{+}$ OLCs and $Sox2^{+}NG2^{+}$ OPCs showed that ERβ-ligand treatment had no effect in EAE WT and EAE CKO mice. **P < 0.01; ****P < 0.0001.

Overall, neuroprotective effects of ERβ-ligand treatment has now been tested on neurons, astrocytes, oligodendrocytes, microglia and peripheral myeloid cells to determine functional significance in two different demyelinating disease models of MS. The results permitted critical insights herein regarding *in vivo* mechanisms of neuroprotection by contrasting effects in some cells (myeloid DC/MΦ and oligodendrocytes) with lack of effects in others (neurons, astrocytes, and resident microglia). While much work remains to fully elucidate the mechanisms of ERβ-ligand treatment on oligodendrocyte maturation and enhancing remyelination, the studies presented here bring several important features of neuroprotection provided through ERβ activation, and suggest promising directions for clinical applications in the future.